Renal Tubular Transport of Drugs in Healthy and Diseased Kidney

Alenka Chapron

A dissertation

submitted in partial fulfillment of the

requirements for the degree of

Doctor of Philosophy

University of Washington

2018

Reading Committee:

Danny D. Shen, Chair

Kenneth E. Thummel

Catherine Yeung

Program Authorized to Offer Degree:

Pharmaceutics

University of Washington

Abstract

Renal Tubular Transport of Drugs in Healthy and Diseased Kidney

Alenka Chapron

Chair of Supervisory Committee:

Danny D. Shen

Department of Pharmaceutics

In this thesis work, I applied traditional and innovative bioengineering approaches to develop an *in vitro* model of renal proximal tubule with human proximal tubule epithelial cells (PTECs) that is particularly suited for drug transport studies. The use of human PTECs has thus far been hindered by the lack of complete understanding of their cell morphology and functioning *in vitro*.

At the initial stage of our development, freshly isolated human PTECs were successfully expanded through conventional culturing, which afforded an adequate cell source. When passaged PTECs were grown on permeable supports, they maintained their polarity, barrier integrity, transporter expression (mRNA and protein immunocytochemistry) and activity. We then developed a novel 3D culture of human PTECs in a Nortis microphysiological system (MPS). Under continuous flow, PTECs in the MPS sustained long term viability up to 28 days;

they also maintained the expression of prototypical proximal tubule markers (e.g. E-Cadherin, aquaporin 1, SGLT2, γ-glutamyl transpeptidase), cellular structures (e.g. cilia), and critical synthetic and metabolic functions. The next key step of development involved co-culturing of human PTECs with human umbilical vein endothelial cells (HUVECs) in a dual-channel Nortis MPS to establish a vascularized proximal tubule MPS. This system is uniquely designed to investigate the multiple steps involved in the renal tubular secretion of compounds; it allows for independent vascular (basolateral) and tubular (apical) perfusion and provides multiple readouts, including fluorescence microscopy and effluent analysis. Regular fluorescent and 2-photon imaging technique were applied to track a fluorescently labelled dextran from its entry into and leakage from the vessel, diffusion through the interstitium, and ultimately its passage across the PTEC tubule; in fact, PTEC was shown to be the limiting barrier in dextran's translocation across the tubulo-interstitium. Through a series of radiolabeled solute experiments, permeability across the PTEC tubule was demonstrated to be several-fold higher for *p*-aminohippuric acid (PAH) than mannitol and dextran, both of which are paracellular permeability markers. Importantly, these findings yielded a favorable prediction of PAH renal clearance upon *in vitro−to−in vivo* scaling. Thus, our vascularized proximal tubule MPS appears to be a promising in vitro model for investigations of renal tubular drug secretion.

The last part of my thesis work focused on alterations in renal secretory clearance of drugs in renal impairment. Dosing adjustments in chronic kidney diseases (CKD) have traditionally relied on serum creatinine as a biomarker of glomerular filtration rate (GFR). However, a number of drugs associated with adverse drug events in CKD undergo renal secretion, a process localized to the proximal tubule. In an evaluation of the available literature to-date, I showed that the renal clearance for some drugs decline less rapidly than (Group A),

more rapidly than (Group B), or proportionately to (Group C) creatinine clearance in advancing kidney disease. It is important to note that, in healthy subjects, all these drugs are extensively secreted via the proximal tubule and minimally reabsorbed along the entire tubule. These findings point to the complexity in the handling of drugs by the proximal tubule in CKD, and challenge the traditional assumption that secretory clearance decline in parallel with glomerular filtration rate, whereby creatinine clearance can serve as a guide for drug dosing adjustments.

Contents

Acknowledgements

I am indebted to many individuals who have helped me in acquiring my PhD degree. Foremost, I would like to thank my advisor Danny Shen for his endless patience, guidance and teaching. His continued support has allowed me to further my professional growth, as well as expand my knowledge of pharmaceutical sciences and translational pharmacology. I will forever fondly remember our numerous meetings, during which we discussed science and many other interesting aspects of life.

I would also like to thank other members of the thesis committee: Ken Thummel, Cathy Yeung, Joanne Wang, Ed Kelly, and Jonathan Himmelfarb for providing their critical inputs and this way improving my thesis research. Special thanks goes to Brian Werth, who served as a Graduate Student Representative (GSR). Furthermore, I would like to thank other faculty, students and staff in the Department of Pharmaceutics, for making our department a welcoming work environment.

I owe deepest gratitude to my loving mom and dad, and my sister with her family, who all rooted for me in these past 6 years from far away. It was always a pleasure to return home to Slovenia during holidays and spend time with them.

Lastly, I would like to thank my husband and my best friend Brian Chapron for being such an incredible work colleague. I will forever be grateful for all the crucial advice and technical assistance that he gladly offered, no matter how busy he was with his own work.

Dedication

To Chapron, Jaklic and Kunze families

1. Introduction

1.1 Background

1.1.1 Considerations in prediction of drug renal excretion during drug development

The primary physiological role of the kidney is to maintain water and electrolyte homeostasis through elimination of solutes that are in excess, and reabsorption of essential solutes (e.g., glucose) and electrolytes (1). In addition, the kidney is also one of the most important drug eliminating organs. It has been estimated that of the 200 most prescribed drugs, 32% are predominantly renally eliminated (2). Hence, a critical need exists to understand renal elimination of drugs to guide drug dosing, particularly at the preclinical to early clinical stages of new drug development.

In the nephron (kidney's structural and functional unit), drugs undergo three sequential processes: passive glomerular filtration, which is followed by active secretion and reabsorption processes in the kidney proximal tubule. Net elimination of drugs via the kidney (i.e., renal clearance) can be described in simple terms by the following relationship:

$$Cl\,renal = (fu \cdot GFR + Cl_S) \cdot (1 - Fr) \qquad \text{Equation 1}$$

where $fu * GFR$ represents filtration clearance of unbound drug, Cl_{Sec} represents secretory clearance, and Fr represents the fraction of the filtered and secreted drug that is subsequently reabsorbed (via passive and active processes). As illustrated by the following scenarios, an estimate of drug renal clearance can reveal the general handling of a drug in the kidney:

- If overall drug renal clearance is greater than glomerular filtration, then net active tubular secretion must occur.

- If renal clearance of a compound is less than glomerular filtration, then net reabsorption process must occur.
- Drugs that exert renal clearance numerically close to filtration clearance can undergo glomerular filtration only, or are subjected to an opposing interplay between tubular secretion and reabsorption resulting in a net loss that is close to glomerular filtration.

Of the renally eliminated drugs currently most prescribed in the market, the majority (92%) undergo net renal tubular secretion (2). Thus, to predict the renal clearance of drugs accurately, active secretion across the proximal tubule should be investigated.

Proximal tubule secretion is a multi-step solute delivery process consisting of carriage by blood into the peritubular capillaries via the efferent (post-glomerulus) arterioles, diffusion or extravasation out of the capillary channel into an adjacent interstitium, passage through the intervening interstitium with its supportive cell types, and vectorial transport across the tubular epithelium. The last step is mediated by one or more transporters located on the basolateral (uptake transporters, e.g. OAT1/2/3, OCT2), and apical (efflux transporters, e.g. MATE1/2K, P-gp, BCRP, MRP2/4) sides of the proximal tubule epithelial cell.

Identification of individual transporters involved in the renal tubular secretion of a drug can readily be ascertained with cell lines or cell membrane vesicles over-expressing a single human transporter isoform. However, proximal tubule secretion of solutes and drugs represents the joint actions of uptake transporter(s) located on the basolateral membrane, and efflux transporter(s) located on the apical membrane of polarized proximal tubule epithelium, which together exhibit complex kinetics requiring sophisticated analysis and modeling. In particular, we need preclinical (*in vitro* and/or animal) models that would allow us to quantify the contribution of individual

transporters at the two membrane domains as well as their coordination in effecting trans-epithelial drug secretion (3).

1.1.2 Existing *in vitro* models of renal tubular drug secretion

Several preclinical models support studies of renal secretory transport of drug molecules, each with its own advantages and limitations.

a) ***In vivo* animal models** permit studies of renal tubular secretion in a complete physiological environment. Because species differences in kidney blood flow, plasma protein binding, and renal transporter expression exist (4, 5), the information on tubular secretion acquired from animal studies should in general be interpreted with caution. The contribution of a single transporter (or multiple transporters) to the overall drug renal clearance (as well as intratubular drug accumulation) can also be studied in a transporter gene knock-out model (6). However, it has previously been shown that knock-out animals often suffer other alterations in transporter functions, not just the target transporter gene modulation (7).

b) **Isolated perfused kidneys, kidney tissue slices and isolated renal tubules**. Similar to *in vivo* animal models, these models also possess fully intact renal transporter systems, and are as such, among *in vitro* models, most representative of *in vivo* environment (8, 9). Isolated perfused kidneys and tubules can be used for drug flux studies, while tissue slices only allow for the assessment of drug uptake largely across the basolateral membrane. A major experimental handicap of these models is their limited viability, up to only a few hours after isolation and preparation. Lastly, the

proper use of these models is technically challenging and requires significant surgical expertise.

c) **Multiple-transfected overexpressing transporter cell systems**. Although not exerting a full complement of transporters as seen *in vivo*, polarized mammalian cells (such as MDCK II cells) overexpressing human isoforms of transporters located on respective basolateral and apical membranes were previously shown as a useful model to elucidate the vectorial transport pathways across a tubular epithelium, particularly those of organic cations (e.g., basolateral hOCT2, and apical hMATE1) (10, 11). Because drug renal transporters generally appear to lack a high degree of specificity, transfection of multiple transporters (human isoforms) may be necessary to fully capture the tubular handling of a drug in these model systems. Also, at present we cannot precisely control the final expression level and activity of the transfected protein(s) to precisely mimic what exists in vivo. Another complication is the potential interference from background activities of some constitutively expressed transporters (e.g., canine OCT2 and P-gp in MDCK II cells, (12, 13)).

d) **Primary cell cultures**. Past investigations of the cellular physiology and pharmacology of the human renal tubule have been conducted mostly using human proximal tubule epithelial cells grown in monolayer (2D) cultures (14-16); more details on the characterization are available in the Introduction of Chapter 2. Thus far, freshly isolated cells grown in culture for up to 2 weeks have been reported to maintain activity of the entire complement of renal transporters, as seen in the human proximal tubule *in vivo* (14, 15). When using these cells as an *in vitro* monolayer model, several limitations associated with the model should be considered:

i. Cell isolation: Currently, cells can be isolated from human tissues via culturing in selective media that only supports growth and proliferation of proximal tubule epithelial cells (17), micro-dissection (17), enzymatic dissociation (18), centrifugation on Percoll density gradient (15), immunomagnetic cell sorting (18), or any combination of the aforementioned techniques (19). Differences in isolation protocols may result in different purities of proximal tubule cell populations, which may directly affect reproducibility and make side-by-side comparisons of models challenging.

ii. Cell viability and phenotypic stability: When compared to continuous cell lines, primary monolayer cultures of human proximal tubule show reduced viability. It has been reported that *in vitro* cells survive and maintain their proximal tubule phenotype for up to 5-6 passages, for a total of 40-50 days in culture (18, 20). A de-differentiated state of cells has been demonstrated after passage 5 (21). To overcome the lack of cell sourcing, several groups first isolated and then immortalized human proximal tubule epithelial cells (22, 23). While longevity in culture and reproducible sourcing are practical advantages of this approach, the altered biology of immortalized cell lines is a serious drawback.

iii. Changes in transporter expression: During time in culture and cell passage, human proximal tubule epithelial cells have been shown to suffer from reduced transporter expression (defined by reduction in transporter mRNA levels) (23-25), and hence potentially reduced transporter function.

Currently, there is a critical need for robust, predictable *in* vitro models of the human proximal tubule that can be applied to assess renal tubular secretion as a potential clearance pathway for new molecular entities in drug development. Given the overall species difference in physiology as well transporter expression and function, primary proximal tubule epithelial cells of human origin have recently gained considerable attention, and continuing efforts in the research community to overcome this model's shortcomings are currently directed to more faithfully recapitulate *in vivo* human proximal tubule environment.

1.1.3 Three-dimensional cell culture platforms

Accumulating evidence suggests that the choice of a platform for cell culture and/or culturing protocol significantly influence the performance of an *in vitro* cell model (16). Three dimensional (3D) cultures that would better recapitulate the biostructural scaffolding and microenvironment in vivo, often referred to as microphysiological systems (MPS), represent the latest advance in bioengineering. The following section offers a brief overview of recently reported MPS model of the human proximal tubule.

a) DesRochers et al. constructed a culture of immortalized human renal cortical epithelial cells (NKi-2) that were grown on Transwell permeable supports and embedded in an extracellular matrix consisting of a 50:50 mixture of rat tail collagen I and Matrigel to promote cell differentiation and *in vivo*-like phenotype (22, 26) Cells were in immediate contact with culture media from the top (insert) and bottom (well). After 2 weeks in culture, cells grew and organized into branching structures that resembled tubule formation; tubules were still observed at 8 weeks of culture. Cells in the model expressed E-Cadherin protein as a marker

of a polarized epithelial cell, as well as OAT4 transporter protein, and MRP2/4 mRNA. Importantly, expression of OAT1 transporter protein was restored compared to regular NKi-2 monolayer culture. A disadvantage of this model is poor accessibility to luminal fluid that prevents quantitative sampling when performing basolateral-to-apical (or bidirectional) transport assays. In addition, a relatively thick extracellular matrix hinders high-resolution imaging that allows for real-time assessments of drug intracellular accumulation (22).

b) Fukuda et al. used commercially available passaged human proximal tubule epithelial cells, and cultured them on a type 4 collagen-coated 6-channel microscopy slide that is suitable for flow experiments and perfusion assays. The flow of culture media was maintained via a peristaltic pump; flow enabled maintenance of fluid shear stress (FSS) on the apical side of cells equaling 0.5 dyne/cm^2 (which is close to *in vivo* 1 dyne/cm^2) (27). When comparing gene expression levels in cells cultured under static and fluidic conditions, a number of genes appeared to be FSS-responsive; notably, MATE2-K mRNA increased 5.3-fold in cells that were cultured under flow for 24 hours. This increase in MATE2-K mRNA was reversible, and resulted in an increase in MATE2-K transporter activity as measured by increased intracellular accumulation of DAPI, a transporter substrate. Furthermore, the findings pinpointed the expression of MATE2-K gene to be regulated by an Nrf2 signaling that becomes activated in response to FSS. This study demonstrated that a microfluidic culture of passaged human proximal tubule epithelial cells can be a good system for evaluating regulatory mechanisms of gene expression under continuous flow. However, lack of access to the basolateral side of cells prevents this model from being used for the assessment of vectorial transport of drugs, mimicking transfer of a compound from a blood capillary into the tubule lumen (28).

c) Jang et al. reported development of a “kidney-on-a-chip” constructed with commercially

available passaged human proximal tubule epithelial cells grown in a polydimethylsiloxane (PDMS) microfluidic device consisting of a luminal flow channel, and interstitial compartment. Specifically, cells were grown on a membrane separating the channel and interstitial (static) compartment. With this model, they studied the effects of fluid flow (and FSS with a value of 0.2 dyne/cm^2 as claimed to be operative *in vivo*) on the expression and activity of several renal proximal tubule proteins. They also conducted a comparative set of studies with cells grown in Transwell. Cells in the microfluidic model exhibited a much improved phenotype (increased height, increased number of primary cilia, enhanced expression of Na^+/K^+ ATPase and aquaporin 1) compared to 2-D culture. Notably, albumin uptake and glucose reabsorption were significantly increased, although the extent of the later process still remained much lower than that observed *in vivo.* Finally, increased P-gp activity determined via reduced intracellular accumulation of calcein was demonstrated under fluidic conditions. However, Jang et al. limited their studies to cells grown in culture for only 6 days. In addition, while the model is well posed to assess tubular handling of drugs on the apical side of the epithelium, it does not permit vectorial transport assays (29).

d) Jansen et al. reported findings of an established bioengineered kidney tubule consisting of conditionally immortalized human proximal tubule epithelial cells grown on a type 4 collagen and L-Dopa double-coated polyethersulfone hollow fiber membranes (HFM). Basolateral side of cells is attached to the outer layer of HFM, and continuous perfusion is applied through the fiber, allowing for basolateral delivery of drugs/compounds. Initially, the authors demonstrated measurable OCT-mediated transport via determining of ASP^+ (an organic cation) intracellular accumulation (25). Because OAT mRNA levels (and hence presumably OAT protein levels) were absent, human OAT1 and OAT3 gene constructs

were transfected into cells to allow for studies of organic anion transport. When compared to cells seeded in a Transwell device, OAT1 mRNA levels in cells cultured on HFM were significantly increased (app. 6-fold). Furthermore, the utility of the model was demonstrated by measuring the excretion of endogenous uremic solutes across the epithelium. One major limitation of this model appears to be high leakage of inulin (up to 10% of perfused input) demonstrating extensive passage of the compounds via the paracellular route.

In summary, reasonable progress has been made towards establishing a microphysiological model of human renal proximal tubule that would permit investigations of tubular secretion. At this point, one should ask what features an ideal *in vitro* model of human proximal tubule should possess. Based on the above-mentioned studies, an ideal model should:

- Allow for adherence of cells on an extracellular matrix that is non-rigid (ideally matrix that is native to human kidney) which promotes epithelial cell polarity and differentiation
- Allow for assembly of cells into tubule lumen, rather than "sheet" culture (i.e., tubulogenesis)
- Enable extended viability of cells so that immortalization of cells is not necessary
- Enable cells to maintain barrier characteristics, and at the same time express a whole complement of renal transporters present *in vivo*
- Offer culture of cells under continuous flow to support cell differentiation and function
- Possess two or three engineered compartments for estimation of tubular secretion: a basolateral compartment mimicking the blood capillary lumen and interstitium or separate vascular and interstitium compartments, and an apical compartment mimicking the tubule lumen; these compartments should allow for quantitative sampling that permit estimation

of clearance measurements that is theoretically scalable to the *in vivo* state

- Allow for high-resolution imaging that reveals handling of drugs and solutes in real-time, particularly intracellular accumulation
- Offer the possibility for integration of multiple cell types, i.e., epithelial cells, pericytes, and microvascular endothelial cells, in a spatial alignment that would fully reconstitute a tubulo-interstitial environment. Previously, cell-cell interactions have been demonstrated to improve overall functioning of cells cultured in microphysiological systems (30). It is reasonable to believe that a proximal tubule epithelial cell functioning *in vivo* is not only auto-regulated, but is subjected to remote signaling and other ways of cell-cell communications, which should also be recreated *in vitro*.

Along with studies to assess renal tubular secretion in a new drug development setting, the MPS model of a human proximal tubule might also prove useful for other applications. In particular, it could be applied to understand drug-drug interactions at the level of the human renal proximal tubule, and the effects of accumulating intracellularly endogenous inhibitors (uremic solutes) that are known to accumulate in chronic kidney disease (CKD). Thus, findings acquired with the MPS may ultimately provide important guidance for planning clinical drug-drug and renal impairment studies.

1.1.4 Modelling effects of CKD on renal tubular secretion

Chronic kidney disease (CKD) is a growing health and economic burden in the U.S. (31). Cardiovascular complications are common in advanced stages of CKD and are associated with excessive accumulation of endogenous waste products, a syndrome known as uremia that arises

from a decline in excretory function (32-34). The clearance of drugs predominantly removed by the kidney is also significantly hindered in CKD (35). To avoid drug accumulation and adverse reactions, the dosage of renally excreted drugs needs to be reduced in patients with CKD. Dose adjustment traditionally has been guided by the rise in serum creatinine concentration, a biomarker of deteriorating glomerular filtration (35, 36). Over the years, it has been assumed that during CKD, decline in the two main components of renal excretory function, glomerular filtration and proximal tubular secretion, occurs synchronously; i.e., serum creatinine is a biomarker for overall nephron function. Despite dosing adjustment based on creatinine measurements, adverse drug reactions due to unanticipated accumulation remain a problem in CKD (37). Some of the literature related to CKD suggests that serum creatinine has limited value in predicting the clearance of drugs that undergo extensive proximal tubule secretion (tenofovir for example (38)), implying that CKD may have differential effects on glomerular filtration and tubular secretion. Indeed, it has been proposed that uremic solutes that are known to accumulate in later stages of CKD have the potential to inhibit tubular secretion of drugs (39). This inhibition may impede the renal clearance of drugs beyond what one might expect from an estimate of residual intact nephrons based on estimated creatinine clearance, and hence explain systemic accumulation (and adverse effects) in CKD patients. This question has thus far not been answered systematically; at this point, it is unknown whether a decline in drug renal clearance of (particular) drugs truly does not follow a decline in estimated creatinine clearance in a parallel manner, and if so, how does tubular secretion deviate from filtration in CKD.

1.2 Research directions

The main objective of my thesis is to develop a microphysiological system model of the human proximal tubule that may offer the first, high fidelity *in vitro* system for in vitro-to-in vivo prediction of renal clearance of highly secreted drug substrates. This new proximal tubule MPS should also serve as the beginning step of modeling the effects of chronic kidney disease (CKD) on drug secretion by the human renal tubule. Below is a brief description of my thesis accomplishments in each of the following chapters.

Chapter 2, details a culturing protocol that maintained and expanded freshly isolated human proximal tubule epithelial cells over multiple passages. I characterized the barrier characteristics of cells grown on permeable supports, showed the expression of renal transporters via determining their mRNA and protein levels, and attempted to modulate mRNA expression of organic anion transporters (OATs). Finally, I optimized the experimental conditions for conducting OAT assays.

Chapter 3 described the development and characterization of human proximal tubule MPS model. I demonstrated that in the defined microenvironment, cells maintained the following salient morphological and physiological properties relevant to their *in vivo* function: (i) cell viability sustained for over 4 weeks; (ii) cell polarity demonstrated by differential expression of Na^+/K^+ ATPase and tight junction ZO-1; (iii) expression of typical proximal tubule markers; (iv) glucose reabsorption, glutathione re-uptake, and breakdown of glutamine under acidic pH; and (v) homeostatic regulation of Vitamin D metabolism.

In **Chapter 4**, I continued to refine the human proximal tubule MPS reported in Chapter 3. I described the successful development of a vascularized proximal tubule MPS model, and showed how this model recapitulates the requisite steps involved in proximal tubule secretion in

vivo, specifically free passage of solutes across the vascular endothelium into the interstitial matrix, and the tubular epithelium posing as a tight cell barrier for transcellular diffusion of solute into the tubule lumen. My results also demonstrate for the first time the possibility of constructing a rudimentary human renal tubule-interstitium-capillary network. Ultimately, we provide insights that inform the in vitro – in vivo scaling and physiological modelling of the secretory transport of a model solute — *p*-aminohippuric acid by the organic anion transport system.

Lastly, in **Chapter 5** I analyzed the available literature on the pharmacokinetics of drugs in renal impairment. We show that for select drugs, creatinine clearance (or other measures of glomerular filtration) does not accurately predict alterations in renal clearance across mild to severe stages of CKD. Our key finding is that in the case of drugs for which glomerular filtration measure fails to predict renal clearance well, proximal tubule secretion plays a dominant role in the overall renal clearance. This points to the need for better understanding of renal drug secretion in CKD.

The need for a predictive, in vitro human proximal tubule model has been repeatedly raised by clinical practitioners, regulatory agencies, and pharmaceutical industry. Nonetheless, this area of research has languished for the past decades due to the lack of technological advances or innovation. The proximal tubule MPS described in this thesis represents a fresh and innovative experimental paradigm that will allow unprecedented investigations into coordinated drug transport processes occurring in the proximal tubule epithelium, and eventually the impact of pathophysiology as a result of chronic diseases. I hope my work could ultimately lead to a more informed and sophisticated approach to drug dosing adjustment beyond the current creatinine-based methods; for example, the use of uremic solute biomarkers that pinpoints the ongoing interference of tubular drug transport function.

2 Conventional culture of passaged human proximal tubule epithelial cells on Transwell permeable supports: barrier characteristics, transporter expression, and secretory function

2.1 Abstract

In the following chapter, I show efforts to develop an *in vitro* model of cultured human proximal tubule epithelial cells that would permit investigation of the mechanism and kinetics of drug transport across the human proximal tubular epithelium. Specifically, I studied vectorial transport of organic anions in human proximal tubule epithelial cells cultured on permeable supports under static conditions. Results show that cultured human proximal tubule epithelial cells maintain the polarity, barrier integrity, transporter expression and activity that are required for further investigation of the underlying mechanisms of coordinated basolateral-to-apical (i.e., secretory) transport of drug/solute across the proximal tubule epithelium.

2.2 Introduction

In vitro culture of primary proximal tubule epithelial cells (PTECs) sourced from human tissue is challenging. Often, lack of tissue supply and limited viability of cells in culture prevent their extensive use. Despite these shortcomings, much effort has been directed over the years toward establishing a competent *in vitro* model of human proximal tubular epithelium that recapitulates key structural features and physiological functions, including tubular drug/solute secretion. Until recently, investigations were performed with PTECs grown on cell culture plates (40-42) or permeable supports. The latter format enables studies of PTECs' barrier permeability, which have reported variable trans-epithelial electrical resistance (TEER) values, ranging from as low as 20 Ω*cm^2 to as high as 500-600 Ω*cm^2 (15, 18, 23, 26). Interestingly, *in vivo* proximal tubule epithelium has consistently been labelled as a "leaky" epithelium; proximal convoluted tubule has been said to exhibit almost no electrical resistance, while proximal straight tubule (where the secretion of most drugs and solutes occur) exhibits resistance to some extent (43). Hence, heterogeneity of the isolated proximal tubule cell populations may explain the phenotype variability observed *in vitro.* In addition, variable cell culture conditions between different research laboratories can also significantly affect barrier integrity (44).

Culturing of PTECs on permeable inserts has been shown to maintain epithelial cell differentiation and polarization. Using transmission electron microscopy, several groups have demonstrated essential features of a functioning proximal tubule epithelium, including presence of tight junction proteins on the border between apical and lateral cell membrane, microvilli on the apical membrane, basolateral infoldings, cuboidal or columnar cell shape, and high density of mitochondria (26, 40, 42, 45). On the other hand, some investigators have shown increased levels of α-smooth muscle actin and loss of E-Cadherin, indicating that PTECs in culture

undergo epithelial-mesenchymal transition and lose their epithelial phenotype over time (46). A complex interplay between differentiation and de-differentiation processes may thus be occurring in culture, and it is not clear to what extent this affects the secretory function of proximal tubule epithelial cells.

In vivo, PTECs maintain expression of transporter proteins critical in vectorial transport of drug / solutes (47, 48). Because species-differences in transporter type and polarized localization have been reported, it is assumed that the use of human PTECs would yield more accurate *in vitro* parameters and better predict *in vivo* drug secretory clearance (49-51). At present, mRNA levels of all drug transporters shown in Figure 1.1 (Introduction chapter) have been confirmed in freshly isolated human PTECs. Over time in culture, mRNA levels were shown to decrease (24). Notably, non-detectable OAT1/2/3 transporter mRNA has repeatedly been reported in cultured PTECs (23, 52). At the protein level, expression of transporters has been confirmed by immunocytochemistry and Western blotting in freshly isolated cells and after being in culture up to 2 weeks post-isolation (14, 15). The expression of a few transporter proteins has also been shown in immortalized cell lines, although no systematic analysis has been conducted (22). It is thus not known if and to what extent observed decreases in mRNA levels translate into reduction of protein levels in cultured PTECs.

Until now, freshly isolated human PTECs (grown for up to 2 weeks in culture) gained the most attention as an *in vitro* renal secretory model of organic anion transport. In this model, *p*-aminohippurate (PAH) permeability (P_{app}) in the basolateral-to-apical direction was estimated to be approximately 1.5×10^{-5} cm/s. PAH permeability was significantly reduced in the presence of probenecid (OAT and MRP inhibition), MK-571 (MRP inhibition), cimetidine (OAT inhibition) and estrone-3-sulfate (OAT3 inhibition). It is important to note that PAH transport characteristics

in cultured PTECs have not been consistently demonstrated; in one study, 50 μM PAH transport was inhibited only by 15% in the presence of 500 μM probenecid (14), while in another 10 μM PAH transport was inhibited by as much as 80% in the presence of 10 μM probenecid (15). This suggests that while freshly isolated PTECs maintain measurable organic anion transport function, factor(s) that are presently unknown may affect transporter expression activities in the epithelial monolayer *in vitro*.

Due to the disappearance of OAT mRNA over time, a longer-term culture of human PTECs spanning multiple passages has thus far been considered inappropriate for the investigation of organic anion transport (53). In an attempt to restore the OAT mRNA levels, Masereeuw et al. have recently transfected an immortalized PTEC cell line (ciPTEC) with OAT1 and OAT3 gene constructs (54). After successful transfection, cells were grown in monolayers and inhibition kinetics of organic anion uptake into cells was determined. Generated IC_{50} values were very similar to previously reported IC_{50} values from single transporter over-expressing cell systems. However, these constructed models have an artificially altered transporter expression ratio and would be expected to have altered coordination between the overexpressed basolateral (OAT) transporters and the comparatively low, endogenously expressed, apical (MRP) transporters.

In summary, current *in vitro* models of human PTECs pose challenges that are inherently related to the cell phenotypic origin and *in vitro* culture conditions. In the work reported in this chapter, we endeavored to: (i) develop a culturing protocol that would enable us to successfully maintain and expand human PTECs through subcultures or passaging; (ii) determine mRNA expression of drug transporters in cultured PTECs over time and explore ways to upregulate their mRNA expression; (iii) determine the protein expression of transporters involved in organic

anion transport by mass-spectrometry based proteomics; and (iv) establish optimal experimental conditions for conducting Organic Anion Transporter (OAT) activity assays. Collectively, these methodological studies have enabled us to improve the yield and quality of human PTECs derived from human kidney surgical wastes and biopsies in support of the drug transport permeability studies with the vascularized proximal tubule MPS described in the chapter 4.

2.3 Materials and methods

2.3.1 Chemicals and reagents

Fluorescein isothiocyanate (FITC)-dextran (average MW 10 kDa), bovine serum albumin, hydrocortisone, Triton X-100 and probenecid were purchased from Sigma-Aldrich (St. Louis, MO). D-Sucrose was obtained from Fisher Scientific (Itasca, IL). 16% Formaldehyde (methanol free) was purchased from Polysciences (Warrington, PA). ^{14}C-PAH (40.2 mCi/mmol) was obtained from Perkin Elmer (Waltham, MA). Phosphate-buffered saline with or without calcium and magnesium (PBS+/+ or PBS-/-), Hanks balanced salt solution with calcium and magnesium (HBSS+/+), 50:50 Dulbecco's modified eagle medium with Ham's F-12 (DMEM/F12), penicillin-streptomycin-amphotericin B, insulin-transferrin-selenium A solution (ITS-A), fetal bovine serum (FBS), 0.05% Trypsin EDTA, ProLong Gold Antifade reagent with 4',6-diamidino-2-phenylindole (DAPI), TRIzol and Taqman gene primers were purchased from Thermo-Fisher (Waltham, MA).

Alexa Fluor 594 conjugated donkey anti-rabbit IgG, Alexa Fluor 594 conjugated donkey anti-mouse IgG, Alexa Fluor 488 conjugated donkey anti-mouse IgG, Alexa Fluor 488 conjugated donkey anti-rabbit IgG, Alexa Fluor 488 conjugated donkey anti-rat IgG, rabbit OAT3, mouse MRP2, mouse Na^+/K+ ATPase were obtained from Abcam (Cambridge, MA);

rabbit OAT1, rabbit villin were obtained from Fisher Scientific (Pittsburgh, PA). Rat MRP4 was obtained from Enzo (Farmingdale, NY). Mouse collagen IV, 6-well and 12-well tissue culture plates, 24-well Transwell^{TM} plates with accompanying transparent and translucent permeable supports (0.4 µm pore size) were obtained from Corning (Corning, NY).

2.3.2 Human proximal tubule epithelial cell isolation and culturing

Human PTECs were isolated from human cortical tissues obtained during kidney surgery as reported in our recent publication (55) and Chapter 3. The use of human tissue was approved by the University of Washington Institutional Review Board (# STUDY00001297). Cells were isolated from cortical tissues within 24 hours post-surgery. In brief, the renal cortical tissue (approximate size 0.3 cm^3) was manually diced and then incubated in 1mg/mL solution of collagenase type IV for 30 min in an incubator-shaker (37°C, 250 rpm). Collagenase activity was stopped with the addition of horse serum. Supernatant (containing cells) underwent centrifugation, followed by a wash with culture media. Cell pellet was resuspended and plated in tissue culture flasks. Cells were allowed to attach overnight, and media was replaced the next day to remove glomeruli, red blood cells and other, non-surface attached cells. Cells were cultured in a hormonally defined, serum-free DMEM/F-12 media containing hydrocortisone (50 nM), antibiotic-antimycotic (1% v/v), and insulin-transferrin-selenium (1% v/v). Absence of serum in media prevented growth of fibroblasts or other cell types requiring serum during cell culture. Cells were grown until confluency (p0) and then cryopreserved (in a cell freezing medium containing 10% FBS and 10% DMSO). Following a thaw, cells were expanded in tissue culture flasks (coated with collagen IV at 5 µg/mL) to passages 1-3 before use in experiments. Cells were split in a 1:2 ratio, with approximate population doubling time of 7 days. Cell

splitting required a double PBS -/- wash, followed by a 2-3 min exposure to 0.05% trypsin treatment that was quenched with culture media containing 10% fetal bovine serum (FBS).

2.3.3 Cell culture and characterization on permeable supports

Permeable supports were first coated with extracellular matrix for 60 min and then washed with PBS -/-; collagen IV at a concentration of 5 µg/mL (equivalent to 1 µg/cm^2) was routinely used. Cells were then seeded on permeable supports at a desired density (no. of cells/mL media). Cells were allowed to attach for 3-5 hours, and then media was replaced. Subsequent media changes occurred daily. When required, cells were also washed with HBSS+/+ to prevent accumulation of cell debris on the surface of monolayer. Confluency of the monolayer was assessed every 2 days via bright field imaging of cells on a Nikon Ti fluorescent microscope. Cell polarity and membrane orientation (i.e., basal membrane attaching the insert support, and apical membrane facing the culture medium in the insert) was determined by immunocytochemistry and imaging on a Nikon A1 confocal microscope. Barrier integrity of the cell monolayer was assessed by measuring trans-epithelial electrical resistance (TEER) using a Millicell ERS electrode that was equilibrated in a pre-warmed culture medium. Measured TEER was subtracted from TEER acquired on a blank insert (background), and the value was multiplied by the surface area of the insert (0.33 cm^2) to get a final TEER estimate.

2.3.4 Drug permeability assays

Prior to conduct of activity assays, TEER values of inserts were measured; inserts with approximate (and pair-matched) value of 200 Ω*cm^2 were used for the subsequent experiments. Activity assays were conducted in the following manner. Inserts were first washed with a defined transport solution that was pre-warmed at 37°C; 700 µL of test solute solution (containing 5 µM PAH in the presence or absence of 150 µM probenecid, or 0.1 mg/mL FITC-Dextran) was then

added into the basolateral compartment (well), and 300 µL was added into the apical compartment (insert). Experiment was performed at 37°C and 5% CO_2 (in a tissue culture incubator). Every 10 minutes, the plate containing inserts was gently shaken (to minimize the unstirred water layer). A 30 µL sample was taken from the apical compartment at 30 and 60 minutes post-initiation of experiment, respectively, and replaced with 30 µL of blank transport solution (the transfer rate of compound was pre-determined to be in the linear range for up to 120 minutes, data not shown). Determination of apparent permeability coefficient (P_{app}) was done via the following equation:

$$P_{app} = \frac{dA/dt}{C_0 * SA}$$

Where *dA/dt* represents the rate of a solute transfer from the basolateral into apical compartment under sink conditions (30-60 min), *SA* is the surface area of the permeable support (cm^2), and C_0 is the initial concentration in the basolateral compartment.

2.3.5 RNA isolation and RT-PCR analysis

Cortical tissue chunks (approximate size of 20 mm^3) were collected into Eppendorf tubes and 0.5 mL of Trizol solution was added. Then, the chunks were mashed and suspension was immediately stored at -80°C. For the assessment of the effects of potential mRNA modulators, cells were seeded on tissue culture wells or tissue culture flasks. Media containing the modulator was replaced daily in order to prevent the degradation and reduction of modulator concentration, resulting in decreased modulator exposure to cells. After treatment was complete (48 hours), cells were collected in 0.5 mL of Trizol and immediately stored at -80°C. Total RNA from collected samples was isolated according to the manufacturer protocol for Trizol reagent. Then, RNA pellet was dissolved in nuclease-free water and the concentration was determined using a Nanodrop spectrophotometer ND-2000 (Thermo Fisher). Reverse transcription of RNA into

cDNA was conducted according to the manufacturer's instructions for the high-capacity cDNA reverse transcription kit. Real-time polymerase chain reactions (RT-PCR) were conducted using TaqMan gene expression primers for the following genes: OAT1/2/3, OCT2, MRP2/4, P-gp, BCRP, MATE1/2K. Calcitriol (at 500 nM concentration) effects on the CYP24A1 gene was routinely used as a positive control. The ΔCt method, using glyceraldehyde 3-phosphate dehydrogenase (GAPDH) as a housekeeping gene, was used to quantify relative amounts of mRNA in all samples.

2.3.6 Immunocytochemistry of proximal tubule epithelial cells

Human proximal tubule epithelial cells were grown on transparent permeable supports. On day 7, cells were fixed with 4% formaldehyde solution (containing 2% sucrose) for 10 minutes. This step was followed by incubation with 50 mM NH_4Cl for 30 minutes (for neutralization of formaldehyde). If heat-mediated antigen retrieval was required for a specific antibody, then cells (fixed on inserts) were incubated in a solution of 0.05% Tween-20 in 10 mM sodium citrate buffer (pH = 6) for 20 minutes at 100°C. Afterwards cells were cooled to room temperature, and the blocking step was performed with a solution of 0.1% Triton X-100 and 5% bovine serum albumin in PBS+/+ (PTB) for 30 minutes. Primary antibodies, diluted in PTB, were then introduced into the inserts at the following concentration: rabbit villin 1:100, rabbit OAT1 1:20, rabbit OAT3 1:100, rabbit ZO-1 1:100, mouse Na^+/K^+ ATPase 1:100, mouse MRP2 1:50, rat MRP4 1:50. Following a wash with PBS+/+, secondary antibodies, diluted 1:1000 in PTB, were added. The cells were again washed with PBS+/+ and then lastly exposed to DAPI (1:4 dilution in PBS+/+) for staining cell nuclei. Negative controls represented samples that were not incubated with primary antibodies. Finally, samples were imaged on Nikon Ti (regular

fluorescent) or Nikon A1 confocal microscope and images were processed with NIS Elements BR 4.10.01 software.

2.3.7 Transporter proteomics

Cells were grown in tissue culture flasks or plates. Prior to detachment, an approximate cell number was estimated based on the cell coverage of the culture surface. Culture media was removed and cells were washed twice with PBS -/-. Two mL volume of PBS -/- was then added and cells were scrapped from the surface. The suspension was collected and centrifuged at 4000 *g* for 10 minutes. PBS -/- was aspirated and cell pellet was stored at -80°C. Quantitation of transporter proteins in samples was conducted in a similar manner as previously reported for fresh cortical tissues (48). In brief, samples underwent total membrane isolation, followed by the quantification of total membrane proteins with the BCA assay. Total membrane proteins were then reduced, denatured, alkylated, and digested as previously described (48). Surrogate peptides for transporters and proximal tubule markers were selected, and final quantitation was conducted by LC-MS/MS.

2.3.8 Statistical analysis

Data are presented as mean ± SD. Technical replicates (n=4) were routinely conducted in all experiments. Whenever possible, cells originating from multiple donors (up to 3) were used. All analyses and data presentation were performed using GraphPad Prism version 7.0.

2.4 Results

2.4.1 Barrier properties of human proximal tubule cell monolayer grown on permeable supports

First, we investigated the effects of the cell seeding density on the establishment of a PTEC barrier as determined by trans-epithelial electrical resistance (TEER). Typically, researchers seed a reasonably low number of cells on one insert (i.e., 50,000 cells on an insert with surface area of 0.33 cm^2) and allow cells to populate the insert with time (10). In some circumstance, a sufficient number of cells is seeded to completely cover an insert (56). As shown in Figure 2.1A, TEER values slowly increased with time and reached a peak on days 6-7. TEER value clearly depended on seeding densities, suggesting that, a higher number of passaged PTECs cells is needed to establish a competent barrier, as compared to most continuous cell lines (10). Another factor that was shown to affect TEER value is the type of extracellular matrix protein coating (collagen IV versus collagen I) on the insert prior to cell seeding. As shown in Figure 2.1B, cells grown on inserts that were coated with collagen IV (1 $\mu g/cm^2$) displayed significantly higher TEER value than cells that were grown on non-coated inserts. Finally, through daily inspection of the cell monolayer under a microscope we found that cells were prone to detachment during vacuum suctioning with a Pasteur pipette in replacing the culture media. We modified our practice by carefully replacing culture media with a single channel pipette, which eliminated the problem and yielded the highest reported TEER values, approximately 200 $\Omega*cm^2$ between days 6 through 10 post-seeding (Figure 2.2).

2.4.2 Characteristics of human proximal tubule cell monolayer grown on permeable supports

Human proximal tubule cells formed a monolayer with a cobblestone appearance; this morphology has previously been reported for several types of cell monolayers of barrier epithelia (42). Dome formation was also observed, although it appeared to be dependent on several factors: (i) cell source (donor), (ii) number of passages the cells have undergone, and (iii) profound ability of cells to lay down extracellular matrix. Formation of domes was also observed if cells were exposed to Matrigel (0.25 mg/mL) overnight, irrespective of the passage number and/or source. At 7 days post-seeding, cell grown on inserts repeatedly exhibited excellent cell viability, with minimal cell death. Cells also polarized, as shown by selective localization of Na^+/K^+ ATPase to the cell basolateral side and ZO-1 to the border between cell apical and lateral side (Figure 2.3).

2.4.3 Transporter mRNA expression

In fresh cortical tissues, mRNA was measurable for the entire panel of renal tubular transporters, including organic anion transporters (OAT1-3), organic cation transporter (OCT2), ATP Binding Cassette proteins (MRP2/4, P-glycoprotein and Breast Cancer Resistance Protein), and Multidrug and Toxic Compound Extrusion (MATE) transporters (Figure 2.4). Following prolonged culturing (2-3 weeks), there was a general decline in transporter mRNA expression. In particular, mRNA levels of OAT1/2/3 were absent in cultured PTECs from all donors.
Given the importance of OAT-mediated transport for our future tubular secretion studies with organic anions, we attempted to restore or boost the mRNA levels of these transporters in human PTEC cultures by investigating: (i) typical transcriptional activators of enzymes and transporters involved in drug disposition; (ii) modulators that would specifically target transcription sites of

OAT genes, and/or have previously been shown to regulate OAT mRNA levels; (iii) compounds that would circumstantially affect OAT mRNA levels. A detailed list of compounds and their tested concentrations is presented in Table 2.1. Unfortunately, none of the experiments with the above list of modulators yielded any positive findings.

2.4.4 Determination of transporter protein levels

Proteomic quantitation of drug transporters in fresh human renal cortical tissues has previously been reported by our research group (48). Accordingly, our present goal was to determine transporter protein levels in passaged human PTECs. Preliminary quantitation using mass spectrometry based proteomic analyses showed measurable expression for some, but not all, transporter proteins in PTECs (Table 2.2).

Measurable levels of OAT3 protein were found, despite the confirmed loss of OAT3 mRNA. MRP protein levels on the other hand were not detectable; this apparent loss can be explained by: (i) lower number of proximal tubule cells in a culture collection than in fresh cortical tissue sample; (ii) already low levels of these proteins in fresh cortical tissues that were close to the limit of the LC-MS/MS assay quantitation (48). Our minimum goal was to assess presence or absence of transporters OAT and MRP transporters; hence, we tried the alternative qualitative technique of immunocytochemistry that in some cases could be more sensitive than quantitative proteomics. Indeed, all transporters relevant in the tubular secretion of organic anions (OAT1/3 and MRP2/4) were shown to be expressed in passaged human PTECs (Figure 2.5).

2.4.5 Optimization of organic anion transport assays

First, we determined the most optimal transport media for conduct of the transporter activity assays by measuring PAH permeability in different culture media and buffers. Since

there is general concern that regular culture media may contain substrates of transporters which can interfere with the activity assays. In particular, we were concerned with OAT3 substrate penicillin G at 100 units/mL and OAT substrate phenol red at 21.5 uM. We compared PAH permeability measurements between regular culture medium and culture media without these respective compounds. In addition, PAH permeability in 3 different types of buffers was also assessed. As seen in Figure 2.6, PAH permeability did not differ significantly among the three culture medias tested, indicating that presence of penicillin G and phenol red at their specified levels is not a concern. More importantly, HBSS +/+ buffer appeared to be the most optimal transport medium, i.e., with the highest PAH P_{app} ($1.08 \pm 0.49 \times 10^{-5}$ cm/s).

In order to assess paracellular solute passage across PTEC monolayer, we considered the use of FITC-Dextran (MW≈10 kDa). The observed P_{app} value (from basolateral to apical side) for FITC-Dextran was $6.10 \pm 7.45 \times 10^{-7}$ cm/s (Figure 2.7). Thus, in the current model, PAH P_{app} value is 17.7-fold greater than that of FITC-Dextran, and is comparable to the previously reported values in freshly isolated primary PTECs ($P_{app} \approx 1.5 \times 10^{-5}$ cm/s) (15).

Initial experiments with PAH as a model organic anion solute, and probenecid as a typical OAT and MRP inhibitor yielded no success. Paradoxically, PAH flux or permeability increased in the presence of 200 µM or 2 mM probenecid relative to that of PAH only control group (data not shown). Although similar surprising results have been previously reported in a clinical study investigating benzylpenicillin as a biomarker of tubular secretion function, they could not be explained mechanistically (57). One potential explanation that we considered was the confounding effect of [Na^+] present in the commercial supply of probenecid in the form of sodium salt. The increased concentrations of [Na^+] co-administered with probenecid may have affected the activity of Na^+/K^+ ATPase, which may in turn affect the activity of OAT

transporters, thereby resulting in an apparent increase in PAH permeability; i.e., masking the presumed inhibition of PAH transport by probenecid. In order to eliminate such an artifact, we switch to using probenecid in its free acid format final concentration of 150 µM. We then observed the expected reduction in PAH permeability, by an average of 61% (Figure 2.7). Had our transport media contained serum or purified albumin, this approach would likely not be necessary, since probenecid binds extensively to plasma proteins – f_U in plasma is 0.1 (58).

2.5 Discussion

In this chapter, we presented significant progress in optimizing the culturing of passaged human PTECs on Transwell permeable supports for secretory transport studies. Freshly isolated human PTECs have been used in the quantitative assessments of tubular secretion (15). For many investigators, it is not feasible to work with such a model, since the cell source is not readily available. We successfully expanded human PTECs prior to insert seeding (up to passage 4); typically, 1 million PTECs are isolated and harvested from fresh cortical tissues and could be expanded to 8 million (which represented a sufficient number of cells for one assay). This increase in cell supply may help to overcome cell resource limitation and widen the use of PTECs in culture models.

In contrast to general thinking, we have shown that human PTECs maintain their apical-basolateral polarity when passaged and grown on permeable supports (Figure 2.3). Just as important, we have also shown that the cells retain their barrier function; in particular, they exhibit a reasonably high TEER values after 6 days in culture. In our experience, the barrier formation was highly dependent on seeding enough cells to cover the permeable support and achieve confluency. At times, TEER was reported to be as high as 600 $\Omega*cm^2$; inserts with such

high TEER values had visible cell clustering to form bilayers. Passaged human PTECs grown on permeable supports should be monitored regularly inspected under the light microscope in order to assure that only PTEC monolayers showing cobblestone appearance, and with TEER values near 200 Ω*cm^2 are used in transport studies.

Disappearance of mRNA of OAT transporters in proximal tubule cells or derived cell lines has previously been reported in the literature (23, 52). Thus far, an explanation for this phenomenon has not been reported. We attempted to restore OAT mRNA levels using agents that previously have been reported to regulate OAT transcription pathways, with the assumption that a single missing variable (modulator, or stressor) is the cause for decreased mRNA expression. At this time, we believe the loss of OAT mRNA is a part of a much more complex process, potentially also involving other PTEC gene transcriptional pathways. In the future, we propose that a more comprehensive approach be taken – e.g., by comparing RNA sequencing (RNAseq) or microarray data between PTECs that have not yet been plated for *in vitro* culture and cells that have been passaged and cultured *in vitro.* Then, the clustering of all PTEC genes that are either reduced or not reduced can be determined. Despite the loss of mRNA for some transporters, we have successfully determined the presence of these same transporter proteins using LC-MS/MS proteomics and immunocytochemistry. As expected, these transporter proteins have longer turnover $t_{1/2}$ than mRNA and have thus "persisted" longer in *in vitro* culture of passaged PTECs (for up to p#5 for cells from certain tissue donors). Thus, passaged human PTECs still show expression of transporters relevant for vectorial transport of organic anions, which makes them a viable *in vitro* model, a potential tool for investigating underlying mechanisms proximal tubular secretion.

Besides tackling the limitation of cell culturing, we believe additional characteristics unique to human PTECs should be considered in future drug transport studies. For instance, the physiological role of human proximal tubule epithelium is to maintain endogenous solute (e.g., Na^+, H^+, HCO_3^-, phosphate, glucose, water) homeostasis. All afore-mentioned ion transport processes are tightly regulated, and intimately inter-connected. It is known that such drug or xenobiotic transport is coupled to or regulated by endogenous ion transport. As an example, the activity of OAT transporters has previously been shown to be Na^+-dependent. Just as important, the activity of MATE transporters is dependent on luminal pH or H^+ gradient. As a result, the choice of cell culture media and its electrolyte composition may be critical in determining the basal activities of transporters, and the functioning of a human proximal tubule epithelial cell as whole. In my opinion, it is not surprising to see highly variable drug transport permeability data in the literature, as nearly each research laboratory adopts its own culture media and culturing protocols that may specifically affect the functioning of these cells. Systematic and careful studies to identify the most optimal composition of cell culture media for permeability studies with human PTECs and recommendations for a standardized culturing protocol across laboratories would thus be a welcome addition to the scientific literature.

In summary, we provide fresh insights into the isolation, propagation and culturing of human proximal tubule epithelial cells for *in vitro* studies of renal tubular drug transport. Optimization of cell culture techniques geared specifically for culturing of passaged human PTECs should lay the foundation for more robust and reproducible experiments on the regulation of drug transport permeability across the human proximal tubule epithelial cell barrier, including the detail steps of basolateral uptake from the interstitium, intracellular processing, and apical efflux into the tubular lumen.

2.6 Figures

Figure 2.1. Measurements of trans-epithelial electrical resistance (TEER) of PTECs grown on permeable supports.

Dependence of TEER values on the cell seeding density (A) and extracellular matrix coating (B) for human PTECs grown on permeable supports. Data are shown as mean ± S.D. (n=4 technical replicates using cells isolated from a single donor).

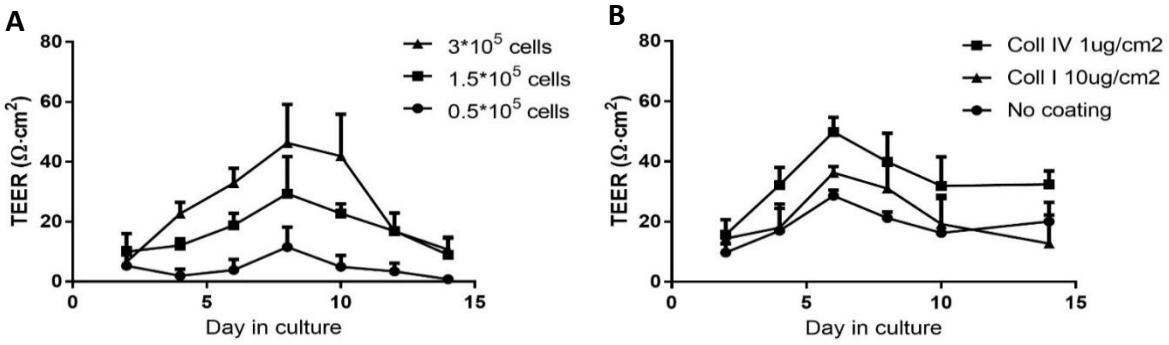

Figure 2.2. Measurements of TEER following optimization of culture of PTECs grown on permeable supports.

Trans-epithelial electrical resistance values when cell seeding density is 1.5 x 10^5 cells/insert, inserts are pre-coated with collagen IV, and media is removed with a single-channel pipette. Data are shown as mean ± S.D. (n=4 technical replicates using cells isolated from a single donor).

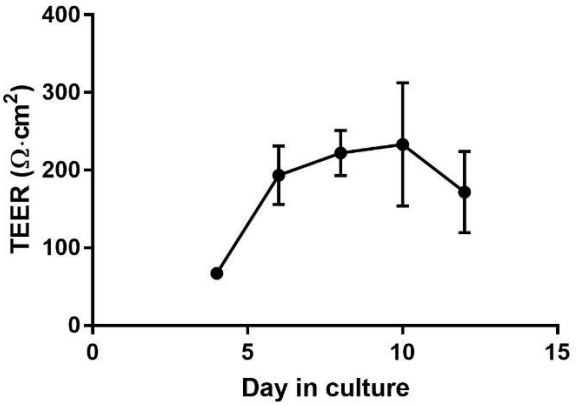

Figure 2.3. Morphology and polarity of human PTECs.

(A) Cobblestone appearance of monolayers of passaged human PTECs grown on permeable supports. (B) Presence of domes on a monolayer (arrows). (C) Live (green) and dead (red) staining denotes excellent cell viability. (D) Human PTECs polarize on permeable supports as shown with Na+/K+ ATPase (green) and ZO-1 (red). (E) Human PTECs forming domes also polarize as shown with Na+/K+ ATPase (green) and villin (red). (F) A cross-section of a dome. Magnification: 40x (A,B,C), 600x (D) and 400x (E and F). Representative images of cells isolated from a single donor.

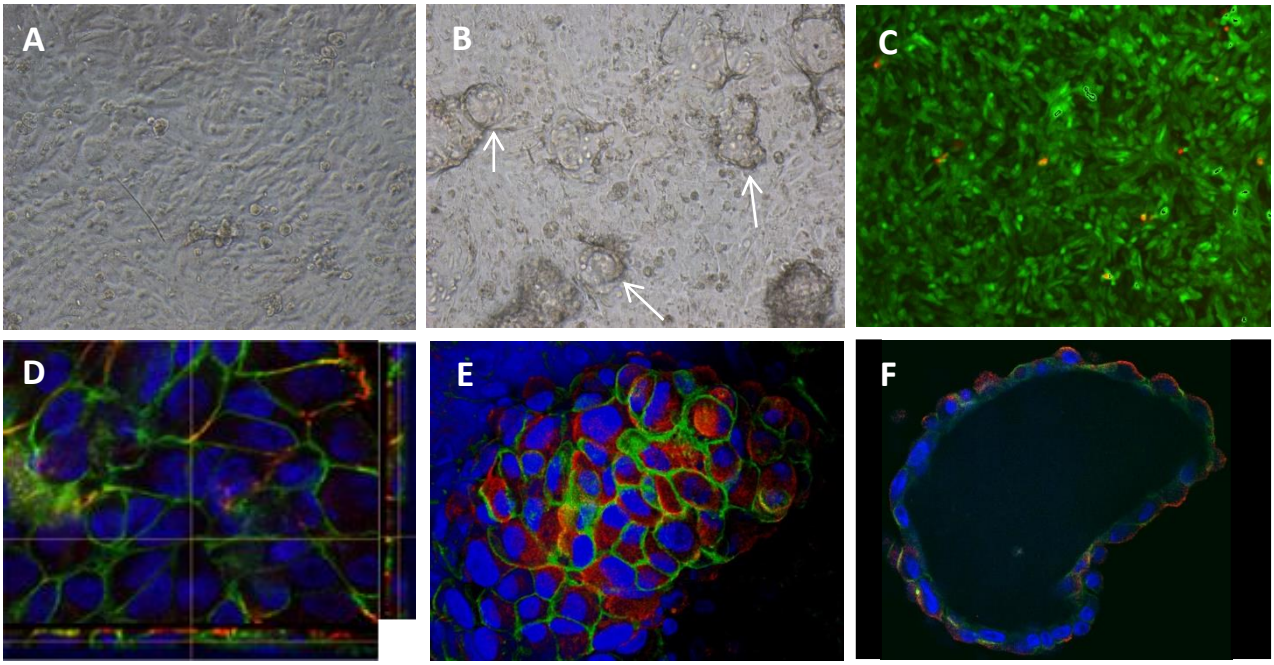

Figure 2.4. mRNA transporter expression in fresh cortical tissues and in cultured human PTECs.

(A) mRNA expression of transporters in cortical tissues (n=3 donors). One sample had no OAT3 transcripts detected. (B) mRNA expression of transporters in cultured cells (n=3 donors). OAT1/2/3 transcripts were not detected, P-gp transcript was detected in 2 donors, and BCRP, MATE1/2K transcripts were detected in 1 donor. A.U., arbitrary units.

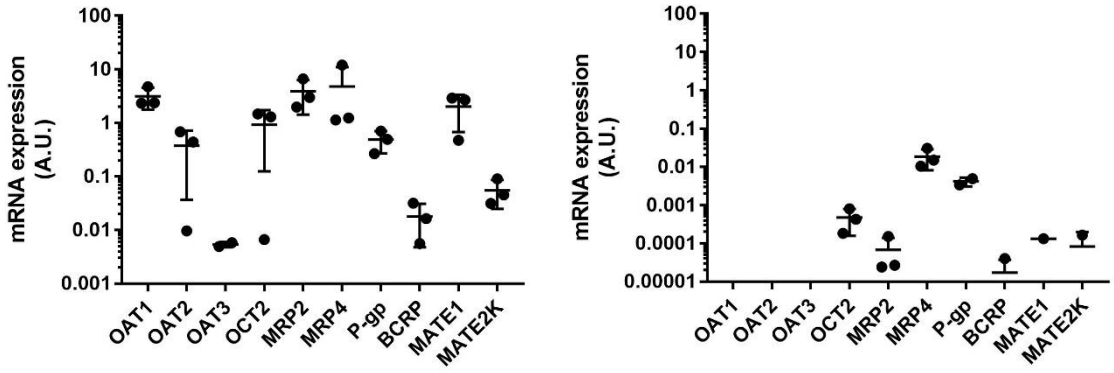

Table 2.1. List of compounds that were investigated for their potential to restore or boost OAT mRNA levels in cultured human PTECs.

Modulator	Concentration(s)	Rationale for testing and references
All trans retinoic acid	1 µM	Regulator of enzyme expression via RXR, regulator of OAT mRNA *in vivo* in choroid plexus (personal communication)
Calcitriol	500 nM	Regulator of enzyme (CYP 450) and transporter (intestinal MRP2) expression via VDR (59, 60)
Dexamethasone	50, 100, 500 nM	Regularly used in induction and maintenance culture medium for hepatocytes; promotes differentiation, suppresses proliferation; shown to stimulate PAH transport *in vivo* (61)
Na butyrate	1, 5, 10 mM	Histone deacetylase (HDAC) inhibitor, frequently used to increase transporter expression in singly-transfected over-expressing cell lines (56)
5-Aza-2'-deoxycytidine	100 µM	Inhibitor of DNA methylation, shown to restore OAT3 mRNA in Caco-2 cell line (62)
FBS	2%, 10% (V/V)	Common supplement (up to 10% V/V) in culture medium for proximal tubule epithelial cells (15)
Triiodothyronine (T_3)	4 pg/mL	Common supplement in culture medium for proximal tubule epithelial cells; stimulates cellular metabolism; OAT1 gene transcription site contains T_3 binding region; shown to stimulate PAH transport *in vivo* (61)
Epidermal growth factor (EGF)	10 ng/mL	Common supplement in culture medium for proximal tubule epithelial cells, affects growth, proliferation, differentiation (63)
Linoleic acid	20 µM, 250 µM	Endogenous ligand for HNF-4α gene (64); increased mRNA HNF-4α levels are associated with increased levels for OAT1 mRNA
Berberine	10 µM	Exogenous ligand for HNF-4α gene (65); increased mRNA HNF-4α levels are associated with increased levels for OAT1 mRNA

Table 2.2. Transporter protein expression as determined via quantitative LC-MS/MS proteomics.

Values represent peak areas. Values <100 are not detectable (ND). Na^+/K^+ ATPase was used as cell membrane marker and dicarbonyl/L-xylulose reductase was used as a proximal tubule marker to verify the proximal tubule origin of cells. OCT2 transporter expression was not measured in one sample.

Donor	Passage	App. no. of cells / sample	Day in culture	Na^+/K^+ ATPase	Proximal tubule marker	OAT1	OAT3	OCT2	P-gp	SGLT2
Donor 1	P3	100,000	5	2196	1210	ND	ND	281	96	ND
Donor 2	P5	100,000	5	2243	672	ND	106		243	ND
Donor 2	P5	200,000	30	11773	5459	ND	977	1486	600	559

Figure 2.5. Cultured PTECs express OAT1/3 and MRP2/4 transporters for up to 7 days in culture as shown by immunocytochemistry.

Addition of blank serum instead of primary antibody did not result in fluorescence for any of the tested transporters. Representative images of cells isolated from a single donor. 200x magnification.

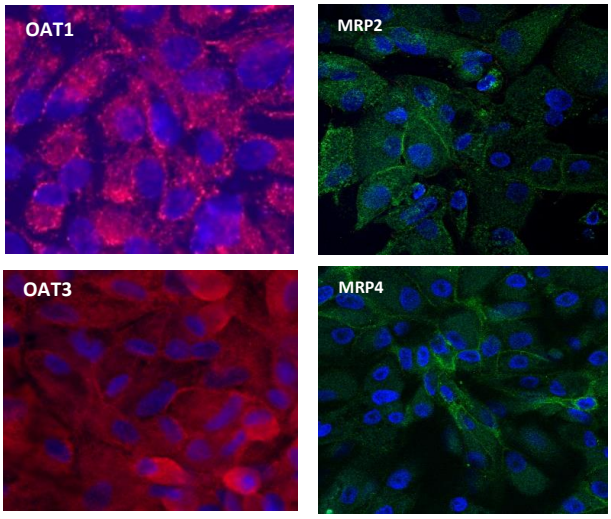

Figure 2.6. Determination of the most optimal transport solution for conducting activity assays.

(A) PAH P_{app} in different culture medias. (B) PAH P_{app} in different buffers relative to that of regular culture media. Data are shown as mean ± S.D. (n=4 technical replicates using cells isolated from a single donor).

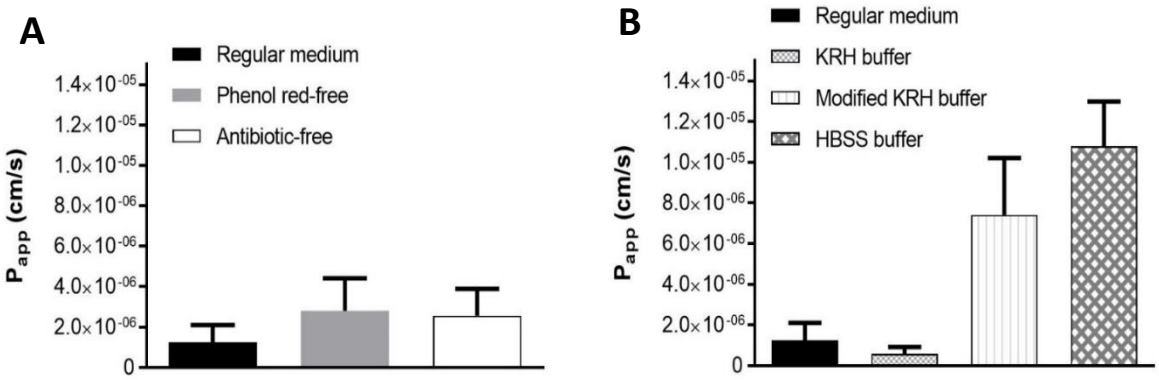

Figure 2.7. Apparent permeability measurements of PAH and FITC-Dextran.

(A) P_{app} of 5 μM PAH and 0.1 mg/ml FITC-Dextran. (B) Percent (%) inhibition of PAH P_{app} by probenecid (OAT and MRP inhibitor). All assays were conducted in inserts with TEER values exceeding 130 Ω*cm^2 that were pair-matched. HBSS (+/+) was used as a transport buffer. Data are shown as mean ± S.D. (n=4 technical replicates using cells isolated from a single donor).

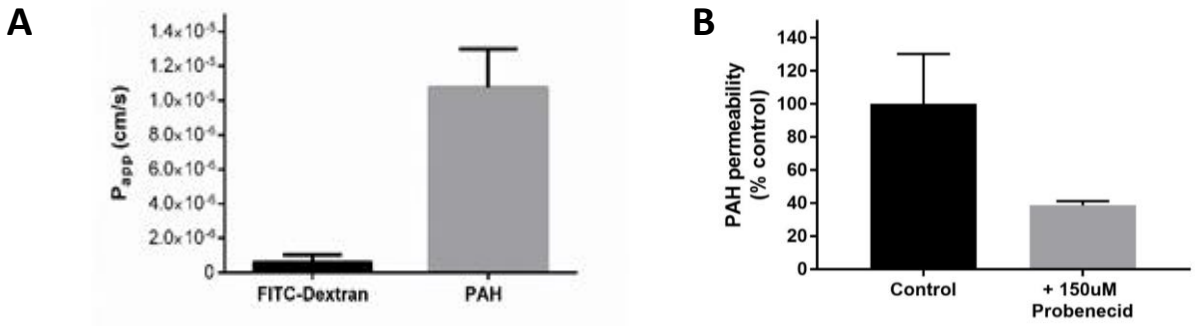

3 Development of a Microphysiological Model of Human Kidney Proximal Tubule Function

This chapter was published in its entirety in Kidney Int. 2016 Sep;90(3):627-37. Co-first-authorship was shared with Brian Chapron and Elijah Weber.

3.1 Abstract

The kidney proximal tubule is the primary site in the nephron for excretion of waste products through a combination of active uptake and secretory processes, and is also a primary target of drug-induced nephrotoxicity. Here, we describe the development and functional characterization of a 3-dimensional flow-directed human kidney proximal tubule microphysiological system. The system replicates the polarity of the proximal tubule, expresses appropriate marker proteins, exhibits biochemical and synthetic activities, as well as secretory and reabsorptive processes associated with proximal tubule function in vivo. This microphysiological system can serve as an ideal platform for ex vivo modeling of renal drug clearance and drug-induced nephrotoxicity. Additionally, this novel system can be used for preclinical screening of new chemical compounds prior to initiating human clinical trials.

3.2 Introduction

Several publicly funded initiatives now seek to drive the development of innovative, human cell derived preclinical models that would accelerate the drug development process, shorten the time it takes to move a new molecular entity into early clinical trials, and reduce the excessively high failure rate of clinical trials. Our goal is to apply flow-directed microphysiological technologies to model the physiological functions of the human kidney proximal tubule, as it plays a vital role in active secretory and reabsorptive transport of drug molecules and is a primary site of drug-induced nephrotoxicity due to these concentrative processes (2). While existing cell culture and animal models of proximal tubular function have utility, there are serious limitations stemming from functional deficits of conventional cell culture systems and differing physiology between animal models and humans.

In this report, we describe the development of a 3D microphysiological system (MPS) of the human proximal tubule. The kidney tubule MPS exhibits long-term viability, retains polarized expression and function of proteins essential for reabsorptive and secretory transport, responds to physiological stimuli, and performs critical biochemical synthetic activities.

3.3 Materials and Methods

3.3.1 Cell isolation, culture, and seeding in MPS platform

Human kidney tissue was obtained from specimens obtained during surgical resection of renal cell carcinoma performed at the University of Washington Medical Center. Human subjects protocol was approved by the University of Washington Institutional Review Board. Healthy portions of the surgical specimen were dissected, stored at 4°C in HBSS buffer containing penicillin-streptomycin, and processed for isolation of proximal tubule epithelial cells within 24

h has described previously (19). Cells with passage number 1 through 4 were used in the subsequent 3D culture experiments.

The 3D MPS platform used in these studies was developed by Nortis Inc. (Seattle, WA) and details of its construction have been reported by Tourovskaia et al (30). For cell seeding, MPS platforms were filled with extracellular matrix of 6 mg/mL rat tail collagen type I (Ibidi, Madison, WI) at 4°C. MPS platforms were left for 30 minutes at 4°C for matrix settling, and then stored at room temperature overnight. Microfibers inserts were removed from the device and the channel was coated with collagen type IV (5 μg/mL, BD Biosciences, Bedford, MA) over 1 h.

Confluent monolayer cultures of proximal tubule epithelial cells (PTECs) were treated with 0.05% Trypsin-EDTA to obtain single-cell suspensions. PTECs were washed, counted, and resuspended at a concentration of 15-20 × 106 cells/mL and ~5 μL of cell suspension was injected into the collagen IV-coated lumen of the MPS. Cells were allowed to adhere for 24 h before initiating media flow at 0.5 μL/min. Cell coverage and integrity of the tubule structure were assessed under light microscopy on a weekly basis. Additionally, cell viability was assessed using a LIVE/DEAD® Viability/Cytotoxicity assay (Invitrogen, Carlsbad, CA). For all of the experiments conducted, MPS platforms contained PTECs grown for 2-3 weeks after initial cell seeding.

3.3.2 Immunocytochemistry and imaging

Proximal tubule epithelial cells in MPS platforms were fixed with 10% Buffered Formalin Acetate (Fisher Scientific, Pittsburg, PA) for 1 h, permeabilized with 0.5% Triton X-100 (Sigma-Aldrich, St. Louis, MO), and blocked with 0.1% bovine serum albumin for 40 min. Primary antibodies were then applied overnight at 4°C and fluorescently labeled secondary

antibodies were applied for 1 h at room temperature. Cells were mounted using SlowFade gold (Invitrogen, Carlsbad, CA) medium. Phase contrast and fluorescent images were acquired as described in Supplementary information (Supplementary materials and methods). For analysis of MPS ultrastructure by transmission electron microscopy (TEM), devices were fixed in 1/2x Karnovsky's fixative (2.5% glutaraldehyde with 2% formaldehyde in 0.1M buffer). Samples were post-fixed in osmium tetroxide and processed, sectioned, and examined according to protocols as described previously (66).

3.3.3 γ-Glutamyl transpeptidase (GGT) activity

The presence and functioning of γ-glutamyl transpeptidase (GGT) was demonstrated by metabolism of a γ-glutamyl substrate—glutathione disulfide (GSSG) or the oxidized form of glutathione in MPS cultured with PTECs grown to >50% confluency. To test for GGT activity, proximal tubule MPS were perfused with culture media at 1 μL/min containing 4 μM of GSSG; effluent samples were collected at hourly intervals for a total of 4 hours. After the first phase of collection, the platforms were perfused overnight using fresh media to ensure sufficient washout of GSSG. To verify specificity of GSSG processing by GGT, platforms were re-perfused with 4 μM GSSG in the presence of GGT inhibitor—acivicin (1 μM), and effluent samples were collected hourly for a total of 4 hours. GSSG concentration in the effluent perfusate was measured by liquid chromatography-tandem mass spectrometry (LC-MS/MS). Results are presented as recovery of GSSG expressed as % of nominal input in the presence and absence of GGT inhibitor. Additional analytical details are presented in Supplementary information (Supplementary materials and methods).

3.3.4 ATP assay

Generation of ATP via cellular respiration by PTECs was tested. MPS cultured PTECs were treated with 1 μM antimycin A (Abcam, Cambridge, MA) or 0.01% DMSO for 24 hours followed by measurement of ATP using a luminescent ATP detection kit (Abcam, Cambridge, MA) with slight modification. Briefly, cells were removed from the devices by injecting approximately 50μl of detergent (Abcam luminescent kit, part 8206000) into the injection port allowing cells to be collected at the luminal outflow port. Cell lysates were transferred to a white opaque 96-well plate (Corning Costar, Corning, NY) to complete the kit procedure and luminescence was quantified using a PlateLumino luminometer (Stratec Biomedical Systems AG, Gewerbestr, Germany). A five-point ATP standard curve (10μM-1mM) was generated and used to convert relative luminescence units to ATP concentration.

3.3.5 Ammoniagenesis

The ability to secrete ammonia in response to acidification was evaluated in MPS platforms cultured with PTECs grown to >50% confluency. The MPS were initially perfused with PBS (pH 7.4) at a flow rate of 1 μL/min for 4 hours; effluent was collected at 2-h intervals. After 4 h, the perfusate was switched to PBS buffered to an acidic pH of 6.9, and 2-hourly collection of effluent was continued for another 4 h. Samples at hour 4 were analyzed for ammonia concentration using a colorimetric ammonia assay kit (Abcam, Cambridge, MA). Effluent ammonia concentrations at acidic and physiological pH conditions were compared.

3.3.6 Glucose reabsorption

Glucose reabsorption via sodium-glucose cotransporter 2 (SGLT2) was demonstrated in the MPS. Platforms were perfused with media for at least 2 weeks prior to being tested for glucose reabsorption. Glucose uptake was assessed using a fluorescent glucose analog 2-NBDG

(2-deoxy-2-[7-nitro-2, 1, 3-benzoxadiazol-4-yl) amino]-D-glucose; Cayman Chemicals, Ann Arbor, MI). Twelve hours prior to testing, PTEC perfusion was switched to culture media with a lower, physiological glucose concentration (100 mg/dL). After 12 hours of pretreatment, MPS platforms were perfused with media containing 200 μg/mL (0.6 mM) of 2-NBDG either in the absence or presence of inhibitors apigenin (50 μM) or dapaglifozin (0.5 μM) for 2 hours at 37°C. Platforms were then washed and imaged using a Nikon Eclipse Ti-S and inverted spinning disk microscope in phase contrast and fluorescent modes and fluorescent signal quantified using ImageJ software.

3.3.7 25-$(OH)_2$ vitamin D_3 metabolism

Conversion of 25-OH vitamin D_3 to its physiologically active and inactive metabolites was assessed in the MPS. Cells cultured from three separate donors were evaluated in triplicate for a total of 9 MPS platforms. PTECs were cultured for 2-3 weeks prior to the addition of 1 μM 25-OH vitamin D_3 (Toronto Research Chemicals, Toronto, Canada) to the cell culture media containing 2% fetal bovine serum (FBS) to minimize adsorption of vitamin D_3 metabolites. Inflow rate of 25-OH vitamin D_3-containing media was set at 0.5 μL/min and outflow was collected daily for 3 days and stored at -80°C. LC-MS/MS analysis of 25-OH vitamin D_3 and its primary metabolites was conducted using a previously established method (67) with modifications described in the Supplementary information (Supplementary materials and methods). Formation clearance (CLf) for the three dihydroxy-vitamin D_3 metabolites (1α,25-(OH)2 vitamin D3, 4β,25-(OH)2 vitamin D_3, and 24,25-$(OH)_2$ vitamin D_3) was plotted over time. The method for calculating CLf is described in Supplementary information (Supplementary materials and methods).

3.3.8 Vitamin D receptor-mediated regulation

To evaluate the inductive effects of 1α,25-(OH)2 vitamin D3 (calcitriol) on the 24-hydroxylation of 25-OH vitamin D3 (calcidiol), a group of MPS devices (n=5) were exposed to 1 μM calcidiol in the presence or absence of 0.5 μM exogenous calcitriol. Effluent was collected for 3 days and stored at -80°C until LC/MS-MS analysis of 24,25-(OH)2 vitamin D3 and calcidiol concentrations. Following treatment, RNA was extracted using Tri-reagent. In order to assess the more rapid effects of calcitriol co-administration on gene expression, additional MPS were treated for 5 hours prior to collection in Tri-reagent. Total RNA was reverse transcribed to cDNA using reverse transcription kit wit (Life Technologies, Carlsbad, CA). Assessment of the effects of calcitriol on the expression of genes relevant to calcidiol metabolism (CYP24A1, CYP27B1 and VDR) was conducted using TaqMan Gene expression assays (Life Technologies, Carlsbad, CA) on a CFX Connect Real-Time PCR Detection System (Bio-Rad Laboratories, Hercules, CA). Relative quantification of mRNA was determined using GAPDH as the housekeeping gene.

3.3.9 Secretory transport of organic solutes

Secretory transport of solutes was assessed using dual channel MPS platforms as depicted in Supplementary Fig. 3.3; one channel was populated with PTECs with an average 85% confluent cell coverage, the other channel remained cell-free and served as a pseudo-vascular channel for delivery of substrates to the basolateral aspect of the tubular epithelium. Substrate solute was added to the media flowing through the cell-free channel. Competitive inhibitors were introduced into the media flowing through both channels. The rate of flow through both channels was set at 1 μL/min. Effluent from both channels was collected hourly. To assess secretory transport of PAH, 1 μCi/mL 14C-PAH or 2 μM equivalent of PAH or 10 μM indoxyl sulfate

(Sigma-Aldrich, St. Louis, MO) was introduced into the cell-free channel. Appearance of solute in the PTEC channel effluent was measured in the presence or absence of 2 mM probenecid. Interaction in secretory transport between PAH and indoxyl sulfate was assessed by examining 1 μCi/mL 14C-PAH transport in the presence of 2 mM indoxyl sulfate. The appearance of radiolabeled PAH in the effluent was measured by liquid scintillation counting. Concentration of indoxyl sulfate in the effluent was measured by a previously established LC-MS assay with modifications (68). Details on the LC-MS assay are presented in Supplementary information (Supplementary materials and methods). The MPS experiments depicted in Figure 3.8B, 3.9A and 3.9B used 9, 8 and 7 MPS, respectively. A minimum of 3 MPS were assigned to each inhibitor treatment and control groups. Hourly time points were aggregated and presented as a mean ratio of the amount of test substrate appearing in the PTEC channel effluent relative to its nominal input amount into basolateral channel ± inhibitor. Error bars reflect the standard error of the mean of the aggregated time points for each experiment. For comparative purposes, transport of PAH was measured in Transwell™ as previously described (56). Details on the protocol and modifications are available in Supplementary information (Supplementary materials and methods).

3.3.10 Statistical Analysis

Data are reported as means ± standard errors. Each constructed model of PTECs in MPS represented an experimental replicate. For comparison of means, statistical tests were applied using GraphPad software (La Jolla, CA).

3.4 Results

3.4.1 Structural Recapitulation of the Proximal Tubule Microenvironment

The stepwise construction of a microphysiological model of human proximal tubule is presented in Fig. 3.1Ai-iv. Human primary proximal tubular epithelial cells (PTECs) were grown in monolayer cultures following isolation from renal cortical tissue. After about 7 days in culture, the cell monolayers displayed a uniform cobblestone-like appearance with dome formation that is characteristic of PTECs (Fig. 3.1Aii) (15, 26). Following seeding into the MPS, PTECs adhered to the channel surface and grew to form a tubule-like structure (Fig. 3.1Aiv); its physical dimension is close to that reported for the proximal portion of the renal tubule in the human kidney (i.e., 6 mm long × 120 μm thick in the MPS compared to 14 mm long × 40 μm thick in vivo) (69). In its present format, the MPS holds approximately 5000 PTECs. Microfluidic technology allowed media perfusion, which exposed PTECs to fluid shear force at the apical surface and delivered nutrients continuously under normoxic conditions (Fig. 3.1Aiii) (3, 30). PTEC in 3D culture exhibited excellent viability (>95%) for up to 4 weeks, as demonstrated by extensive green fluorescent Calcein AM signal in live cells with minimal red fluorescent signal indicative of dead cells (Fig. 3.1Aiv). Cell surfaces showed fairly even expression of CD13 (aminopeptidase-N) and E-Cadherin, markers of epithelial origin, for at least 28 days (Fig. 3.1B1-4). Proximal tubule origin of the final culture was verified by consistent immunohistochemistry (IHC) staining for aquaporin-1 (Fig. 3.1B5-6) and lotus lectin (Supplementary Fig. 3.1), while signal for aquaporin-2, prominin 2 and uromodulin, markers of distal tubule and/or collecting duct cells, was absent in both 2D cultures and MPS (Supplementary Fig. 3.1). It is interesting to note that KIM-1, a marker of acute kidney injury, is expressed in PTECs cultured in 2D, but is absent in MPS devices (Supplementary Fig. 3.1). This

suggests that flow directed culture coupled with three-dimensional architecture confers a less injured, more quiescent phenotype within the MPS. Transmission electron microscopy (TEM) images of PTEC ultrastructure showed representative density of mitochondria, Golgi apparatus, and rough endoplasmic reticulum. Tight junctions and short microvilli at the apical surface were also observed, as well as basolateral interdigitations between neighboring cells, the latter being characteristic of proximal tubules in vivo (Figure 3.2A1/A2 and Supplementary figure 3.2) (69). Polarization of PTECs was shown by localization of the tight junction protein ZO-1 to the luminal (apical) aspect of the PTEC tubule, and localization of Na+/K+-ATPase to the lateral interface between neighboring cells and the basal border between PTECs and collagen substrate (Fig. 3.1C). Cilia formation in response to fluid shear stress was evidenced by positive staining of acetylated tubulin in rod-like structures that originate close to the cell nucleus; the ciliary process averaged 10 ± 3.5 μm in length (Fig. 3.2B1/B2).

3.4.2 Recapitulation of Proximal Tubule Physiological Functions

Reclamation of glutathione is an essential biochemical function of renal proximal tubule in vivo (70). The reclamation process is mediated by γ-glutamyl transpeptidase (GGT), which normally mediates the transfer of glutamyl moiety from glutathione to an acceptor amino acid as part of the γ-glutamyl cycle, a pathway for the synthesis and degradation of glutathione. Selective IHC staining for GGT in the MPS revealed enriched localization of the enzyme at the luminal aspect of the PTEC structure (Fig. 3.3A). GGT mediates a comparable reaction for the oxidized form of glutathione, glutathione disulfide (GSSG) (Fig. 3.3B) (71), which is a more chemically stable substrate for assessing the activity of γ-glutamyl transpeptidase in proximal tubule MPS. PTECs within the MPS were perfused with media containing 4 μM GSSG in the presence or absence of the irreversible GGT inhibitor acivicin (1 mM). The recovery of GSSG in

the effluent was low (<1.5%), demonstrating extensive catalytic activity of GGT; in the presence of acivicin, an approximate 2-fold increase in GSSG recovery was observed over 2-4 hours (Fig. 3.3C).

The proximal tubule is responsible for nearly 90% of glucose reabsorption in the kidney, which is mediated primarily by glucose transporters, including SGLT2 (72). Selective IHC staining for SGLT2 in the proximal tubule revealed its expression and localization at the apical surface (Fig. 3.4A). To confirm functioning of SGLT2 in the PTEC tubule microenvironment, glucose reabsorption was demonstrated by perfusing the proximal tubule in the MPS with a fluorescent glucose analog, 2-NBDG (200 μg/mL) in the presence or absence of either a SGLT2/GLUT inhibitor (apigenin 50 μM) or a SGLT-2 specific inhibitor (dapagliflozin, 0.5 μM). PTEC layer showed strong green fluorescent signal demonstrating avid cellular uptake and accumulation of 2-NBDG. Fluorescent signal intensity of 2-NBDG decreased significantly in the presence of both inhibitors, indicating blockade in uptake of the fluorescent glucose analog into epithelial cells (Fig. 3.4B-F). It is worth noting that the magnitude of effect for both inhibitors (25-30%) is similar to the clinical efficacy of SGLT2 inhibitors (30-50%) despite in vitro predictions of 90% inhibition (73).

To demonstrate that the primary cells we use to populate the MPS generate their ATP energy source from mitochondrial oxidative phosphorylation as opposed to aerobic glycolysis i.e. the Warburg effect (74), we measured cellular ATP levels in the presence and absence of antimycin A. As seen in Fig. 3.5, exposure to 1 μM antimycin A for 24 h resulted in a 2-fold drop in ATP content. A similar magnitude decrease was also observed in PTECs cultured in monolayer (data not shown).

Renal proximal tubules respond in vivo to a drop in either blood or luminal filtrate pH with an increased generation and secretion of ammonia (Fig. 3.6A). To demonstrate this physiological response, PTECs were exposed to a decrease in MPS luminal perfusate pH from 7.4 to 6.9. PTEC cells in the MPS responded with an approximate 3-fold increase in effluent ammonia concentration (pH 7.4—0.55 mM NH3, pH 6.9—1.56 mM NH3) (Fig. 3.6B).

The proximal tubule epithelium is known to be a critical site for bioactivation of vitamin D. Systemically available 25-OH vitamin D_3 (calcidiol) is converted to bioactive 1α,25-$(OH)_2$ vitamin D_3 (calcitriol) through the action of cytochrome P450 27B1 (CYP27B1). Metabolism of calcidiol to relatively inactive metabolites also occurs in the kidney via cytochrome P450 24A1 (CYP24A1). When seeded into the MPS, PTECs demonstrated the ability to metabolize calcidiol to quantifiable levels of bioactive calcitriol, inactive 24,25-$(OH)_2$ vitamin D_3 and 4β,25-$(OH)_2$ vitamin D_3 (Fig. 3.7A) (75). Overall, the formation clearance (i.e., formation rate normalized by substrate concentration) for 24,25-$(OH)_2$ vitamin D_3 was significantly greater than that of calcitriol and 4β,25-$(OH)_2$ vitamin D_3. This finding is consistent with metabolism of calcidiol in vivo, where circulating concentrations of 24,25-$(OH)_2$ vitamin D_3 are known to be higher than those of both calcitriol and 4β,25-$(OH)_2$ vitamin D_3 (67). In order to further explore vitamin D homeostasis, MPS-seeded PTECs were challenged with additional exogenous calcitriol (500 nM), a Vitamin D Receptor (VDR) ligand. Induction of the VDR-regulated 24-hydroxylation pathway was observed (Fig. 3.7B). This increase in 24,25-$(OH)_2$ vitamin D_3 formation was accompanied by a rapid (5 hours) and sustained (72 hours) accumulation of mRNA transcripts for CYP24A1 (Fig. 3.7C). No apparent changes in gene expression of CYP27B1 (Fig. 3.7D) or VDR (Fig. 3.7E) were observed.

3.4.3 Secretory transport of organic solutes

Circulating organic solutes, including drugs and xenobiotics, can undergo secretion into the tubular lumen by means of active transport across the renal tubule epithelium. Secretory transport of the prototypical organic anion, para-aminohippurate (PAH) across PTEC monolayers was evaluated in both conventional Transwell™ permeable cell culture inserts and the MPS, in the presence and absence of a competitive inhibitor, probenecid. No change in apparent permeability (Papp) was observed in the 2D Transwell™ system upon addition of probenecid (Fig. 3.8A). However, within the MPS the relative appearance of PAH in the effluent from the PTEC lumen was reduced approximately 4-fold in the presence of probenecid (Fig. 3.8B). These data support the involvement of basolateral uptake (OAT1/3) and/or apical efflux (MRP2/4) transporters in the observed vectorial transport of PAH in the MPS (76). We further evaluated transport in the MPS using the endogenous anionic uremic solute, indoxyl sulfate (Fig. 3.9A). As compared to PAH, indoxyl sulfate output in the PTEC channel effluent was approximately 20% lower, but exhibited a similar degree of inhibition by probenecid. In addition, an interaction between PAH and indoxyl sulfate was demonstrated; co-perfusion with indoxyl sulfate decreased secretory transport of PAH by 1.8-fold, suggesting a competition of the two solutes for the same organic anion transporters (Fig. 3.9B).

3.5 Discussion

We have demonstrated that in a flow-directed MPS, human PTECs attach to supportive collagen extracellular matrix and self-assemble to form a 3D tubular structure (3, 30). Furthermore, cells maintain renal epithelial differentiation and characteristic morphology in this microenvironment for an extended period of time. In contrast, PTECs grown in conventional 2D

monolayer cultures often show limited longevity and loss of distinctive epithelial phenotype due to lack of fluidic mechano-sensory input (29) and other stimulus elements present in the native microenvironment in vivo. Also, in contrast to conventional 2D culture, PTECs grown in the MPS polarize with proteins selectively localized to the basolateral and apical aspects of the tubular epithelium and exhibit expected morphological and functional phenotypes of proximal tubule epithelium in vivo out to 28+ days (69, 77).

We also demonstrated proximal tubular origin for the majority of epithelial cells in culture by IHC staining of differential markers of kidney epithelial cells (viz., aquaporin 1, aquaporin 2, and SGLT2). Structurally, PTECs in the MPS exhibited polarized structure based on localization of domain-marker proteins. Assessment of ultrastructure by transmission electron microscopy revealed the hallmarks of a competent epithelial barrier, as well as healthy mitochondria and characteristic basolateral membrane interdigitations. The apical brush border expressed functionally active SGLT2 transporter (Fig. 3.4) and GGT enzyme (Fig. 3.3). Although brush border microvilli on the cultured PTECs were not as abundant as in freshly isolated cells (69, 77), this is consistent with literature reports of low microvilli density in traditional PTEC monolayer cultures (14, 26). Metabolic competence of the cultured PTECs was confirmed by their capability for ammoniagenesis and vitamin D biotransformation. In the case of vitamin D, this metabolic competence was accompanied by retention of some of the machinery critical to maintaining vitamin D homeostasis in vivo.

The human kidney tubule MPS recapitulates the perfusion delivery and transport pathway of a secreted solute in vivo in that the test solute is perfused into a surrogate vascular channel, diffuses through the pseudo-interstitial space, and undergoes uptake and efflux across the epithelial barrier into the flowing perfusate in the tubular luminal channel. We demonstrated

robust trans-epithelial transport of organic anionic (PAH, indoxyl sulfate) solutes that were sensitive to selective transport inhibitors. The results showed some inter- and intra-MPS variability, which can be attributed to (i) interindividual variability in expression of proximal tubule transporters, and (ii) instability in effluent flow as a result of the porous and pliable collagen extracellular matrix. Nonetheless, the human proximal tubule MPS demonstrates applicability for assessing renal tubular secretion of drugs that was not observable using PTECs in a Transwell™ system. Our work lays a foundation for further investigation of the complex, coordinated uptake and efflux transport processes at the tubular epithelium.

A number of 3D tissue engineering models have been developed that attempt to mimic the proximal tubule structure and function ((25, 29, 70, 78), for reviews see (3, 79)). A number of these systems utilize a monolayer of cells adhered to a microporous membrane coated with a thin layer of an ECM protein component, often collagen IV or laminin. The importance of a 3D tubular architecture is reinforced by the observation that transplantation of 2D sheets of porcine renal proximal tubule cells onto dorsal subcutaneous tissue of nude rats results in increasingly complicated tubular structures with altered expression of surface markers as the 2D sheets convert to their native structure in vivo (80). It has become increasingly evident that the composition (81), microtopography (82, 83), and rigidity/elasticity (84, 85) of the ECM substrate on which a cell adheres can dictate the cells' morphology, phenotype, proliferation, and even fate. Unlike systems using microporous membranes, the tubular structures formed in our microphysiological system are surrounded by ECM whose composition and rigidity/elasticity can be modified to best recapitulate in vivo-like cellular function. Additionally, our microfluidic system enables co-culture of a variety of cell types in the matrix compartment and the proximal

tubule channel, permitting critical cell-cell and cell-matrix interactions, without interference from artificial scaffold materials.

The system described herein represents a milestone in cell culture modeling of human kidney in that it is possible to achieve a functional 3D construct of human proximal tubule in vitro in a microfluidic device that more faithfully reflects the native microenvironment of the renal tubulo-interstitium. There have been earlier attempts in recapitulating a functioning 3D proximal tubule. DesRochers et al. (22) constructed a static 3D culture of proximal tubular cells by culturing immortalized human renal cortical epithelial cells (NKi-2) suspended in an extracellular matrix consisting of a 50:50 mixture of rat tail collagen I and Matrigel. Maschmeyer et al. (86) cultured immortalized cell line RPTEC/TERT-1 on a PET membrane within a four-organ-chip device under continuous flow. While longevity in culture and reproducible sourcing are practical advantages, the altered biology of immortalized cell lines is a serious drawback. The observation that the PTECs in our MPS self-assemble into 3D tubular structure may help to recapitulate proximal tubular functionality more effectively than previous monolayer or dispersed culture systems.

More recently, Jang et al. reported development of a ’kidney on a chip’ with similar goals to our project. The MPS reported by Jang et al consisted of a PTEC epithelial monolayer exposed to an apical fluid shear stress was capable of reabsorbing glucose in the range of approximately 2% of the nominal input (29). Notably, our kidney tubule MPS achieves approximately ten fold higher glucose reabsorption than that noted by Jiang et al, that is responsive to SGLT-2 specific inhibition, thus more closely replicating expected physiological functions. Efficient apical glucose uptake is one of the key functions of proximal tubules in vivo. In addition, our proximal tubule MPS also exhibits organic solute transport functions that will

permit its application in the study of renal drug clearance mechanisms. In contrast to the work of Jang et al, we are also able to demonstrate physiologically regulated PTEC cytochrome P-450 function in the biosynthesis of vitamin D sterols. Finally, our system demonstrates maintenance in vitro of an epithelial cell phenotype for up to 28 days, whereas the system employed by Jang et al. was tested for only up to four days.

In pioneering work by Humes and colleagues the development of a renal tubule assist device (RAD) also recapitulated multiple aspects of proximal tubular physiological function ex vivo. Similar to what we observe in our MPS, the RAD also demonstrated glucose reabsorption, glutathione metabolism and PAH secretion (70). The RAD, as the name implies, was developed for the purpose of providing proximal tubule replacement therapy in the setting of kidney failure, while our kidney on a chip was designed for the specific purpose of improving the drug development as part of the NIH organs on chips consortium. Thus the RAD was designed to support renal function in vivo on a macro scale while our MPS is primarily designed for predictive toxicity testing on a micro scale. Given the divergent goals for development of the RAD and our proximal tubule on a chip, it is not surprising that each system has both comparative strengths and weaknesses. In the RAD system media is perfused across a flat cell sheet in a 1 mm wide channel that attempts to mimic lumenal shear stress. In contrast, our microphysiological system enables the creation of a 120 μm diameter tubular tissue that is in direct contact with the surrounding 3D ECM, which more closely replicates human anatomy. Additionally species specificity for individual transporters may be a concern, given the use of primary porcine cells in the RAD device, although the RAD tested in clinical trials did make use of human cells (87). Because of the thickness of the hollow fiber dialysis membrane, the RAD

may be less efficient for assessing basolateral secretory organic solute clearance, which is the major mechanism for proximal tubule drug and metabolite elimination.

Conversely, because the hollow fiber design of the RAD allows facile abluminal flow and creation of an interstitial oncotic gradient favoring apical reabsorption, the RAD is superior to the current kidney on a chip design for detecting apical water and electrolyte reabsorption. Despite attempts to measure ion flux in our MPS using lithium as a marker of sodium transport in the presence and absence of inhibitors targeting either Na+H+ exchanger or Na+K+ ATPase, we were unable to recapitulate this function (data not shown). While this is not a major limitation of the MPS for assessing organic drug elimination by the kidney as there is limited active apical reabsorption of organic xenobiotics (88), nonetheless we are currently developing a two-channel microfluidic kidney MPS, with the second channel allowing a peritubular microvascular endothelia as we have recently described (89), to be grown within the matrix compartment. This design should provide a biomimetic for a more complex in vivo-like microenvironment that may facilitate assessment of electrolyte and water reabsorption in the proximal tubule. In addition, several studies have shown that co-culturing endothelial cells with proximal tubule epithelial cells enhances in vivo-like epithelial function (22, 85, 86).

In summary, for the first time, we have a high-fidelity system in vitro that allows reliable investigation of the fundamental biology of the renal tubule epithelium; the potential applications include tubular secretion of drugs, xenobiotics and uremic toxins, and the ability to assess toxic injury response. To our knowledge this is the first demonstration of a human proximal tubular cell in vitro system that can effectively model basolateral solute transport, apical solute uptake, and intracellular enzymatic function in a physiologically relevant manner. Moreover, our human kidney proximal tubule microphysiological system has the potential for integration of multiple

cell types, i.e., epithelial cells, pericytes, and microvascular endothelial cells (30), in a spatial alignment that would fully reconstitute a tubulo-interstitial environment. In time, we envision the MPS will be extended to investigation into pathophysiological processes at the tubule-interstitium that underlie acute kidney injury and chronic kidney diseases, as well as transport and metabolic processes governing the renal handling of drugs and environmental toxicants in healthy and disease states.

3.6 Figures

Figure 3.1. PTEC viability and basic functionality in human kidney 3D MPS.

(A) Scheme depicting construction of human PTEC in MPS. (i) Cell isolation from human kidney cortex. (ii) Cell culture in 2D. (iii) Cell seeding and culture in 3D MPS. (iv)Phase contrast and viability of PTEC in MPS at day 28. (B) 3D projection of MPS matrix shows PTEC tubule structure: surface expression of epithelial cell marker CD13 (red) (B1 and B2 - 400X Magnification); cell self-assembly confirmed by E-Cadherin expression (red) (B3 and B4 - 400X Magnification); proximal tubule origin confirmed by expression of aquaporin 1 (red) (B5 and B6 - 400X Magnification). (C) Polarization confirmed by tight junction formation via apical localization of ZO-1 (C1) (green) and basolateral expression of Na+/K+ ATPase (C2) (green). Tubule diameter is ~120 μm. (scale bars: 1Aii, 200 μm; 1Aiv, 50 μm; 1B-1C, all 20 μm).

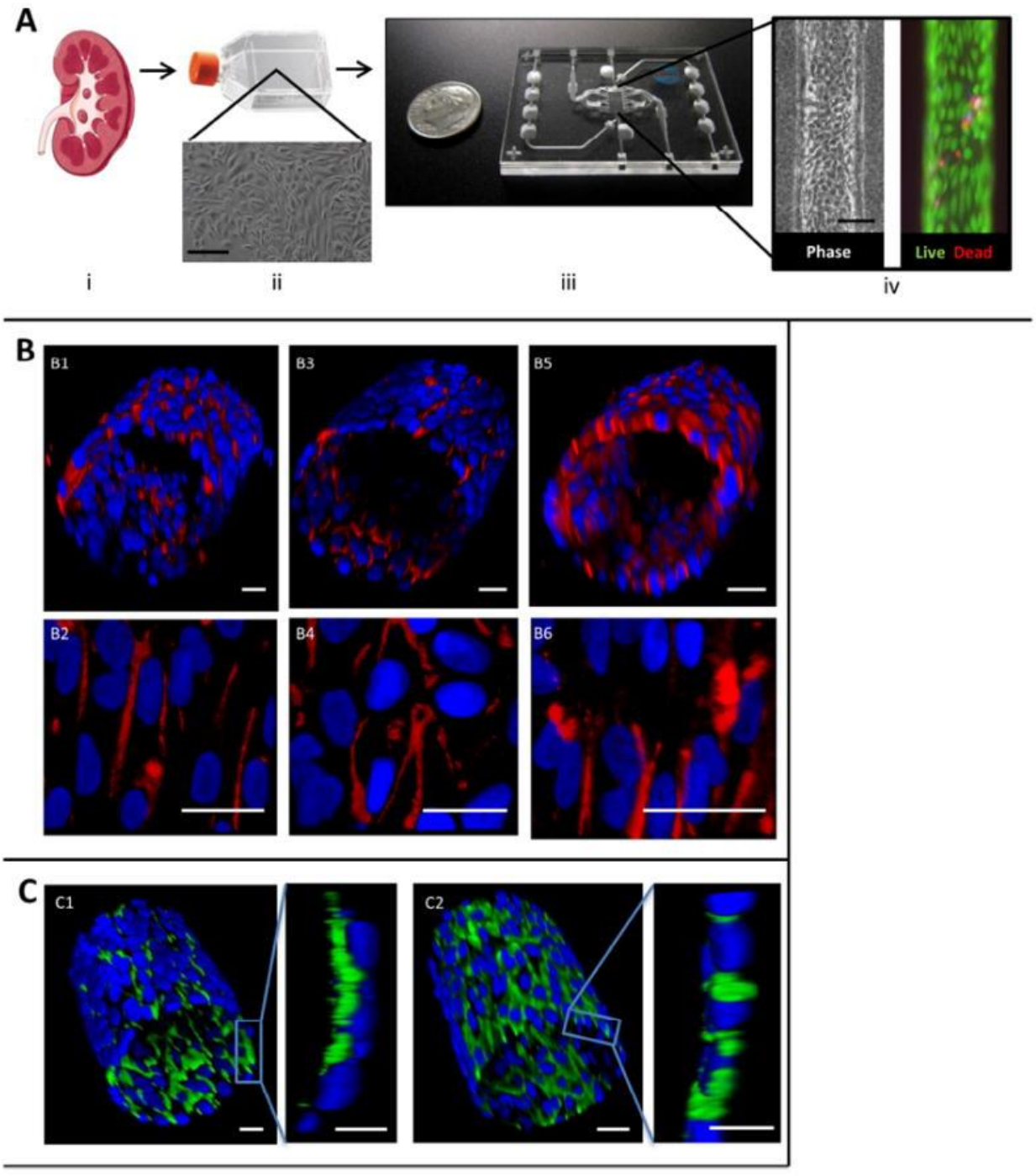
A
i
ii
iii
iv
Phase
Live Dead
B
B1
B3
B5
B2
B4
B6
C
C1
C2

Figure 3.2. Ultrastructure of human PTECs in human kidney 3D MPS.

(A1 and A2) Transmission electron microscopy depicting ultrastructure of PTECs cultured in MPS device. Cellular structure labels: MV-microvilli, M-mitochondria, TJ-tight junction, ER-endoplasmic reticulum, and GA-Golgi Apparatus. (A1 10,000x, A2 30,000x magnification). (B1 and B2) PTECs in MPS form cilia as seen from 2 representative images of single cells stained for acetylated tubulin in red. (scale bars: A1/2, 500 nm; B1, 5 μm).

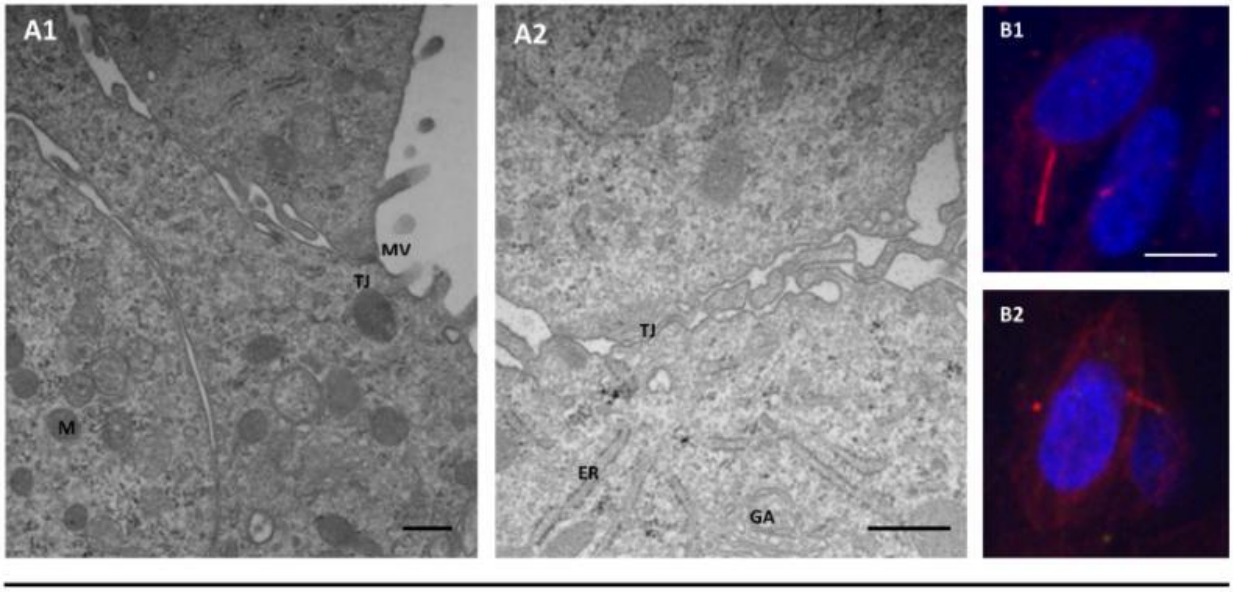

Figure 3.3. GGT activity in human kidney 3D MPS.

(A) Immunocytochemistry reveals proper apical localization of GGT (green) in juxtaposition to nuclei (blue) within the PTEC tubule. (B) γ-glutamyl transpeptidase (GGT) is functionally essential to cleaving the γ-glutamyl moiety from oxidized glutathione and can be inhibited by acivicin. (C) GGT activity as determined by oxidized glutathione abundance in the presence and absence of inhibitor, acivicin (n = 4 MPS devices) (*, P < 0.001, 2-tailed t-test). (scale bars: A, 20 μm-tubule & 10 μm wall).

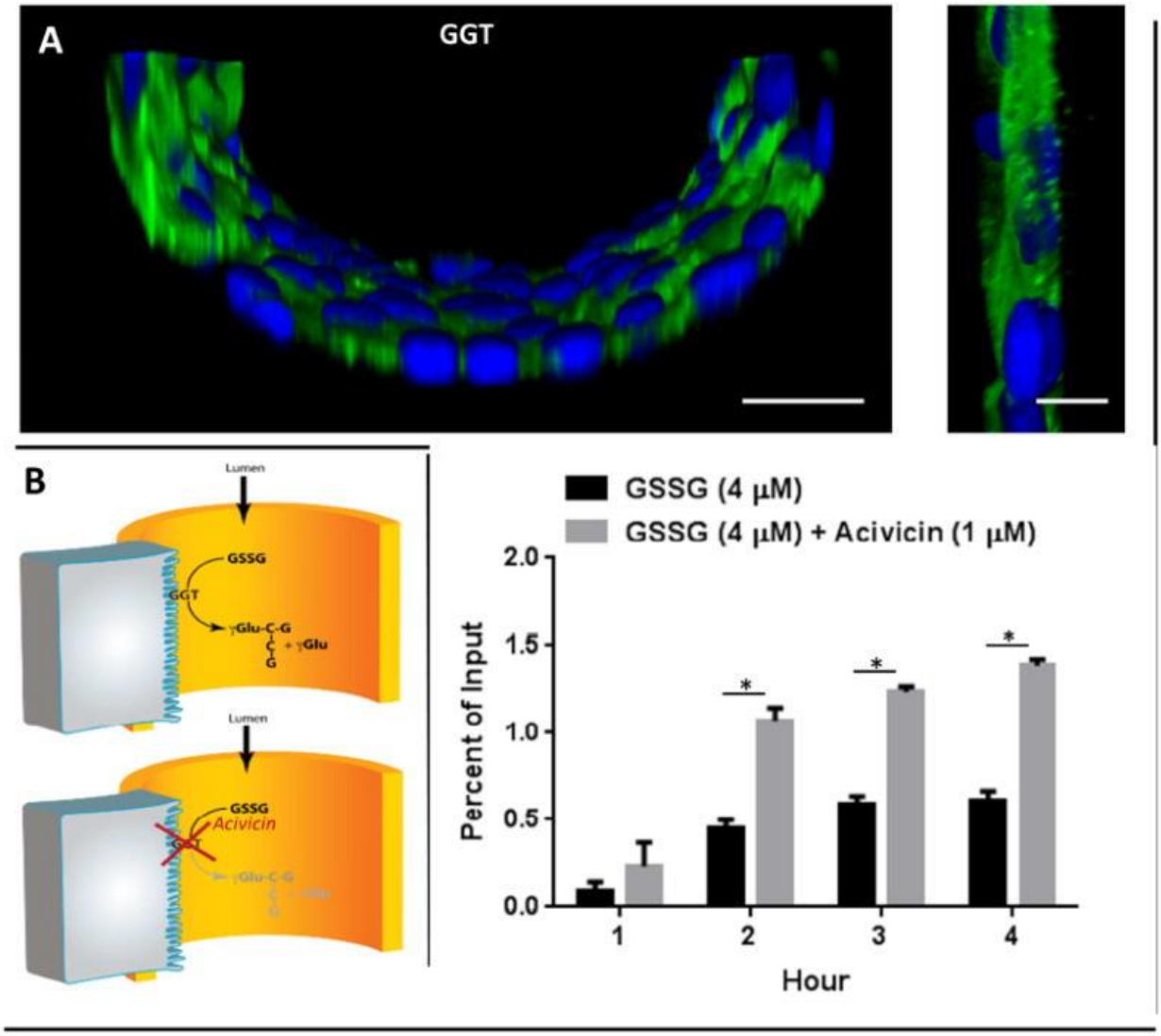

Figure 3.4. Glucose Reabsorption in human kidney 3D MPS.

(A) Glucose is actively reabsorbed from the urine via SGLT2 located on the apical membrane in the PTEC tubule. Immunocytochemistry reveals proper apical localization of SGLT2 (green) in juxtaposition to nuclei (blue). DIC images showing the structure of PTECs in the MPS in the presence and absence of SGLT2 inhibitor, apigenin (B and D). Fluorescent images showing the distribution of the fluorescent glucose analog, NBDG (C and E). NBDG was actively reabsorbed in the absence of inhibitor (C) and was not absorbed in the presence of inhibitor (E). (F) Quantification of cell-associated fluorescent signal following subtraction of auto fluorescence, demonstrating significant reduction of glucose uptake in the presence of inhibitors apigenin and dapaglifozin (n = 3 MPS devices/ group) (*, P < 0.001, unpaired t-test). (scale bars: A, 20 μm tubule and 10 μm wall; E, 50 μm).

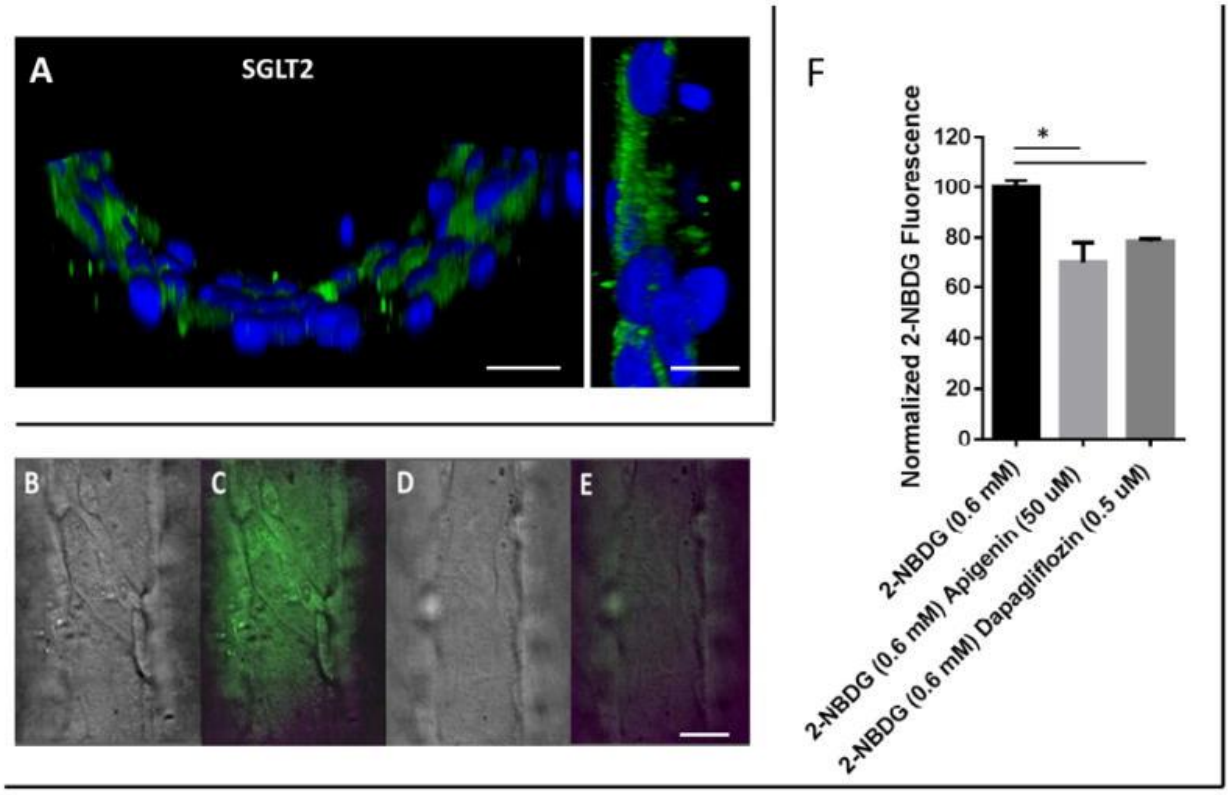

Figure 3.5. ATP formation in human PTECs cultured in 3D MPS.

Cellular ATP content in control and antimycin A treated (1 μM, 24 h) MPS. (n = 3 MPS devices/ group) (*, P=0.05, 2-tailed t-test).

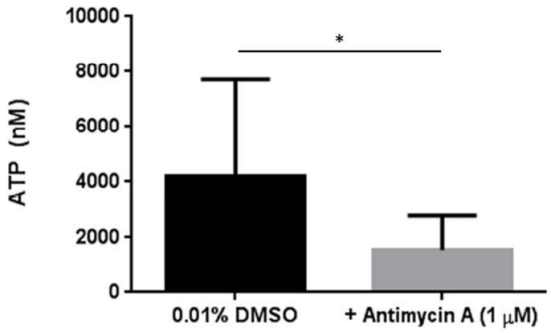

Figure 3.6. Ammoniagenesis in human kidney 3D MPS.

(A) The physiological response to a drop in either blood or luminal pH resulting in the generation and secretion of ammonia in the tubular outflow. (B) With the MPS, luminal media was initially at pH 7.4 and then switched to pH 6.9. Secreted ammonia in the outflow was quantified spectrophotometrically from 4 separate devices after 4 h and was significantly different when exposed to acidic conditions. (*, P = 0.05, 2-tailed t-test).

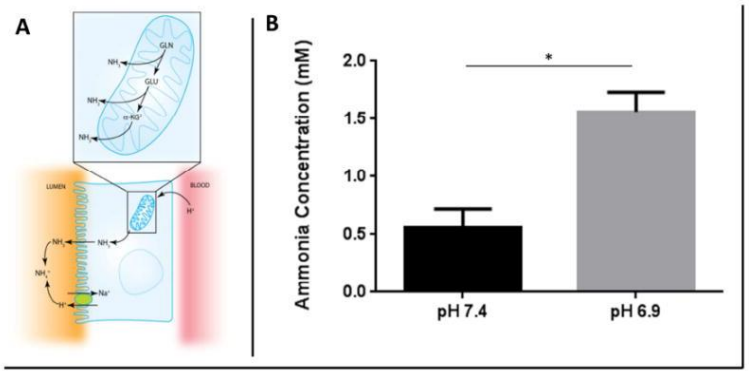

Figure 3.7. Vitamin D homeostasis in PTECs cultured in 3D MPS.

(A) Formation clearance of the 1α,25-$(OH)_2$ Vit D_3 (calcitriol), 4β,25-$(OH)_2$ Vit D_3 and 24,25-$(OH)_2$ Vit D_3 over 3 days exposure of PTEC cultured in MPS to 1 μM 25-OH Vit D_3 (calcidiol). Clearance values are plotted at midpoint of collection interval. Sequential metabolism was assumed to be negligible. (B) Formation clearance of the 24,25-$(OH)_2$-Vit D_3 was greater in MPS-seeded PTEC cultured in media with both 0.5 μM 1α,25-$(OH)_2$ -Vit D_3 (calcitriol) and 1 μM 25-OH-Vit D_3 (calcidiol) than those exposed to 1 μM calcidiol alone. Clearance values plotted at midpoint of collection interval. Sequential metabolism was assumed to be negligible. Baseline data point (×) for formation clearance was determined from experiment presented in (A). Effect of calcitriol on gene expression of (C) CYP24A1, (D) CYP27B1 and (E) VDR in MPS-seeded PTEC. Relative accumulation of CYP24A1 mRNA transcripts was greater in MPS-seeded PTEC cultured in media with both 1α,25-$(OH)_2$ -Vit D_3 (calcitriol) and 25-OH-Vit D_3 (calcidiol) than those exposed to calcidiol alone. Induction of CYP24A1 mRNA occurred rapidly (5 hours) and persisted for the duration of treatment (3 days). No detectable (ND) transcripts of CYP24A1 were observed in the 5 hour "Calcidiol Only" group. There were no substantial changes in CYP27B1 and VDR mRNA expression over the duration of treatment. All genes of interest were standardized to GAPDH.

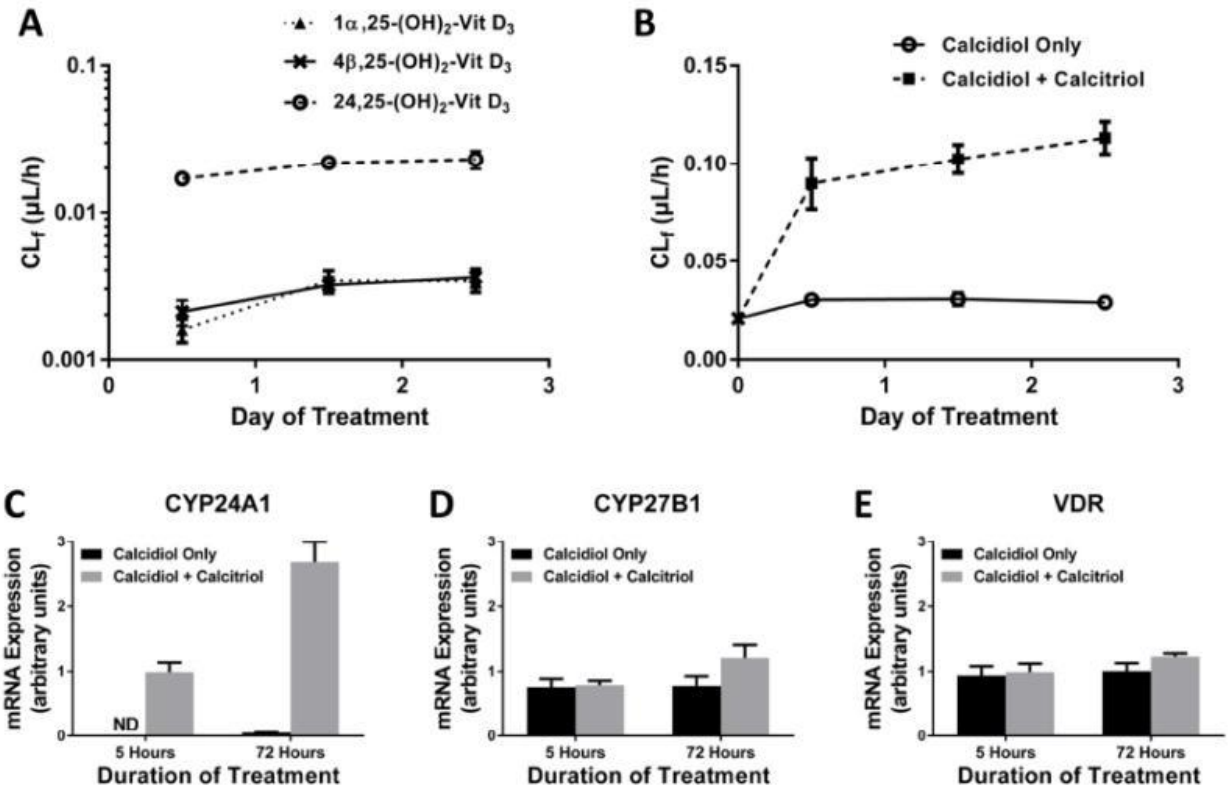
A
1α,25-(OH)2-Vit D3
4β,25-(OH)2-Vit D3
24,25-(OH)2-Vit D3
CLf (µL/h)
0.1
0.01
0.001
0
1
2
3
Day of Treatment
B
Calcidiol Only
Calcidiol + Calcitriol
CLf (µL/h)
0.15
0.10
0.05
0.00
0
1
2
3
Day of Treatment
C
CYP24A1
mRNA Expression (arbitrary units)
Calcidiol Only
Calcidiol + Calcitriol
ND
5 Hours
72 Hours
Duration of Treatment
D
CYP27B1
mRNA Expression (arbitrary units)
Calcidiol Only
Calcidiol + Calcitriol
5 Hours
72 Hours
Duration of Treatment
E
VDR
mRNA Expression (arbitrary units)
Calcidiol Only
Calcidiol + Calcitriol
5 Hours
72 Hours
Duration of Treatment

Figure 3.8. Comparison of trans-epithelial transport of PAH across PTEC monolayers in a conventional 2D Transwell™ and a flow-directed 3D MPS.

(A) In a Transwell ™ monolayer, probenecid had no effect as depicted by no change in the mean PAH Papp values between inhibitor and control group. Papp values were derived as explained in SI Methods. (B) In a flow-directed 3D MPS, probenecid reduced the secretion of PAH by approximately 4-fold.

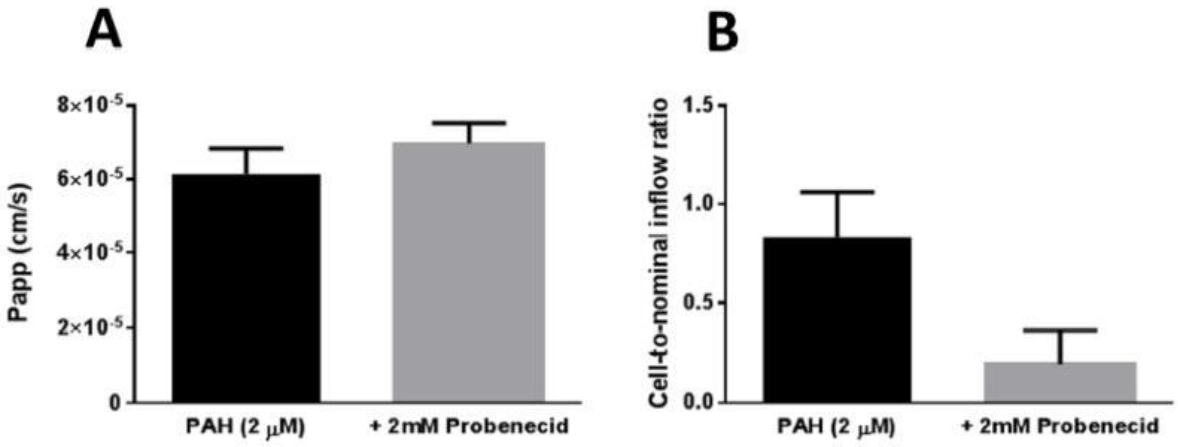

Figure 3.9. Trans-epithelial transport of uremic solute indoxyl sulfate in a flow directed human PTEC 3D MPS.

(A) Indoxyl sulfate secretion in MPS device, inhibitable by probenecid. (B) PAH-Indoxyl sulfate interaction as demonstrated by inhibition of PAH secretion by 2 mM indoxyl sulfate.

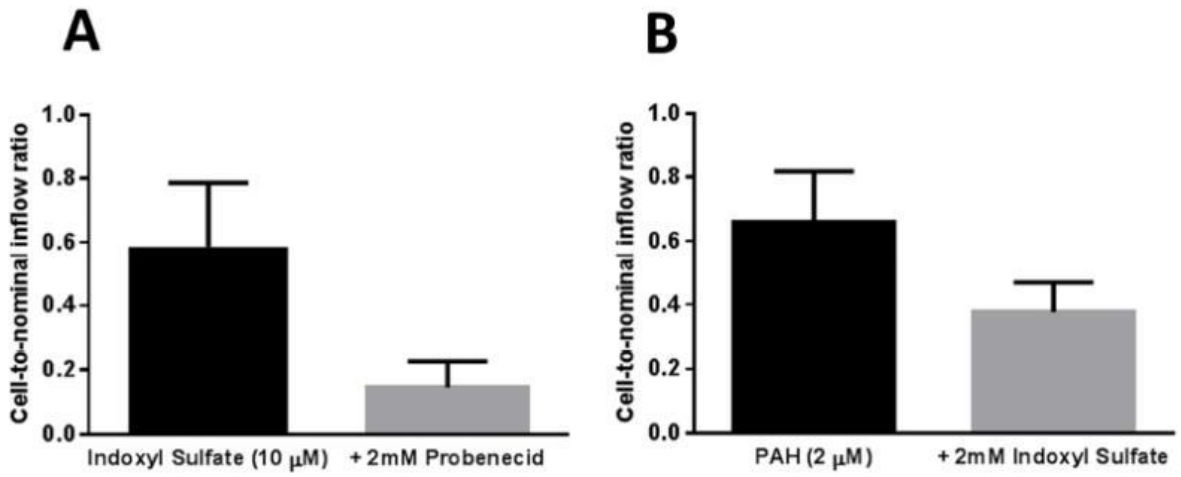

3.7 Supplementary information

Supplementary materials and methods

Immunocytochemistry and Imaging. Proximal tubular epithelial cells in Nortis devices or 8-well plates (Corning, Glendale, AZ) were fixed with 10% Buffered Formalin Acetate (Fisher Scientific, Pittsburgh, PA) or 4% paraformaldehyde in PBS^{++} (Fisher Scientific, Pittsburgh, PA) for 1 hour, permeabilized with 0.5% Triton X-100 (Sigma-Aldrich, St. Louis, MO), and blocked (1% BSA+2% goat serum or 5%BSA) for 40 minutes. Subsequently, cells were incubated with primary antibodies overnight at 4°C. After washing, fluorescently labeled secondary antibodies were added for 1 hour at room temperature and cells were mounted using SlowFade gold (Invitrogen, Carslbad, CA). Primary antibodies included CD13 (mouse, 1:100, Abcam, Cambridge, MA), E-Cadherin (mouse, 1:100, Abcam), ZO-1 (rabbit, 1:100, Invitrogen), Aquaporin 1 (rabbit, 1:100, Abcam), Aquaporin 2 (rabbit, 1:100, Abcam), KIM-1 (mouse, 1:100, R&D Systems, Minneapolis, MN), Na+/K+ ATPase (mouse, 1:100, Fisher Scientific), SGLT2 (rabbit, 1:100, Abcam), GGT (mouse, 1:100, Abcam), Prominin 2 (rabbit, 1:100, Abcam), Uromodulin (mouse, 1:100, Abcam), and acetylated tubulin (mouse, 1:100 Abcam), along with donkey anti-rabbit (1:1000, Abcam) or donkey anti-mouse (1:1000, Abcam) as secondary antibodies. Phase contrast and fluorescent images were taken with a Nikon Eclipse T*i*-S and inverted spinning disk microscope (3i-Intelligent Imaging Innovations, Denver, CO). Acquired images were processed either in ImageJ 1.48v (National Institutes of Health) or Slidebook software (Intelligent Imaging Innovations). Confocal images were captured on a Carl Zeiss LSM 780 confocal microscope (Carl Zeiss Microscopy, Jena, Germany) using a Zeiss C-Apochromat 40x/1.1 water immersion objective. *Z*-sections were taken at 2 µm intervals

through the depth of the tubule, typically a distance of 120 µm. Acquired confocal images were processed in Volocity 6.3 3D Image analysis software (Perkin Elmer, Waltham, MA).

Quantification of immunocytochemistry images. Merged fluorescence images containing antigen and DAPI staining were split into four quadrants then cells exhibiting positive signal were counted and normalized to the number of nuclei in the quadrant. The percent of cells staining positive in the four quadrants was used to calculate a mean and standard deviation for each image.

Secretory Transport of Organic Solutes. Proximal tubule epithelial cells were seeded on the Transwell™ inserts and grown in culture until confluency. 700 µL of media containing 1 µCi/mL ^{14}C-PAH (50 mCi/mmol; purity >97%; Perkin Elmer, Waltham, MA) or 20 µM equivalent of PAH was introduced into basolateral donor compartment in the presence or absence of 2mM probenecid. 330 µL of media was added to the apical receiver compartment. 30 µL of media from the apical receiver compartment was removed at 30 and 60 minutes. Concentrations of PAH in the samples were determined by liquid scintillation counting. Concentrations were used to determine apparent permeability (P_{app}) by using the following equation:

$$P_{app} = \frac{dQ/dt}{C_0 * A}$$

Where dQ/dt is the rate of PAH transfer into the apical compartment, A is the surface area of the Transwell™ membrane, and C_0 is the nominal concentration of PAH in the basolateral donor compartment at t=0. The Transwell™ experiments outlined in Figure 3.8A were conducted in quadruplicate. Data was plotted as mean P_{app} ± standard error of the mean.

Assessment of secretory transport of solutes by the 3D PTEC culture was performed using Nortis™ Dual-Channel microfluidic platforms that have two separate channels/compartments allowing for independent basolateral and luminal perfusion (Supplementary Fig. 3.3). One channel was populated with PTECs with an average channel confluency of 85%, and the other cell-free channel served as a surrogate for normal vascular basolateral input. For assessing the secretory transport of organic solutes, PTECs were isolated from two separate kidney tissue donors. PTECs in the platform were perfused with media in the cell-containing channel for 2-3 weeks. Twenty-four hours prior to experiment, the microfiber rod was removed from the other channel that remained empty. Substrate was perfused through the cell-free channel of the platform, and inhibitor was added to the perfusate for both channels. The rate of media flow was set at 1 µL/min. Effluent from both channels was collected hourly for hours 2 through 4 of the experiment. Effluent volumes were measured gravimetrically and calculated assuming a solution density of 1 g/mL. A sample volume of 10 or 25 µL was aliquoted for assay of substrate in effluent. For the secretory transport of organic anion solutes, ^{14}C-PAH (1 µCi/mL, 50 mCi/mmol, purity >97%; Perkin Elmer, Waltham, MA) and indoxyl sulfate (10 µM, Sigma-Aldrich) were used as prototype substrates. Appearance in the PTEC channel effluent was measured in the presence or absence of probenecid (2 mM, Sigma-Aldrich, St. Louis, MO). The interaction between transport of PAH and indoxyl sulfate was assessed by measuring ^{14}C-PAH output in the presence of 2 mM indoxyl sulfate. Radioactivity of ^{14}C-PAH in the effluent was measured by liquid scintillation counting. The MPS experiments depicted in Figure 3.8B, 3.9A and 3.9B used 9, 8 and 7 MPS respectively. A minimum of 3 MPS were assigned to each inhibitor treatment and control groups. Hourly time points were aggregated and presented as a mean ratio of the amount of test substrate appearing in the PTEC channel effluent relative to its

nominal input amount into basolateral channel in the presence or absence of inhibitor. Error bars reflect the standard error of the mean of the aggregated time points for each experiment.

Analysis of Indoxyl Sulfate. Indoxyl sulfate concentration was performed by stable isotope dilution assay using liquid chromatography-mass spectrometry (LC-MS) similar to the method described by Itoh et al. (68). Protein in samples was precipitated with MeOH at a 1:3 v/v ratio. The supernatant was transferred to a new Eppendorf tube and dried down under vacuum in a Savant Speed Vac concentrator (Thermo-Fisher Scientific, Waltham, MA). The residue was resuspended in 100 µl of 5 mM, pH 6.8 ammonium acetate buffer, and centrifuged at 10,000 x g for 15 min; the supernatant was transferred to a fresh tube and subject to a second centrifugation. Twenty µl aliquots of the final supernatants were loaded onto a CTC Leap Technologies HTS Pal autosampler (Carrboro, NC) and injected onto the LC-MS. Separation of the analyte was accomplished by reversed phase chromatography using a 2.1 mm x 100 mm, 3 µm Waters Atlantis T3 column using a Finnigan Surveyor HPLC pump (Thermo-Fisher Scientific, Waltham, MA) with flow rate set at 200 µl/min. The LC mobile phases were generated from binary mixing of (A) 5 mM, pH 6.8 ammonium acetate buffer and (B) acetonitrile. After an initial wash at 5% B for 1.0 minute, a linear gradient of B from 15% to 60% in 5.5 min was applied to elute analytes; the column was then washed with 80% B for 2 minutes before re-equilibration for the next injection. The retention time for indoxyl sulfate was 4.6 minutes. A Thermo Finnigan TSQ Quantum Ultra triple quadrupole mass spectrometer (Thermo-Fisher Scientific, Waltham, MA) was used for selected reaction monitoring. MS/MS collision energy was set at 20 V and Q2 gas pressure at 1.5 µtorr. The selected ion transitions monitored by MS in negative ion mode were 212 m/z to 132 m/z for indoxyl sulfate and 217 m/z to 137 m/z for its deuterated form. Peak areas for indoxyl sulfate and its corresponding internal standard were

integrated; calibration curve was constructed as analyte-to-internal standard peak area ratio vs amount, upon which analyte concentrations in the samples were estimated.

Analysis of Vitamin D_3 Metabolites. 25-OH vitamin D_3 and its primary metabolites were analyzed in 250 µL aliquots of perfusate samples using a modified LC-MS/MS method previously reported for assay in plasma (67). To improve sensitivity limits, the established method was implemented on a Nexera X2 LC-30AD UHPLC (Shimadzu, Kyoto, Japan) coupled to an AB/SCIEX QTRAP 6500 mass spectrometer (Sciex, Framingham, MA). The following modifications were made to the published method: [1] methanol (MeOH) replaced acetonitrile as the organic mobile phase; [2] the mobile phase gradient was changed to 0-1 min at 35% MeOH, 6-8 min at 65% MeOH, 15-15.5 min at 75% MeOH, 17-19 min at 90% MeOH, 19.2-22.1 min at 35%; and [3] total flow was increased to 0.25 mL/min; [4] injection volume was reduced to 2 µL; [5] column temperature was increased to 45°C; [6] gas temperature was increased to 400°C; and [7] capillary voltage, fragmentor voltage, and collision energy were changed to 5500 V, 70 V and 20 V respectively. Data was acquired and peaks were integrated using Sciex Analyst version 1.6 software.

Formation clearance for the three dihydroxy-vitamin D_3 metabolites (1α,25-$(OH)_2$ vitamin D_3, 4β,25-$(OH)_2$-Vitamin D_3 and 24,25-$(OH)_2$-Vitamin D_3) were plotted as formation clearance (CLf) over time with GraphPad (La Jolla, CA) Prism v. 5.1 using the following equation (1):

$$CL_f = \frac{\frac{dA_m}{dt} + (CL_m \times C_m)}{C_p}$$

Concentration of the respective dihydroxy-Vitamin D3 metabolites was represented by the parameter C_m and the concentration of the parent 25-OH vitamin D_3 was represented by Cp.

Rate of metabolite formation (dA_m/dt) was determined by dividing the observed mass of the formed metabolite by the duration of the 24-hour collection interval. We assumed no sequential metabolism for any of the dihydroxy-vitamin D_3 metabolites during the course of the experiment; clearance of the metabolite (CL_m) was assumed to be negligible and set equal to zero. The formation clearance was then plotted at the midpoint of the collection interval.

Analysis of GSSG. Analysis of GSSG in perfusate samples was accomplished by direct LC-MS/MS without any sample preparation. The HPLC is an Agilent Technologies (Santa Clara, CA) model 1290 equipped with binary pump, thermostated auto-sampler, and heated column compartment. The autosampler compartment was maintained at 4°C. Two µl of sample was injected. The 2.1 mm x 150 mm, 5 µm Develosil Rp-Aqueous C30 column (Phenomenex, Torrance, CA) was maintained at 35°C. The mobile phase consists of 0.1% formic acid (A) and methanol (B) at 0.2ml/min using the following gradient: 0% B held 0-3.5 min, 0-20% over 3.5-6 min, 20% held at 6-8.1 min, 20-0% B at 8.1-8.2 min. The HPLC is coupled to an Agilent Technologies (Santa Clara, CA) model G6410B triple quadrupole mass spectrometer. The MS was operated in the ESI+ mode with the following operating parameters: GSSG transition — m/z 613.0 → 231.0, fragmentor — 135 volts, CE — 36 volts, VCAP — 3500 volts, drying gas — 10 L/min nitrogen @ 350°C, and nebulizer gas — nitrogen @ 35 psi.

As the GSSG appeared to be unstable in cell media even at 4°C in the autosampler, a single standard of GSSG spiked into blank media was injected prior to the samples in order to confirm retention time and estimate instrument response of GSSG. Responses were measured in absolute height counts.

Supplementary figure 3.1. Characterization of renal tubular cell phenotype by immunocytochemistry.

(1A) Quantification of four fields of view for percent of cells expressing antigens shown in panels 1B-I. 1B-I) Representative immunofluorescence images of 2D cultured renal tubular cells evaluated for (B) sodium glucose cotransporter-2, (C) aquaporin-1, (D) CD13, (E) aquaporin-2, (F) lotus-lectin, (G) kidney injury molecule-1, (H) uromodulin, and (I) prominin-2. 1J-M) Immunofluorescence images of 3D MPS cultured renal cells assessed for (J) lotus-lectin, (K) kidney injury molecule 1, (L) uromodulin, and (M) prominin 2. Cells isolated from renal cortical tissue show considerable staining for proximal tubule antigens (aquaporin 1, lotus-lectin, and SGLT2) while minimal staining is observed for antigens expressed in other segments of the nephron (aquaporin 2, uromodulin, and prominin 2). (bar in panels B and J = 100 μm).

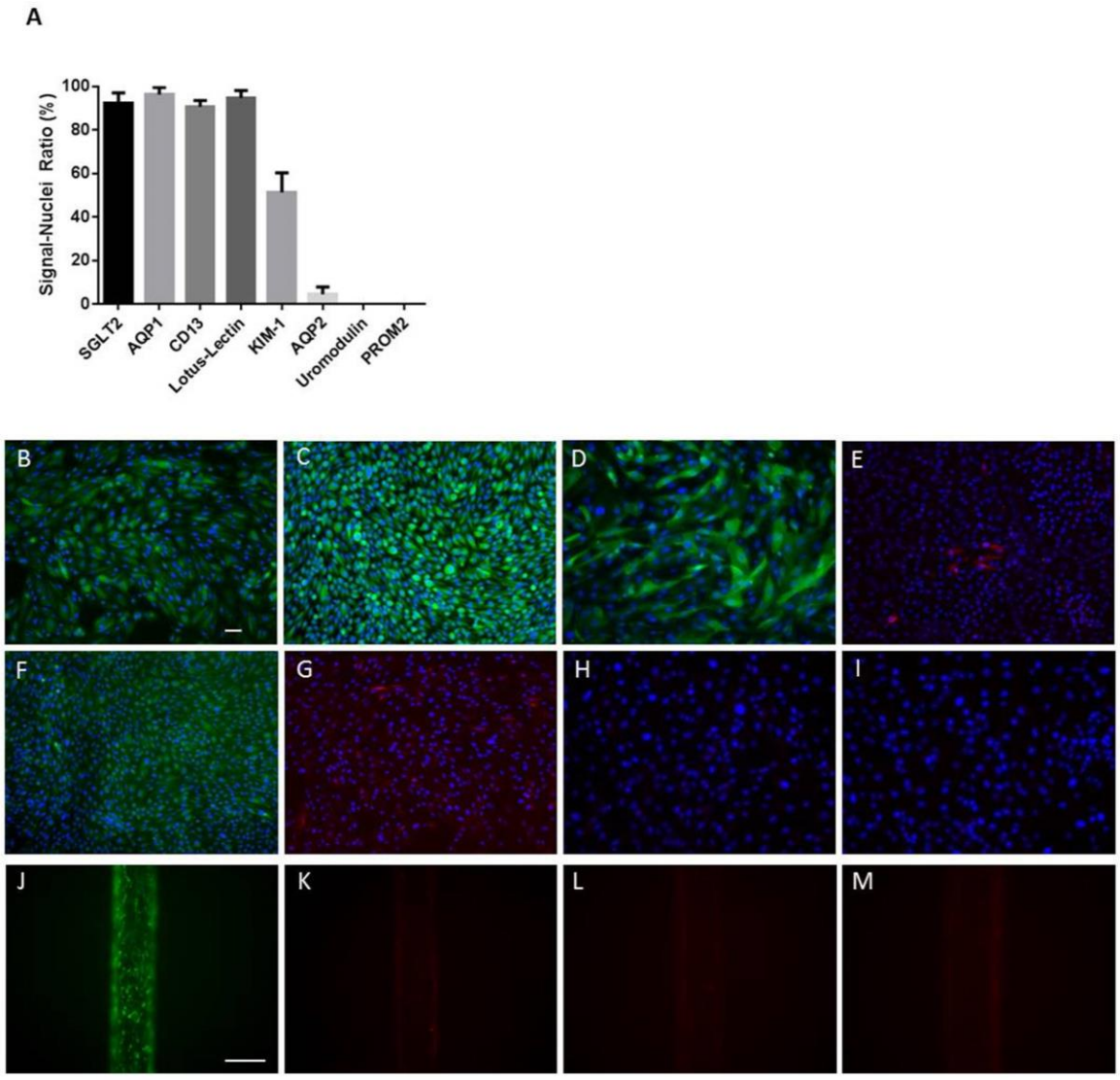
A
Signal-Nuclei Ratio (%)
100
80
60
40
20
0
SGLT2
AQP1
CD13
Lotus-Lectin
KIM-1
AQP2
Uromodulin
PROM2
B
C
D
E
F
G
H
I
J
K
L
M

Supplementary figure 3.2. Ultrastructural characteristics of PTECs cultured in 3D MPS.

Demonstration of basolateral intercellular interdigitations (*) in a human kidney 3D MPS (magnification 12,000x).

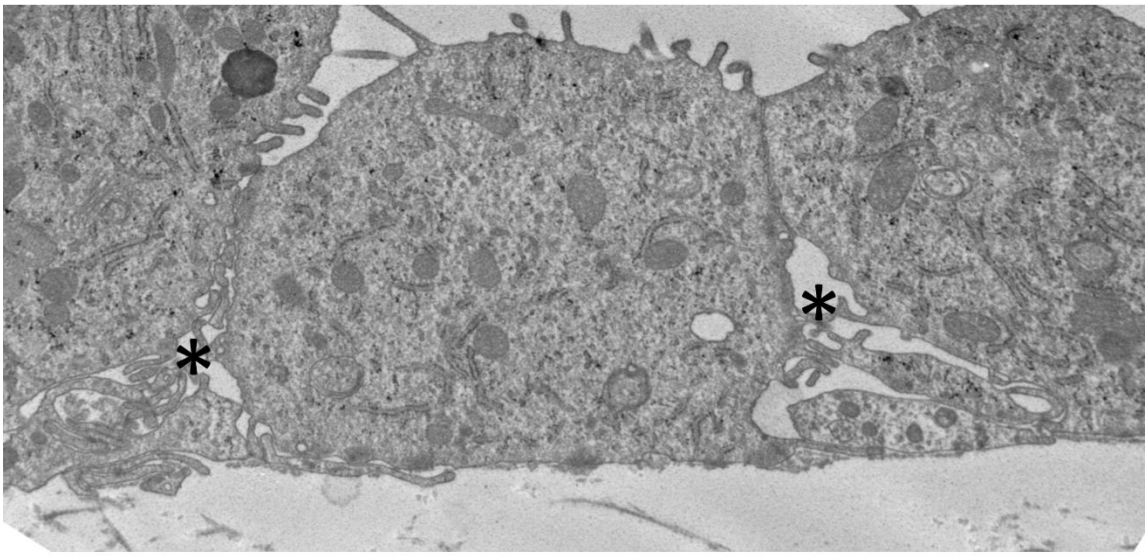

Supplementary figure 3.3. Experimental design for evaluating secretory transport by PTEC in a human kidney 3D MPS.

Substrate ± inhibitor is perfused through the pseudo-vascular channel. Inhibitor is also perfused through the receiving PTEC channel. The effluent media is collected from both channels at designated time points.

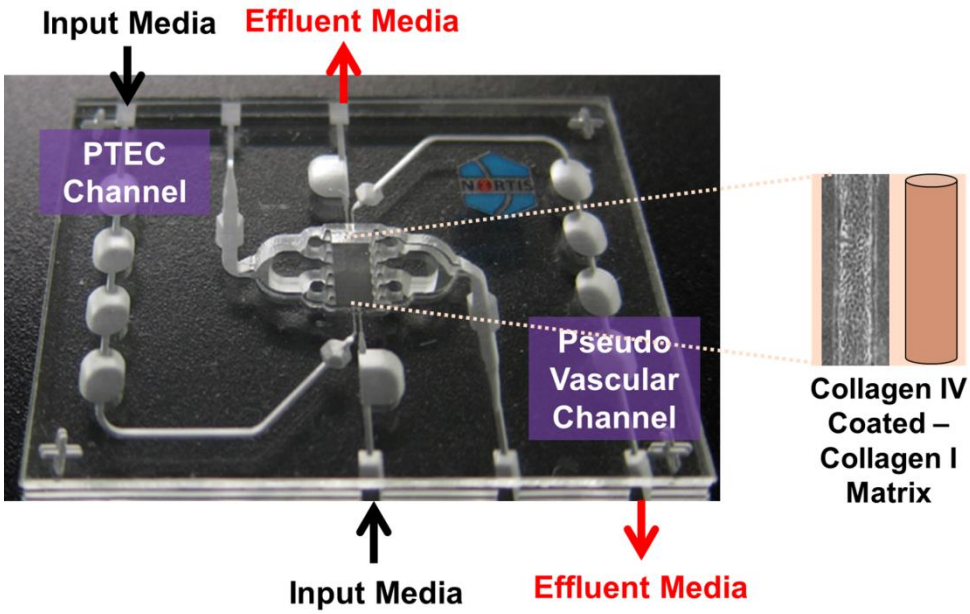

Supplementary figure 3.4. Cell morphology across donors and passages.

(A) Passage 0 cells after 8 days in culture from 68-year old female. (B) Passage 0 cells after 8 days in culture from 60-year old male. (C) Passage 0 cells after 25 days in culture from 66-year old male. (D) and (E) Passage 1 cells after 7 days in culture from 63-year old male. (F) Passage 1 cells after 5 days in culture from 70-year old male. (G) Passage 2 cells after 8 days in culture from 59-year old male. (H) Passage 3 cells after 6 days in culture from 71-year old male. (I) Passage 3 cells after 15 days in culture from 81-year old male. Scale bar = 100 µm.

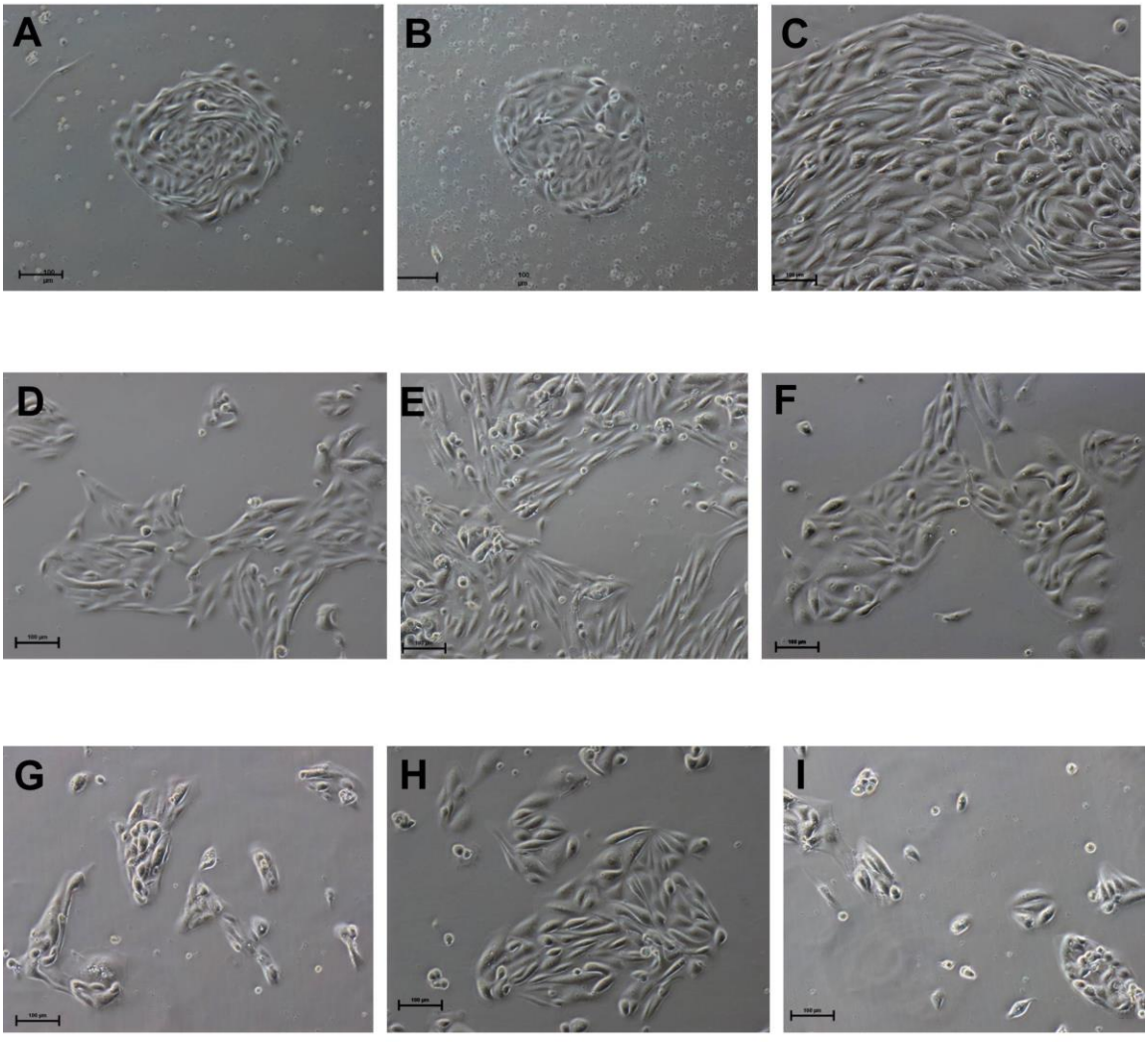

4 An Improved Vascularized Microphysiological System for Modeling of Human Proximal Tubule Drug Secretion

4.1 Abstract

We have developed a vascularized human proximal tubule model in a dual-channel microphysiological system (VPT-MPS), which represents an advance over previous, single cell-type kidney microphysiological systems. Human proximal tubule epithelial cells (PTECs) and human umbilical vein endothelial cells (HUVECs) were co-cultured in side-by-side channels. Over 24 hours of co-culturing, the two cell types maintained their distinct, functionally pertinent morphology. PTECs preserved their polarity as shown by appropriately localized expression of Na^+/K^+ ATPase and tight junction (ZO-1), while HUVECs showed absence of a junctional complex, and instead expressed endothelial cell marker (CD-31). In time lapse functional imaging studies, FITC-dextran passed freely from HUVEC vessel into supporting extracellular matrix, which confirms leakiness of the endothelium (at 80 min, matrix/intra-vessel fluorescence ratio = 0.2). Over time, dextran-associated fluorescence accumulated in the matrix adjacent to the basolateral aspect of PTEC tubule; at the same time, minimal passage of the compound into the tubule lumen was observed (at 80 min, tubule lumen/matrix fluorescence ratio = 0.01). This fluorescence gradient profile is a visual demonstration of proximal tubular epithelium as the rate-limiting barrier in the secretion of a compound in VPT-MPS. In kinetic studies with radiolabel markers, *p*-aminohippuric acid exhibited significantly higher output into the tubule lumen than paracellular markers – mannitol and FITC-dextran (tubule outflow/vessel outflow concentration ratio of 2.4%, vs. 0.5% and 0.4%, respectively). *p*-Aminohippuric acid (PAH) secretion was reduced by 45.8% when probenecid was introduced into the vessel and lumen. This signifies functional expression of organic anion transporters OAT1/3 in PTECs that normally mediate the renal secretion of PAH. The VPT-MPS holds the promise of providing an in vitro platform for evaluating potential for renal secretion as a prominent elimination pathway for new drug

candidates under development and contributing to investigations into the dysregulation of human tubular drug secretion in chronic kidney disease.

4.2 Introduction

Drug secretion by the renal proximal tubule is a multi-step process consisting of passage across the peritubular capillary endothelium, diffusion through the intervening interstitium with its supportive cell types, and vectorial transport across the tubular epithelium. The last step involves coordinated actions of basolateral uptake and apical efflux transporters that shuttle the solute across the epithelial barrier. All these actions occur under continuous blood perfusion through the peritubular capillaries and glomerular ultrafiltrate flow through the tubule lumen (1, 2).

Many advances have been made over the years towards establishing *in vitro* models of cultured proximal tubular epithelial cells that allow transcellular transport studies of endogenous solutes and drug molecules (15, 40-42). Recently, we (55) and others (22, 29, 90, 91) have developed 3D models of the human proximal tubule epithelium comprised of a monoculture of proximal tubular epithelial cells (PTECs) in a microfluidic platform that attempt to recapitulate both the biostructure and physiology of proximal renal tubules. Our group has shown that human PTECs cultured in the microphysiological system (MPS) exhibit: (i) long-term cell viability, (ii) polarized cell morphology and expression of proximal tubule cell markers, and (iii) critical functionality with respect to glucose reabsorption, regulation of vitamin D metabolism, and glutathione reclamation. Initial attempts were also made to study transport of *p*-aminohippuric acid (PAH) and indoxyl sulfate across the PTEC tubule.

In this report, we show development of a vascularized proximal tubule MPS (VPT-MPS), which represents a technical advance over previous, single cell-type kidney MPS models. We characterized functioning of the VPT-MPS in the following respects: (i) sustained expression of respective in vivo cell markers for vascular endothelium and proximal tubule epithelium; (ii)

ready extravasation and diffusion of solute across the interstitial matrix; and (iii) epithelial barrier functions including tight junctions resulting in limited transit of paracellular permeability markers and secretory transport of a prototypical anionic drug substrate, *p*-aminohippuric acid. VPT-MPS should allow future refinements to eventually achieve the construction of a bioengineered human kidney proximal tubule functioning in an in vivo-like micro-interstitium.

4.3 Materials and methods

4.3.1 Chemicals and reagents

Fluorescein isothiocyanate (FITC)-dextran (average MW 10 kDa), bovine serum albumin, hydrocortisone, Triton X-100 and probenecid were purchased from Sigma-Aldrich (St. Louis, MO). D-Sucrose was obtained from Fisher Scientific (Itasca, IL). 16% Formaldehyde (methanol free) was purchased from Polysciences (Warrington, PA). ^{3}H-PAH (40 Ci/mmol) was obtained from American Radiolabeled Chemicals (St. Louis, MO). ^{3}H-mannitol (14.2 Ci/mmol) were obtained from Perkin Elmer (Waltham, MA). Phosphate-buffered saline with (PBS), 50:50 Dulbecco's modified eagle medium with Ham's F-12 (DMEM/F12), penicillin-streptomycin-amphotericin B, insulin-transferrin-selenium A solution (ITS-A), fetal bovine serum (FBS), 0.05% Trypsin EDTA, ProLong Gold Antifade reagent with 4',6-diamidino-2-phenylindole (DAPI) were purchased from Thermo-Fisher (Waltham, MA). Alexa Fluor 594 conjugated donkey anti-mouse IgG, Alexa Fluor 488 conjugated donkey anti-rabbit IgG, Alexa Fluor 594 conjugated mouse ZO1, rabbit OAT3 and rabbit CD31 were obtained from Abcam (Cambridge, MA); rabbit OAT1 was obtained from Fisher Scientific (Pittsburgh, PA), and rabbit Na^{+}/K^{+} ATPase was obtained from Invitrogen (Waltham, MA). Dual-channel MPS platforms were supplied Nortis (Woodinville, WA). Rat tail collagen I was purchased from Ibidi (Martinsried, Germany). Collagen IV was obtained from Corning (Corning, NY). Human umbilical venous

endothelial cells (HUVECs) and EGM-2 bullet kits were obtained from Lonza (Basel, Switzerland).

4.3.2 Isolation of PTECs

Human PTECs were isolated as previously described (55), in accordance with a protocol approved by the University of Washington Human Subjects Institutional Review Board (# STUDY00001297). Detailed kidney tissue donor information is available in Supplementary Materials (Supplementary table 4.1). Following isolation, cells were expanded in tissue culture flasks to passages 1-3 before use in all experiments.

4.3.3 Establishment of vascularized proximal tubule MPS (VPT-MPS)

The inner chamber of Nortis dual-channel MPS platforms was dried, filled with 6 mg/mL of rat tail collagen I, and left overnight to allow the collagen I matrix to solidify. The mandrels of the MPS platforms were then removed, leaving behind two hollow channels through the collagen I matrix. One of two channels in each MPS platform was coated with a 5 µg/mL mouse collagen IV. Human PTECs were then seeded into the collagen IV-coated channel and allowed to attach for 1 hour. A 0.5 µL/min perfusion of DMEM/F12 media containing added ITS-A, 50 nM hydrocortisone, penicillin, streptomycin and amphotericin B was then initiated. Following 5 days under these culture conditions, the epithelial tubule was established and perfusion to the channel was stopped for a brief period. The parallel empty channel was equilibrated with EGM-2 media containing 2% FBS for 2 hours at 1.5 µL/min. Then, HUVECs (passages 5 to 10) were seeded into the equilibrated channel and allowed to attach for 30 minutes to establish an endothelial vessel. Flow to both channels was resumed at 0.5 µL/min with both channels receiving their respective culture medium. All experiments were completed between 8 and 24 hours after HUVEC seeding. Prior to the beginning of experiments, a visual inspection under light

microscope was performed to confirm complete (100%) coverage of both HUVEC vessel and PTEC tubule, respectively. Only VPT-MPS that exhibited even, non-perturbed media flow characteristics (i.e., nearly identical volume of output media from HUVEC vessel and PTEC tubule) were selected for use in functional experiments.

4.3.4 Immunocytochemistry

Vascularized proximal tubule MPS were fixed with a 20-minute perfusion of 4% formaldehyde and 2% sucrose through both channels, followed by a wash with PBS^{++} (containing calcium and magnesium). Blocking of non-specific binding was achieved by exposing the cells to a solution of 0.1% Triton X-100 and 5% bovine serum albumin in PBS^{++} (PTB). Primary antibodies, diluted in 1:100 in PTB, were then introduced into the channels at the following concentrations: rabbit OAT1 1:20, rabbit OAT3 1:100, CD-31 1:50, conjugated mouse ZO-1 1:100, rabbit Na^+/K^+ ATPase 1:100. Following a wash with PBS^{++}, secondary antibodies, diluted 1:1000 in PTB, were perfused. The cells were again washed with PBS^{++} and then finally exposed to a perfusion of a 1:4 dilution of DAPI for staining cell nuclei. Negative controls consisted of perfused samples that were not incubated with primary antibodies; their micrographs are shown in Supplementary Materials. The vascularized proximal tubule MPS platforms were imaged on a Leica microscope and Olympus FV1000 MPE BX61 multi-photon microscope (Center Valley, PA) and processed in ImageJ. For viability assessment of PTECs and HUVECs, LIVE/DEAD® kit (Life Technologies) was used to distinguish between live and dead cells according to manufacturer's instructions. Briefly, Calcein AM (2 μM) and EthD-1 (4 μM) were perfused through the VPT-MPS pre- and post-imaging experiments at a room temperature. The viability was determined by acquiring green and red fluorescent images on a Nikon Ti (Melville, NY) fluorescent microscope.

4.3.5 FITC-dextran extravasation and interstitial diffusion in the VPT- MPS

To characterize the time-course of solute extravasation from the endothelial vessel, we conducted time lapse imaging of fluorescent FITC-dextran (average MW 10 kDa) infused through the vascular channel. The experiment was conducted with 2 VPT-MPS on different experimental days. Confluent VPT-MPS were perfused with EGM-2 media containing 0.1 mg/mL of FITC-dextran at a rate of 1 µL/min for 80 minutes at room temperature on a Nikon Ti (Melville, NY) fluorescent microscope. The VPT-MPS were illuminated with 488 nm excitation light at regular time intervals and images of green fluorescence were acquired at a standardized exposure. ImageJ software was used to quantify relative fluorescence units (RFU) and a ratio of background-subtracted fluorescence was calculated according to Equation 1:

$$Ratio = \frac{RFU\ on\ basolateral\ interstitial\ side\ of\ tubule - background\ RFU}{RFU\ inside\ the\ vessel - background\ RFU} \qquad \text{Equation 1}$$

4.3.6 FITC-dextran tubular uptake in the VPT-MPS

Time course of FITC-dextran (0.1 mg/mL) uptake into the proximal tubule was acquired on a Olympus FV1000 MPE BX61 multi-photon microscope (Center Valley, PA) over 3 hours at a perfusion flow rate of 1 µL/min. The temperature was kept constant at 37°C over the course of imaging; this was achieved by constructing a chamber around the microscope and heating the chamber with 2 egg-incubator heaters. The experiment was conducted with 2 VPT-MPS on different experimental days. The VPT-MPS were exposed to excitation light at regular time intervals and images of green fluorescence were acquired at a standardized exposure. A ratio of background-subtracted fluorescence was estimated according to Equation 2:

$$Ratio = \frac{RFU\ inside\ tubule - background\ RFU}{RFU\ on\ basolateral\ interstitial\ side\ of\ tubule - background\ RFU} \qquad \text{Equation 2}$$

4.3.7 Active tubular secretion in the VPT-MPS

EGM-2 media containing either FITC-dextran (0.1 mg/mL) or radiolabeled mannitol (65 nM) or radiolabeled PAH (4 nM) was perfused through the endothelial vessel, mimicking solute delivery via peritubular capillaries. Effluents from the vessel and the tubule were collected every 2 hours, and solute concentrations in the samples were determined either by fluorescence plate reader (FITC-dextran) or liquid scintillation counting (mannitol and PAH). FITC-Dextran measurements were done in n=7 VPT-MPS (assessed across 3 donors), mannitol in n=5 VPT-MPS (assessed across 2 donors), and PAH in n=4 VPT-MPS (with cells from 1 donor, 2 VPT-MPS per inhibitor and 2 VPT-MPS per control group). Effluent measurements were extended out to 8 hours in order to reach steady-state levels in solute output. This time frame was predicted based upon the estimated half-life of volume turnover given the total perfusion flow rate (1 µL/min) and fluid volume (187 µL) of the MPS platform; i.e., 1/187 min^{-1} or $T_{1/2}$ of 130 min. Equilibration for 4 $T_{1/2}$s was allowed to achieve near steady-state.

4.3.8 Physiologically based pharmacokinetic modelling of *in vivo* PAH renal clearance

Prediction of PAH renal clearance based on data gathered in the VPT-MPS was accomplished through in vitro-to-in vivo scaling in a step-wise fashion. First, estimation of PAH permeability-surface area product (PA) per VPT-MPS was made via the Equation 3:

$$PA = \frac{\Delta A/\Delta t}{C_b} \qquad \text{Equation 3}$$

where ΔA represents amount of PAH collected in the effluent (at 6-8 hour collection interval), Δt represents the time interval (2 hours), and C_b represents concentration of PAH on the basolateral side of the epithelial tubule. The later value is calculated from inflow perfusate concentration of PAH at the HUVEC vessel, corrected for the solute concentration gradient across the interstitial matrix, i.e., between HUVEC vessel and PTEC tubule at steady-state (0.6138; approach to

estimation is available in Supplementary materials). The resultant PAH PA was then scaled to the proximal tubule surface area per nephron, and then per total number of nephrons in the two human kidneys in vivo; the latter is an estimate of unbound secretory clearance of PAH ($Cl_{u,int}$). For the scaling, relevant physiological parameters were acquired from the published literature (1, 92-96). Parameters were collected almost exclusively from human (not animal) kidney studies. Finally, PAH renal clearance was predicted according to Equation 4 as previously proposed by Janku (97):

$$Cl_{renal} = Q_R \cdot \left\{ f_u \cdot F_F + (1 - f_u \cdot F_F) \cdot \left[1 - exp\left(- \frac{f_u \cdot \frac{Cl_{u,int}}{GFR} \cdot F_F}{1 - F_F} \right) \right] \right\} \cdot (1 - F_R) \qquad \text{Equation 4}$$

Where Cl_{renal} represents PAH renal clearance, Q_R represents renal plasma flow (600 mL/min), f_u represents unbound fraction of PAH in plasma (0.8), F_F represents glomerular filtration as fraction of renal plasma flow (0.2), GFR represents the glomerular filtration rate (120 mL/min in healthy subjects), and F_R represents fraction of PAH reabsorbed from the lumen along the tubule. Given that PAH is polar (*LogP* -2.2) and highly ionized at urinary pH (*pKa* = 3.8), tubular reabsorption was assumed to be negligible (F_R = 0).

4.4 Results

4.4.1 Construction and functional characterization of VPT-MPS

The design of the Nortis VPT-MPS and a scheme for modeling the path or steps involved in tubular secretion of a solute is presented in Figure 4.1. This dual channel device permitted the study of solute entry into and extravasation from the endothelial vessel, diffusion across the interstitial matrix, coordinated uptake and efflux of solutes across the tubular epithelium, and finally, collection of solutes in the tubular outflow (Figure 4.1B). In effect, the structure of the VPT-MPS consists of 3 discrete bioengineered compartments: endothelial vessel, interstitial matrix, and epithelial tubule. Initially, proximal tubule epithelial cells were seeded into one channel and allowed to establish a confluent tubule for 5 days. Then, human umbilical vein endothelial cells were used to form the endothelial vessel. Co-culturing of both cell types was limited to the first 24 hours because HUVECs have been shown to form tight junctions after prolonged culture in conventional 2D format (98) (Figure 4.2A). During the initial 24 hours, HUVECs expressed adherent molecule CD31, but had not yet formed tight junctions (lack of ZO-1), thus maintaining the vascular/endothelial phenotype (Figure 4.2B). In contrast, epithelial tubule established from PTECs and cultured for 7 days showed expression of tight junction ZO-1 (Figure 4.2C), demonstrating presence of a formidable cellular barrier. Exclusive presence of CD-31 marker on endothelium and ZO-1 on epithelium (see merged images in Figures 4.2B and 2C) also suggest the lack of any cross-contamination between the 2 cell types in the process of cell seeding and co-culture.

Another critical feature of VPT-MPS was maintenance of epithelial cell polarity (Figure 4.3). In the established culture conditions (i.e., in the presence of serum-defined media and endothelial cells), PTECs continued to expressed Na^+/K^+ ATPase on the basolateral side of the

cells, while tight junction marker ZO-1 were visibly expressed along the lateral and apical borders.

4.4.2 Disposition of FITC-dextran in the VPT-MPS

The spread of FITC-dextran (MW=10 kDa) across all 3 compartments of the VPT-MPS is presented in Figures 4.4 through 4.6. Upon introducing FITC-dextran into the inlet port of the Nortis platform, FITC-associated fluorescence did not appear in the endothelial vessel until app. 30 min afterwards due to the dead volume through the bubble traps. Once FITC-dextran reached the endothelial channel, it rapidly filled the entire endothelial vessel compartment, which was followed by an unrestricted leakage of the marker out of the vessel and into the interstitial matrix. Within the next 10 minutes, FITC-dextran diffused across the interstitial matrix and reached the basolateral side of the epithelial tubule. Representative time-sequenced images of FITC-dextran extravasation and diffusion across the interstitial matrix are shown in Figure 4.4A. A progressive decline in fluorescence intensity across the interstitial distance reflects the diffusion gradient in FITC-dextran concentrations. Also, fluorescence intensity on the basolateral matrix side of the epithelial tubule increased over time: at 80 min, matrix/intra-vessel fluorescence ratio was estimated to be 0.2 (Figure 4.4B).

Since conventional fluorescence microscopy does not allow for removal of out of focus FITC-dextran fluorescence emanating from the matrix above and below the epithelial tubule, we utilized a 2-photon microscope to study the uptake of the marker from the interstitium on the basolateral side of the tubule into the tubule lumen (Figure 4.5). While FITC-dextran readily diffused across the interstitium and accumulated at the basolateral side of the epithelial tubule, it did not significantly translocate into the tubule lumen. The very low level of FITC-dextran fluorescence appearing in the tubule lumen probably reflect access via the paracellular path.

Representative time-sequenced images of FITC fluorescence are shown in Figure 4.5A. An initial sharp decrease in ratio of tubule lumen/interstitium presented in Figure 4.5B was due to rapid buildup of interstitial fluorescence with nearly no increase in tubular lumen fluorescence. The lumen-to-interstitium ratio appeared to have plateaued at 2 hours, to a minimal ratio of 0.01. It is important to note that extended duration of fluorescence imaging in the lower, atmospheric CO_2 environment did not impair the excellent cell viability of either the endothelium or epithelium (Supplementary figure 4.1).

4.4.3 Secretory transport across the epithelial tubule in the VPT-MPS

The disposition or routing of the secretory transport and paracellular markers introduced into the vascular channel were monitored by measuring their effluent concentrations from the endothelial vessel and epithelial tubule channels. Over the course of 8 hours, cumulative recoveries of FITC-dextran, mannitol and PAH from both channels were 97.5%, 85.2% and 91.8%, respectively. As shown in Figure 4.6A and Table 4.1, only trace amounts of FITC-dextran managed to reach the effluent of the tubule (tubule/input ratio of 0.4% at 8 hr), while concentration in the endothelial vessel effluent approached the nominal input level already by 4 hours (vessel/input ratio of 97.1% at 8hr). Like FITC-dextran, mannitol has high polarity and is negatively charged, but it is much smaller in size; it is well-accepted as a marker for paracellular permeability across epithelial barriers (99, 100). At 6-8 hr after initiation of perfusion, mannitol concentration in the vessel effluent began to approach a plateau (Figure 4.6B), somewhat lower than that of FITC-dextran (Table 4.1), possibly due to slower equilibration and/or more extensive distribution in the interstitial space because of smaller molecule size. The level of mannitol in the tubule effluent increased linearly with time and, when standardized to the nominal input, were nearly the same as that of FITC-dextran. PAH was selected as a solute that is known to

translocate across the tubular epithelium by means of passive diffusion and active transport via basolateral uptake and apical efflux transporters (2). The concentration of PAH in the vessel effluent plateaued in 6 hours at a level 75% that of its nominal input, while its concentration in the tubule effluent increased remarkably in an exponential manner over time; it exhibited 5 to 6-fold higher output into the tubular outflow than mannitol and FITC-dextran (tubule outflow/vessel outflow concentration ratio of 2.4%, vs. 0.5% and 0.4%, respectively). The levels of PAH in the tubule effluent were also reduced by 45.8% in the presence of probenecid (Figure 4.6 and Table 4.1), which could be attributed to the inhibition of PAH basolateral uptake via organic anion transporters (OAT1 and OAT3) expressed in the epithelial cells as revealed by immunocytochemistry (Figure 4.7).

4.5 Discussion

Visceral organs, including the kidneys, are highly vascularized, which meets their high metabolic demand for an abundant and efficient supply of oxygen and nutrients. This is also true for delivery of xenobiotics, including drugs, to these organs for detoxification and elimination. Accordingly, the critical need for vascularization of organ or tissue models in a microfluidic platform is well recognized (101, 102). Vascularized MPS has been developed for several organs or tissues, such as the liver (103) and heart (104), as well as tumor-on-chip (105) that employ endothelial cells to form supportive microvasculature. We now report the successful development of a vascularized proximal tubule tissue model (VPT-MPS), a logical progression from our previously established single cell-type proximal tubule model (55). Many improvements and advances are featured in our novel VPT-MPS (a side-by-side comparison of the two models is available in the Supplementary table 4.2). First, VPT-MPS enables controlled

perfusate flow through both channels populated with endothelial and epithelial cells, respectively. Second, while previously devoid, the HUVEC vessel serves as a microvascular conduit for delivery of drugs/compounds to the basolateral side of the epithelial tubule. Third, predictable flow dynamics enable assessments of discrete steps involved in the tubular secretion of drugs/compounds. Depending on the investigative step (Figure 4.1), quantitative assessments of solute concentrations in the output from the tubule and vessel can be performed, or distribution of drugs/compounds within the microfluidic device can be visualized and quantitated by microscopy imaging techniques. For the first time, the salient morphological and functional characteristics of the vascularized proximal tubule are fully investigated, and the utility of the model for pharmacokinetic prediction is further demonstrated through an example of an *in vitro-to-in vivo* scaling of PAH secretory clearance.

Confluent human umbilical vein endothelial cells (HUVECs) are known to develop tight junctions during prolonged culturing. However, when time in culture is controlled and with appropriate choice of culture media, HUVECs can maintain its porous permeability, a hallmark of the peritubular microvasculature (89). This was convincingly demonstrated by the ready and rapid release of FITC-dextran into the interstitial matrix. Furthermore, we demonstrated that the epithelium severely limited the entry of a small-to-medium size solute (10 kDa FITC-dextran) into the tubule lumen, which attests to the integrity of tight junctions expressed in epithelial cells (and lack thereof in the endothelial cells). Thus, VPT-MPS has the appropriate barrier characteristics to serve as an in vitro model for investigations of renal tubular secretion of xeno- and endobiotics.

FITC-dextran and mannitol were employed in the study to define the extent of paracellular diffusion across an epithelial tubule. PAH, a substrate for renal transporters, was

approximately 5-fold more efficiently secreted than mannitol (and 6-fold more extensively secreted than FITC-dextran); the process was partially blocked by a known OAT and MRP transporter inhibitor probenecid. We further undertook in vitro-to-in vivo scaling to predict the renal clearance of PAH based on the intrinsic secretory clearance data obtained from our VPT-MPS. As seen in Table 4.2, the predicted value of PAH renal clearance reasonably approximated (within 3-fold) previously of reported in vivo PAH renal clearance (93).

One limitation with the construction and functioning of the VPT-MPS is the relatively large interstitial distance between the vessel and tubule (~ 1000 μm) compared to what is observed *in vivo* in the human tubule-interstitium, where the approximate distance of the interstitium typically does not exceed a single cell diameter (1). This technical limitation is a common problem observed in other organ-on-chip models and is primarily a physical limitation imposed by the design and architecture of current microfluidic devices (101). The increased distance between the vessel and tubule helped to stabilize the flow characteristics. Importantly, the resultant steady flow dynamics allowed us for the first time to reproducibly assess solute output rate from the tubule channel via serial collection of perfusate outflow. While diffusional distance may complicate kinetic studies critical for quantifying solute secretion by the proximal tubule, there are possible ways to minimize/overcome the interstitial diffusional gap. One possibility is to create branching of the endothelial vessel towards the epithelial tubule by laser boring 3D culture, i.e., branches perpendicular to the existing endothelial channel that shortens the diffusional distance between the two structures. More recently, 3D-bioprinting techniques could potentially create the desired distance between endothelial PTEC channels. Such modification of the existing VPT-MPS would create an endothelial network that better mimics

the renal peritubular microvasculature in vivo and achieve closer proximity to the epithelial tubule.

What are the potential applications of a vascularized proximal tubule tissue model? Although not an aim in this study, VPT-MPS could potentially allow assessment of intracellular accumulation to provide critical kinetic data for modeling the transepithelial transport kinetics of xenobiotic solutes (106, 107). Such approach could then lay foundation for further investigation of underlying mechanisms of drug intratubular toxicity (e.g., tenofovir, (108)). In time, we envision this model to accommodate novel kinetic studies involving small drug molecules bound to plasma proteins (e.g., albumin) or extensively carried by blood cells, as well as therapeutic proteins and nanoparticle drug delivery systems. For example, the presence of a porous endothelial vessel and accompanying collagen I matrix could offer the possibility of studying extravasation of protein and red blood cell-bound solutes into the interstitium, and allows for study of the role of binding-and debinding kinetics of solute highly bound to carrier protein(s) on its access to active transport across the epithelial tubule. Just as important, the VPT-MPS may also be applied to studying the effects of disease states, such as chronic kidney disease (CKD). Currently, cells isolated for culture in the MPS are obtained from the healthy margins of surgically resected renal carcinomas. Cells from individuals with existing tubulo-interstitial disease can also be used to model the effects of these diseases on drug/solute handling by the proximal tubule *in vitro*. This way, multiple underlying mechanisms involving kidney diseases can further be elucidated, such as downregulation or direct inhibition of drug solute transporters caused by circulating endogenous molecules, or if individuals with preexisting kidney disease are more susceptible to nephrotoxins (38, 109, 110). In all likelihood, modelling of tubule-interstitial disease would involve populating the between-channel matrix with relevant interstitial

cell types. To date, we have attempted culturing pericytes in the interstitial matrix with some success (data not shown); thus, it is feasible to creating a triple cell type MPS. We can conceive of further enhancement by incorporating interstitial co-culture of inflammatory cells. The ultimate goal would be to provide a model that offers the possibility of comprehensively evaluating the multifactorial causes and consequences of chronic kidney disease.

In conclusion, we have successfully established and characterized a vascularized kidney proximal tubule model in the Nortis dual-channel microfluidic platform. This model provides the opportunity for further development geared towards the complete reconstruction of a human tubule-interstitium.

4.6 Figures

Figure 4.1. Vascularized proximal tubule MPS (VPT-MPS) construct.

(A) Nortis dual channel platform used for the establishment of vascularized proximal tubule MPS (VPT-MPS). Extracellular matrix space is depicted in pink, vascular media flow path is shown in red and tubular media flow is shown in blue. **(B)** Biologically-relevant steps of proximal tubule renal secretion modeled in the VPT-MPS. **(1)** Entry of solute into peritubular capillaries. **(2)** Extravasation of solute into interstitial space. **(3)** Diffusion of solute across the intervening interstitium. **(4)** Partitioning and facilitated uptake of solute across basolateral epithelial cell membranes. **(5)** Passive partitioning and facilitated efflux of solute across apical epithelial cell membranes. **(6)** Passage of solute into distal portion of nephron.

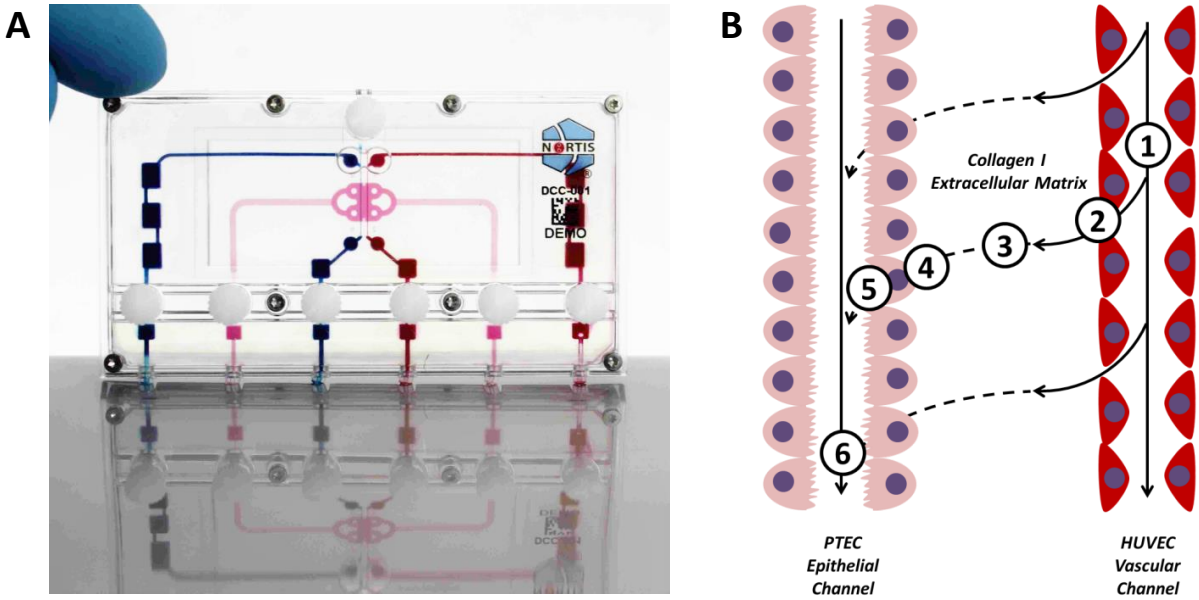

Figure 4.2. Morphological characterization of co-culture in the VPT-MPS.

(A) Step-wise establishment of an epithelial – endothelial co-culture within the VPT-MPS; (i) and (ii) are bright field images of the bioengineered co-culture in the collagen I matrix, (iii) blue fluorescence depicts cell nuclei in epithelial and endothelial cells. Scale bar: 500 µm (40x magnification). **(B)** Endothelial vessel expressed CD-31 (surface expression pointed with arrows), but not ZO-1. **(C)** Epithelial tubule expressed ZO-1, but not CD-31. Fluorescent and differential interference contrast (gray color) images were generated under (B) and (C); 200x magnification. Average epithelial tubule and endothelial vessel diameter is 120 µm. Representative images of cells isolated from a single donor (characterization was reproduced in cells from 3 donors total).

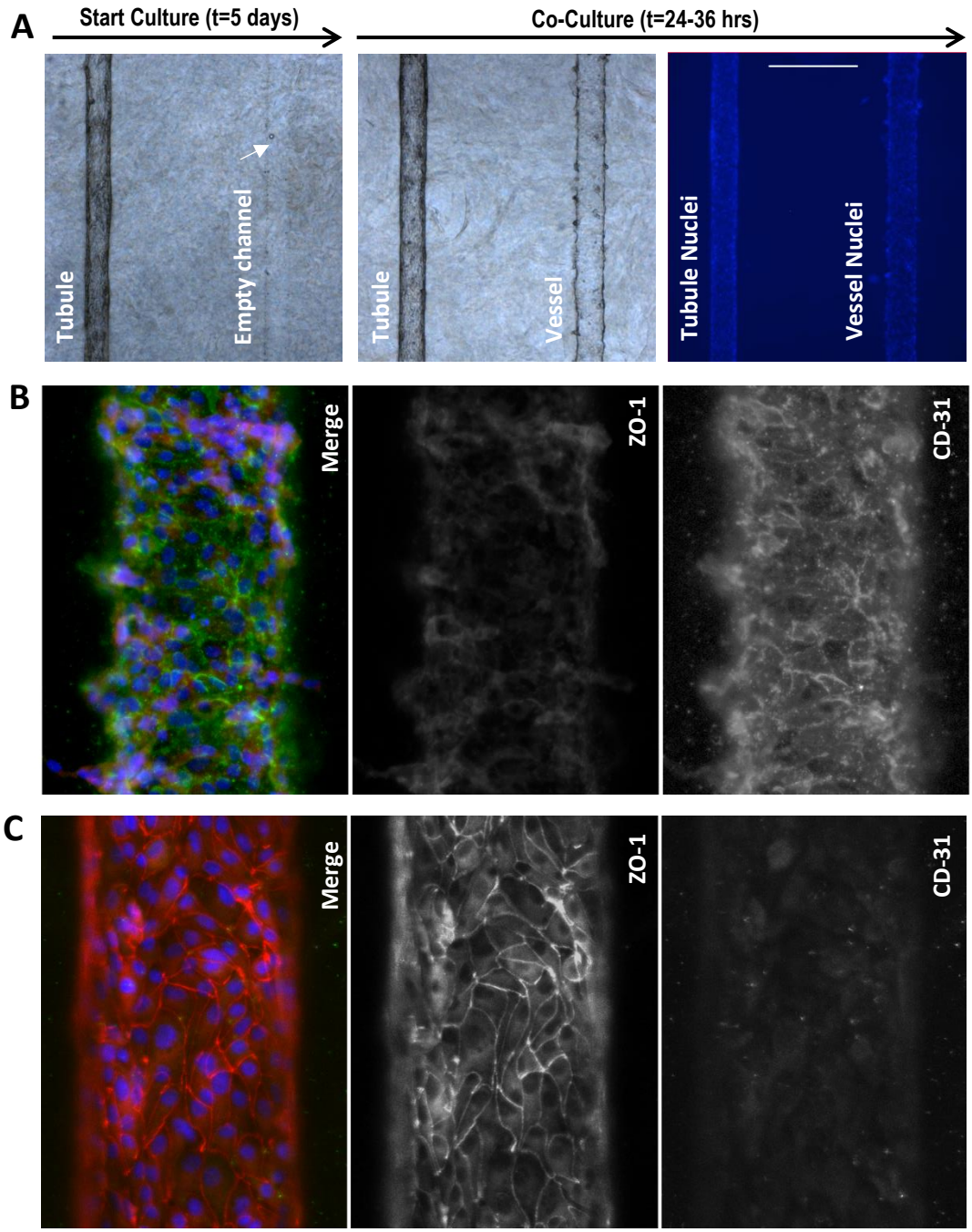
A
Start Culture (t=5 days)
Co-Culture (t=24-36 hrs)
Tubule
Empty channel
Tubule
Vessel
Tubule Nuclei
Vessel Nuclei
B
Merge
ZO-1
CD-31
C
Merge
ZO-1
CD-31

Figure 4.3. Polarized epithelium in the VPT-MPS.

Human proximal tubule epithelial cells in VPT-MPS maintained polarity as demonstrated by basolateral Na^+/K^+ ATPase signal adjacent to the interstitium (red) and ZO-1 signal (green) at the borderline between lateral and apical cellular domains (i.e., toward the tubule lumen). Nuclei are stained in blue. Top left is a merged cross-section image of the tubule, the other 3 images show tubule viewed as a monolayer from the top under 200x magnification. Images of cells isolated from a single donor.

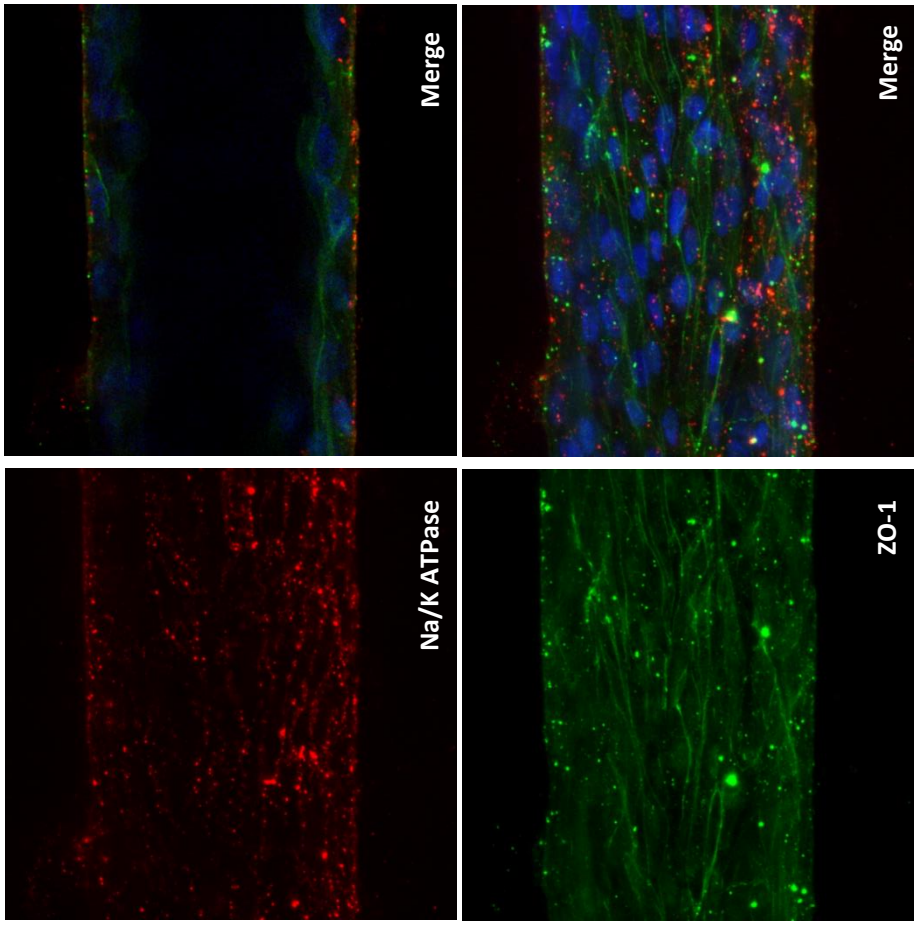

Figure 4.4. Fate of FITC-Dextran in the VPT-MPS.

(A) Fluorescent images showing extravasation of FITC-Dextran and diffusion across the interstitial matrix (diffusional distance ~ 1000 μm) to the epithelial tubule over time. Scale bar: 500 μm (40x magnification); γ-function transformation=0.30. **(B)** Build-up of fluorescence in the matrix adjacent to basolateral aspect of the epithelial tubule relative to fluorescence within the endothelial vessel. Times given are after start of perfusion; initial time delay occurred due to dead volume through bubble traps. Data points at each time represent duplicate experiments using cells from 2 separate donors.

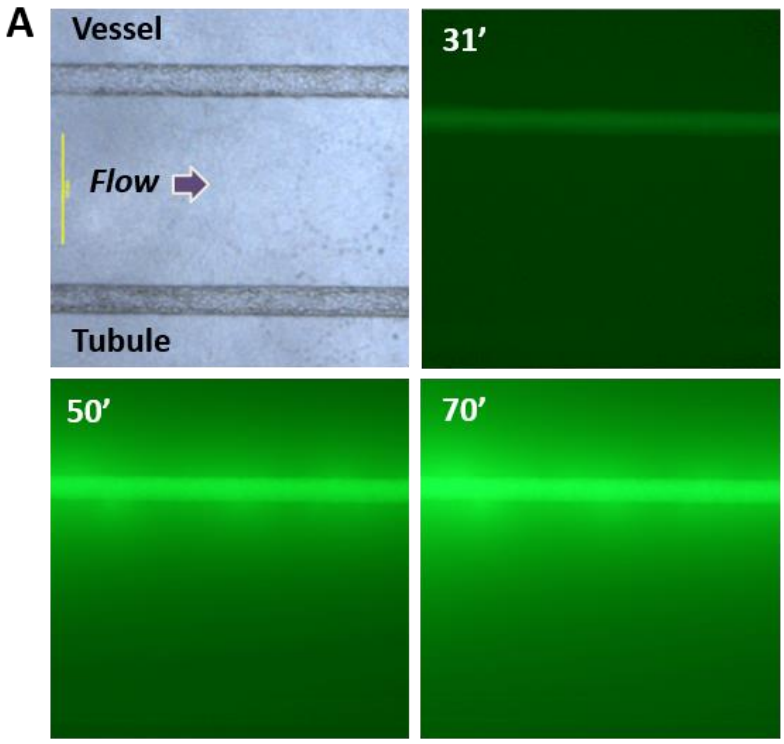
A
Vessel
Flow
Tubule
31'
50'
70'

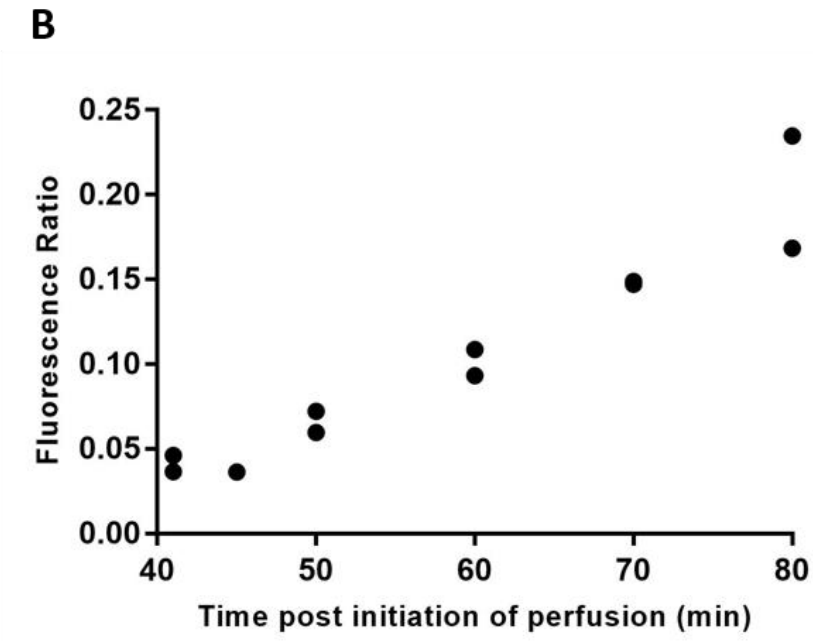
B
Fluorescence Ratio
0.25
0.20
0.15
0.10
0.05
0.00
40
50
60
70
80
Time post initiation of perfusion (min)

Figure 4.5. The extent of FITC-Dextran translocation across the tubular epithelium into the lumen over time.

(A) Representative images of FITC-Dextran accumulation on the basolateral side of the tubular epithelium. Elimination of out-of-plane fluorescence highlighted the true extent of FITC-Dextran translocation; 200x magnification. **(B)** Time-dependent decrease in fluorescence tubule/interstitium ratio; the ratio plateaued at approximately 2 hours. Changes in ratio were due to increased interstitial fluorescence accumulation. Times given are after start of perfusion; initial time delay occurred due to dead volume through bubble traps. Data points compiled from 2 separate experiments (each experiment with a different donor).

A

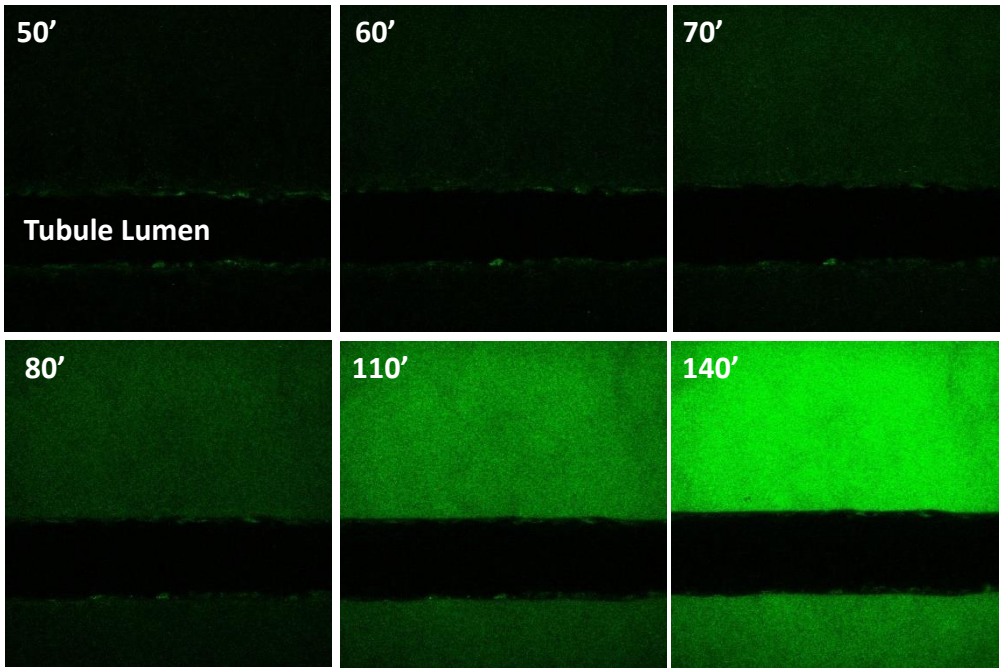
50’
60’
70’
Tubule Lumen
80’
110’
140’

B

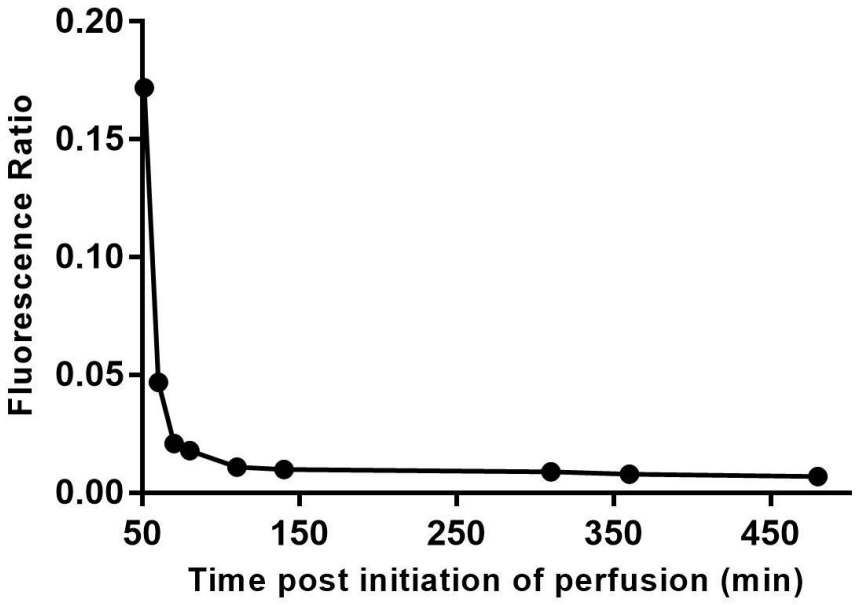
0.20
0.15
0.10
0.05
0.00
Fluorescence Ratio
50
150
250
350
450
Time post initiation of perfusion (min)

Figure 4.6. Handling of secretory transport and paracellular markers in the VPT-MPS. Graphs show concentration-time course of solutes (mean ± SD, or individual data points) when sampled from the respective effluents of endothelial vessel and epithelial tubule. Dotted horizontal line represents vascular input concentration. **(A)** FITC-Dextran. **(B)** Mannitol. **(C)** *p*-aminohippuric acid (PAH) in the absence or presence of inhibitor probenecid (2 mM).

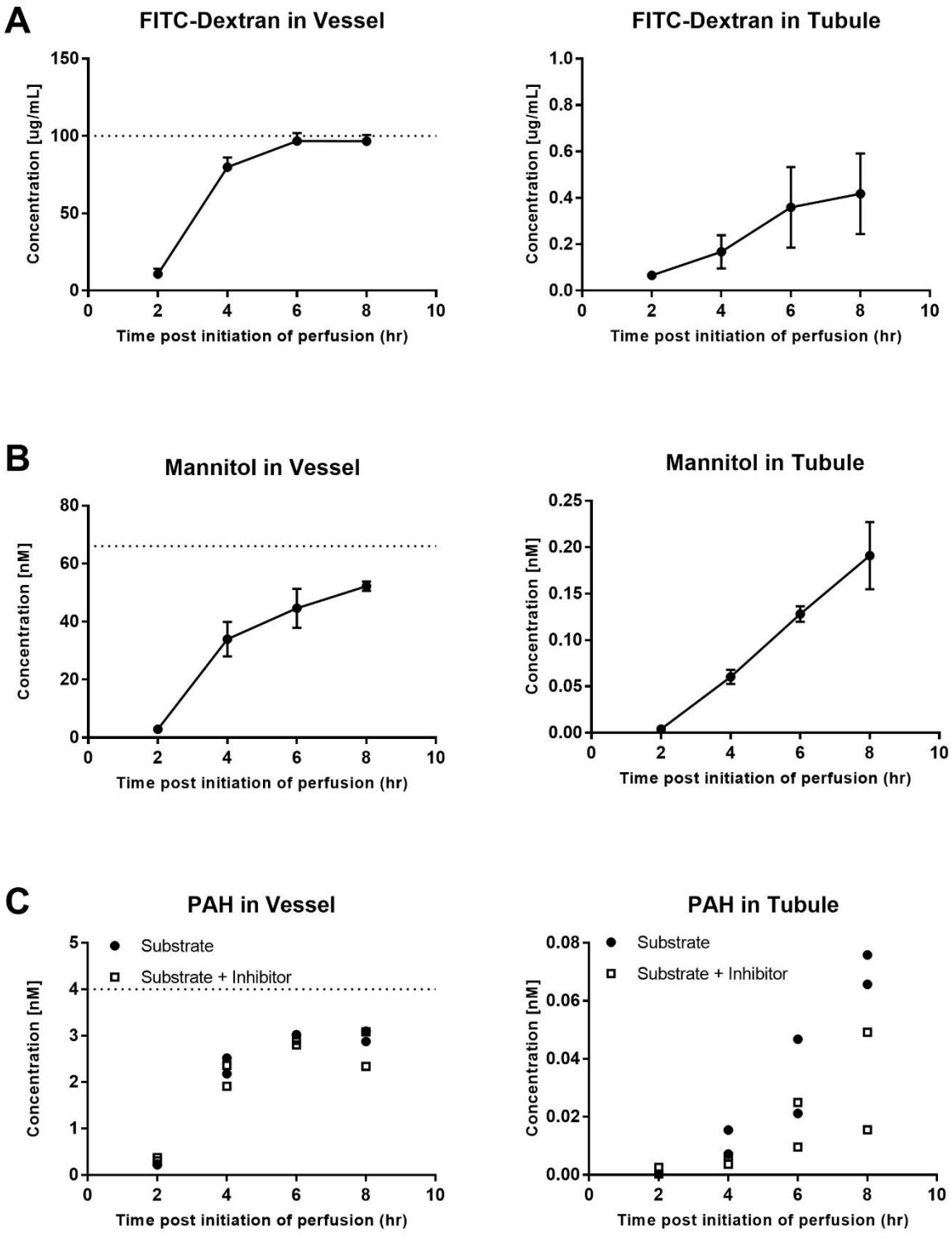
A
FITC-Dextran in Vessel
Concentration [ug/mL]
Time post initiation of perfusion (hr)
FITC-Dextran in Tubule
Concentration [ug/mL]
Time post initiation of perfusion (hr)
B
Mannitol in Vessel
Concentration [nM]
Time post initiation of perfusion (hr)
Mannitol in Tubule
Concentration [nM]
Time post initiation of perfusion (hr)
C
PAH in Vessel
Substrate
Substrate + Inhibitor
Concentration [nM]
Time post initiation of perfusion (hr)
PAH in Tubule
Substrate
Substrate + Inhibitor
Concentration [nM]
Time post initiation of perfusion (hr)

Table 4.1. Handling of solutes in the VPT-MPS.

Concentration data (mean ± SD) of FITC-Dextran (n=7 VPT-MPS), mannitol (n=5 VPT-MPS) and PAH (± probenecid, n=2 VPT-MPS per treatment group) in the effluents at the last collection interval (t=8 hr). Data are either standardized per nominal input, or concentrations in the tubule effluent are compared to that of the concentration in the vessel. VPT-MPS were constructed from cells isolated from 1 donor (PAH), 2 donors (mannitol), or 3 donors (FITC-Dextran).

	Vessel / Input (%)	Tubule / Input (%)	Tubule / Vessel (%)
FITC-Dextran	97.1 ± 4.1	0.4 ± 0.4	0.4 ± 0.4
Mannitol	84.8 ± 8.0	0.4 ± 0.2	0.5 ± 0.2
PAH	89.7	2.1	2.4
PAH (+ probenecid)	81.4	1.0	1.3

Figure 4.7. Determination of transporter expression in PTECs via immunocytochemistry. Cells expressed Organic Anion Transporter 1 (green, left image) and Organic Anion Transporter 3 (green, right image). Nuclei are shown in blue. Average diameter of the tubule is 120 µm (200x magnification). Representative images of cells isolated from a single donor (characterization was reproduced in cells isolated from 2 donors total).

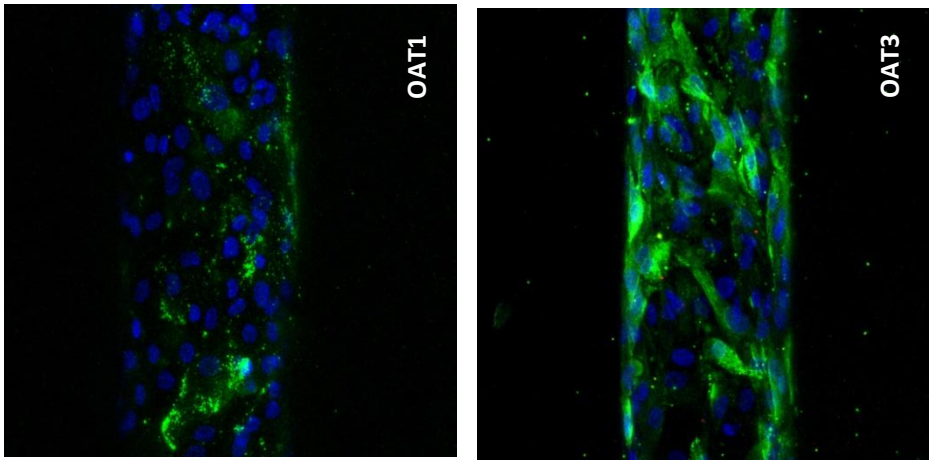

Table 4.2. In vitro-to-in vivo scaling of VPT-MPS secretory clearance data to predict *in vivo* renal clearance of PAH.

Concentrations in the effluent and input were measured from 8-hour collection interval.

Estimation of PAH permeability-surface area product per VPT-MPS		
PA = 0.0345 µL/min		
Estimation of scaling factor		
Parameters	**VPT-MPS**	***In vivo* (human)**
Length (l)	6 mm	15 mm
Diameter (2r)	120 µm	70 µm
Surface area (estimated as π*2r*l)	2.26 mm^2	3.29 mm^2
Ratio	3.29 mm^2 / 2.26 mm^2 = 1.46	
Predicted *in vivo* tubular clearance of PAH		
Cl = 0.0345 µL/min * 1.46 *1,000,000 proximal tubules per kidney * 2 kidneys = 100.74 mL/min		
Predicted *in vivo* renal clearance of PAH		
Cl = 173.9 mL/min		
Ratio observed/predicted renal clearance of PAH		
490 mL/min / 173.9 mL/min = 2.82		

4.7 Supplementary materials

Supplementary table 4.1. Donor information on kidney tissues used for isolation of proximal tubule epithelial cells.

Abbreviations: RCC, renal cell carcinoma.

Donor	Age	Sex	Ethnicity	Pre-existing Conditions	Reason for Nephrectomy	Final Pathology
1	64	Male	White	Diverticulosis, hyperlipidemia, hypothyroidism	Renal mass (right)	Chromophobe RCC
2	53	Male	White	HTN	Renal mass (right)	Clear cell RCC
3	67	Male	White	Prostate cancer, ulcerative colitis	Renal mass (left)	Chromophobe RCC
4	58	Male	White	HTN, hernia	Renal mass (right)	Unclassified RCC with clear cell features
5	62	Female	White	HTN, GERD, previous cervical, thyroid and breast carcinoma	Renal mass (unspecified)	Not available
6	40	Male	African American	Methamphetamine use, Deep Vein thrombosis	Renal mass (left)	Clear cell RCC
7	65	Male	White	None reported	Renal mass (unspecified)	Not available

Supplementary figure 4.1. Cell viability in atmospheric CO_2.

Tubule (consisting of human PTECs) and vessel (consisting of HUVECs) in VPT-MPS maintain excellent cell viability for up to 8 hr when exposed to atmospheric CO_2 during time lapse functional imaging studies.

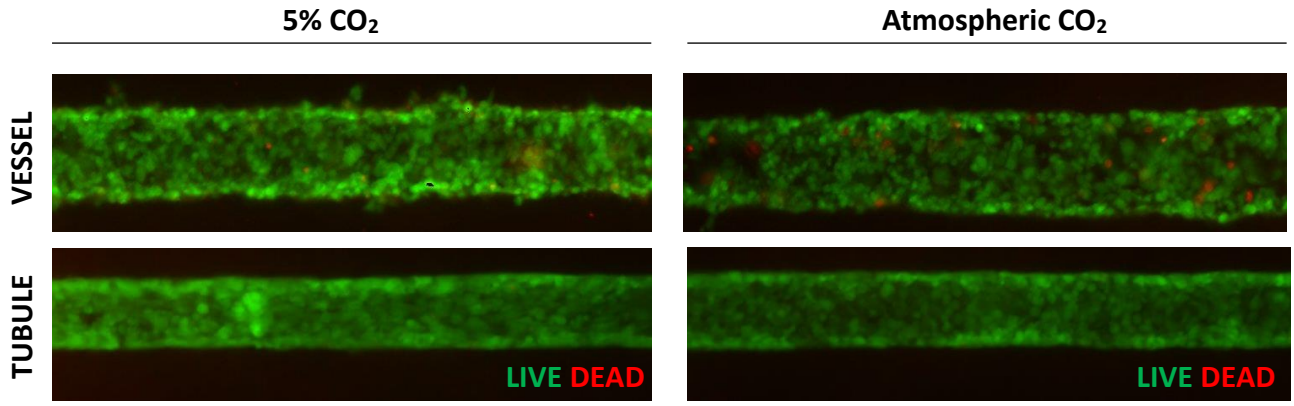

Supplementary table 4.2. Evolution of an *in vitro* vascularized proximal tubule MPS (VPT-MPS).

A side-by-side comparison and improvements in vascularized PT-MPS relative to previously established single-cell MPS model (PT-MPS). "X" denotes either not possible or not tested in a particular model.

Key Characteristics	Model Features	**PT-MPS**	**Vascularized PT-MPS**
		Experimental set-up	
Type of platform		Nortis non-commercial (beta) dual channel platform	Nortis commercial dual channel platform
Design of a transport model	Cell type(s)	Human proximal tubule epithelial cells (PTECs): polarized epithelium	Human proximal tubule epithelial cells (PTECs): polarized epithelium
		X	Human umbilical vein endothelial cells (HUVECs): adhered, leaky and permeable endothelium
	Cell-culture media	Hormonally defined DMEM/F12	PTEC: Hormonally defined (with addition of 2% FBS) DMEM/F12, HUVEC: Lonza endothelial cell culture media
	Interstitium	Collagen I matrix with Collagen IV channel overlay	Collagen I matrix with Collagen IV channel overlay
Perfusion characteristics		Semi-predictable flow dynamics	Controlled flow through both channels
		Solute disposition	
Quantitative effluent sampling	Collection interval	Cumulative 4 hours	Q2: through 8 hours
	Attainment of steady-state levels	X	√ (Vessel)
	Measurement read-out	Solute amount	Solute concentration
	Solutes tested	Solutes subject to active transcellular transport	Solutes subject to active transcellular transport and paracellular transport
Semi-quantitative cell/matrix-associated fluorescence imaging	Measurement interval	X	8 hours
	Attainment of steady-state levels	X	√
	Cell-associated fluorescence (relative to channel/interstitium)	X	√

Supplementary figure 4.2. No primary antibody controls (negative controls) from immunocytochemistry experiments.

A: negative control for figure 4.2B (left), and figure 4.2C (right). B: negative control for figures 4.3 and 4.7. Nuclei are depicted in blue. Red and green fluorescence are nearly absent. Average tubule and vessel diameter: 120 µm (200x magnification).

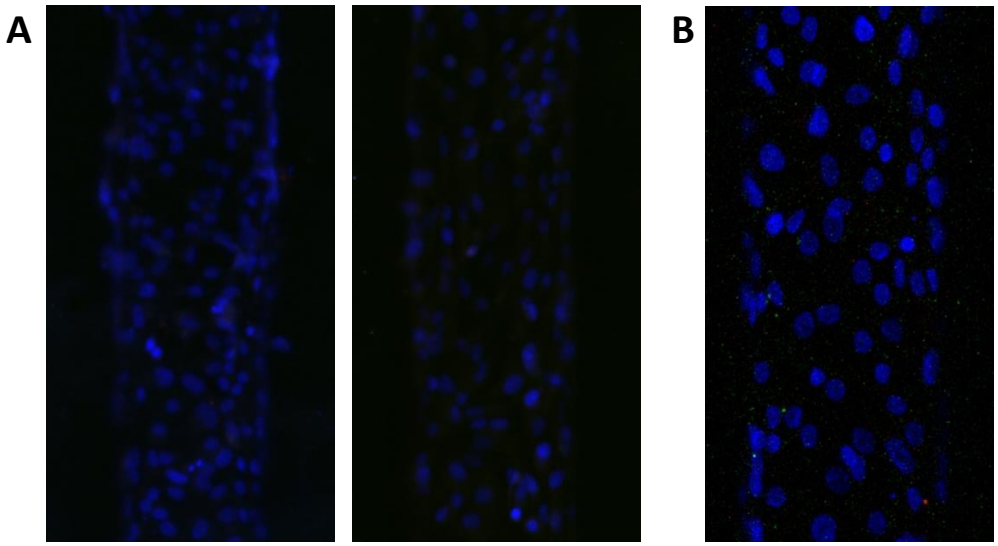

Supplementary figure 4.3. Estimation of concentration gradient across the interstitial matrix in the VPT-MPS.

(A) Time course of FITC-Dextran-associated fluorescence accumulation on the basolateral side of the epithelial tubule. Fluorescence starts plateauing at 180 minutes. (B) Estimation of concentration gradient across the interstitial matrix at and after 180 minutes by extrapolation of matrix/vessel fluorescence ratio results presented in Figure 4.4. Extrapolation was conducted by means of simple linear regression; equation is available as the graph inset.

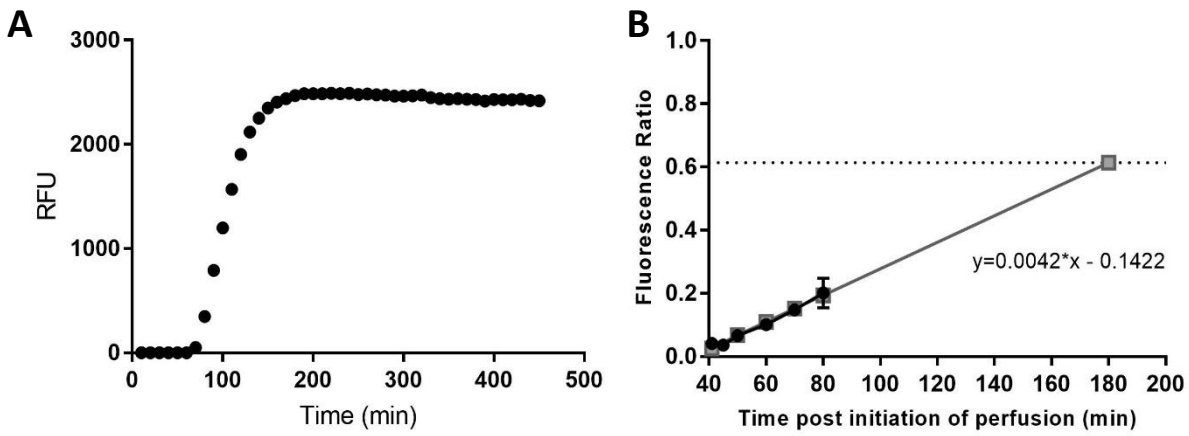

5 Does Secretory Clearance Follow Glomerular Filtration Rate in Chronic Kidney Diseases (CKD)? Reconsideration of the Applicability of Intact Nephron Hypothesis

This chapter was published in its entirety in Clin Transl Sci. 2017 Sep;10(5):395-403.

5.1 Abstract

Dose modification in CKD is based on the assumption that renal excretory processess decline in parallel in CKD. We collected published pharmacokinetic data to assess if measures of glomerular filtration rate (GFR) predict renal clearance changes across CKD severity. For each drug, we calculated $R_{nf,}$ a ratio of renal clearance to filtration clearance. Tweny-one drugs had R_{nf}>0.74 in subjects with GFR>90ml/min, implying filtration and secretion. Thirteen drugs with R_{nf}>0.74 displayed statisticallysignificant change in R_{nf} across GFR (defined as slope of linear regression being statistically different from zero), indicating failure of GFR to predict changes in drug renal clearance/secretory clearance across CKD severity. The dependence was either positive (n=3, Group A) or negative (n=10, Group B). Eight drugs did not show significant correlation (Group C). Investigated drugs were small molecules, mainly hydrophilic, with multiple pKa values. Some were previously characterized as substrates of renal transporters. In conclusion, dosing adjustment in CKD requires a redefinition that, in addition to GFR, includes measures of tubular secretion.

5.2 Introduction

Clearance of drugs that mainly occurs via renal excretion is compromised in patients with chronic kidney disease (CKD). To avoid systemic drug accumulation and adverse reactions in this population, the dosage of renally eliminated drugs requires appropriate reduction. Despite the fact that renal clearance of most medications occurs via secretion by the proximal tubule of the kidneys, dosing adjustment in renal impairment has traditionally relied on serum creatinine as a biomarker of deteriorating glomerular filtration and overall renal function. While creatinine-based approach has been successful for some drugs (eg, with older antibiotics), universal applicability has been questioned (111, 112), with reports appearing as early as 1972 of dose adjustment failures (eg, chlorpropamide; (113)).

The estimation of drug renal clearance reduction using creatinine clearance is based on the "intact nephron hypothesis," which proposes that all renal excretory processes (i.e., filtration, tubular secretion and reabsorption) decline in parallel with disease progression (114, 115). Therefore, it is generally assumed that for a given decline in creatinine clearance in CKD, the decrease in renal clearance of a drug that is either extensively secreted and/or reabsorbed is reduced to approximately the same degree as one that is neither reabsorbed nor secreted (116). Thus far, no systematic investigation or analysis of this assumption has been reported.

There are several reasons to suspect that glomerular filtration and proximal tubule secretion vary among people who have CKD. First, "CKD" encompasses a wide range of kidney diseases that differentially impact the glomeruli, tubules and renal interstitium. Second, proximal tubule secretion is an active, cell-based process, whereas glomerular filtration is passive and primarily determined by size and charge selectivity of the basement membrane. Third, secretion

is subject to inhibition by retained solutes and other medications, whereas filtration is generally impervious to the solute load.

With the present analysis of available literature to-date, our aim was to evaluate whether creatinine clearance (or other measures of glomerular filtration) accurately predict alterations in drug renal clearance across mild to severe stages of CKD. In the long term, the findings may point to the need for further investigation into factors that modulate drug renal clearance in CKD, which in turn may lead to an improved strategy for renal dosing algorithms that would advance personalized use of medications in patients with CKD.

5.3 Methods

5.3.1 Literature review

We created a list of drugs for which pharmacokinetics in renal impairment have previously been characterized. Data were collected from the University of Washington Drug Interaction Database (www.druginteractioninfo.org, accessed in 1/2016) and PubMed (www.ncbi.nlm.nih.gov/pubmed, accessed between 8/2015 and 2/2016). The Pubmed searches were conducted with the following terms: drug name AND pharmacokinetics AND renal impairment. When published data were presented in the form of a graph, relevant portions of the data were extracted with Plot Digitizer 2.6.6 (www.plotdigitizer.sourceforge.net). Only reports showing drug renal clearance data from individual subjects over a range of glomerular filtration rate (GFR) and not receiving dialysis treatment were considered for our analysis; ie, we did not consider reports showing only mean values of drug renal clearance, total (renal and non-renal) drug clearance, or *AUC* data for each stage of CKD. We included all studies irrespective of the chosen measure of GFR (estimated GFR by Cockroft-Gault or Modification of Diet in Renal

Disease - MDRD equation, measured GFR based on creatinine, inulin or ^{51}Cr-EDTA clearance). Publications reporting only drug renal clearance in healthy subjects and patients with severe renal impairment (ie, abbreviated pharmacokinetic studies typically performed for New Drug Applications) were not considered. In order to account for changes in drug plasma protein binding, we collected information on the plasma unbound fraction (f_U) of the drugs on our list. The f_U drug data were recorded either as mean f_U values per CKD stage, or f_U values obtained from healthy subjects with values ≥ 0.80. The latter data were accepted under the assumption that in CKD, plasma protein binding is expected to decrease; hence, only a negligible change in f_U would occur, at a maximum of 20%. When not available in the original publication, the f_U data was collected from DrugBank (www.drugbank.ca, accessed between 8/2015 and 2/2016) or in the case of *p*-aminohippuric acid (PAH) separate literature publications were located (117). For drugs that were included in the final analysis, additional information, such as interaction with renal transporters from reported *in vitro* and *in vivo* studies as well as relevant physico-chemical characteristics (molecular weight, logP, pKa), was collected from the University of Washington Drug Interaction Database, DrugBank, PubChem (https://pubchem.ncbi.nlm.nih.gov/, accessed between 8/2015 and 2/2016) and ChEMBL (ChEMBL, accessed between 8/2015 and 1/2016).

5.3.2 Index for the contribution of non-filtration processes to the overall renal drug clearance

Renal clearance (*Cl renal*) of a drug is described by the following equation (117):

$$Cl\,renal = (fu \cdot GFR + Cl_S) \cdot (1 - Fr) \quad (1)$$

where $fu * GFR$ represents filtration clearance of unbound drug, Cl_S represents secretory clearance, and Fr represents the fraction of the filtered and secreted drug that is subsequently

reabsorbed (via passive and active processes). We estimated filtration clearance of a drug by multiplying individual GFR by the average plasma unbound fraction appropriate for either healthy renal function or subject's stage of CKD. The ratio of $Cl\ renal$ divided by $fu * GFR$ (R_{nf}) is defined as an index to indicate the impact of non-filtration processes upon drug renal clearance (*ie*, either dominance by secretion or reabsorption).

$$R_{nf} = \frac{Cl\ renal}{fu \cdot GFR} = \left(1 + \frac{Cl_S}{fu \cdot GFR}\right) \cdot (1 - Fr). \quad (2)$$

Equation 2 shows that R_{nf} is a function of $Cl_S/(fu \cdot GFR)$ and Fr representing the discrete process of secretion and reabsorption, respectively. According to Equation 2, when $Cl\ renal >> fu * GFR$ in healthy subjects, the drug undergoes net secretion; when $Cl\ renal << fu * GFR$ in healthy subjects, the drug undergoes net reabsorption. Drugs that have a value of R_{nf} close to 1 may undergo glomerular filtration only, or are subjected to an opposing interplay between tubular secretion and reabsorption resulting in a net loss that is more reflective of glomerular filtration.

Our analysis was focused on alterations in the contribution of tubular secretion to renal clearance across the range of CKD; hence, we selected those drugs for which passive reabsorption along the renal tubule is likely to be negligible based upon their physicochemical characteristics (ie, being highly ionized at the luminal filtrate pH). Accordingly, we confined our analysis to drugs with $R_{nf} > 0.74$, a cut-off value set below unity to allow for inter-subject variability we observed in collected GFR in subjects with GFR ≥ 90 mL/min (mean GFR of all studies = 128.6 mL/min with corresponding coefficient of variation = 26%). Thus, $R_{nf} > 0.74$ assures the likelihood that we are dealing with drugs that do not undergo significant net reabsorption in renal tubule, thus avoiding its complication in data interpretation. In the absence of reabsorption ($Fr = 0$), Equation 2 simplifies to:

$$R_{nf} = \frac{Cl\ renal}{fu*GFR} = \left(1 + \frac{Cl_S}{fu \cdot GFR}\right). \quad (3)$$

5.3.3 Differential alterations in renal filtration and secretory processes in CKD

According to the intact nephron hypothesis, secretion and reabsorption processes of a drug decline in parallel with glomerular filtration in CKD; if so, R_{nf} should remain constant across the range of GFR. In contrast, any disproportionate decline in tubular secretion (or reabsorption) relative to glomerular filtration would result in changes in ratio across the range of GFR, which can be presented graphically by plotting R_{nf} as a function of GFR. When R_{nf} increases as GFR declines, secretion clearance declines more slowly than GFR; ie, tubular secretion is better preserved than filtration as disease progresses. For the opposite scenario, ie, when R_{nf} decreases as GFR declines, tubular secretion deteriorates more rapidly than GFR with advancing kidney disease.

5.3.4 Statistical analysis

All statistical analyses were performed in Microsoft Excel and R statistical software (www.R-project.org). A linear regression was used to assess a significant change in R_{nf} (outcome variable) across GFR (predictor variable) by estimating if slope of regression coefficient statistically differs from zero. For each drug, the slope of the linear regression was estimated as a measure of the direction and steepness of the dependence. Based on the regression coefficients, we estimated a fold-change in ratio when GFR decreases from 90 ml/min (value in healthy subjects) to 30 ml/min (CKD stage 3B, www2.kidney.org/professionals/KDOQI/guidelines_ckd/p4_class_g1.htm), which represents

another quantitative measure of the average degree of dissociation in the decline in secretory clearance versus that in GFR.

5.4 Results

Relevant pharmacokinetic data on 27 drugs were found in the literature; in the majority of cases (44%), glomerular filtration rate as an index of CKD progression was determined by measuring 24-hour creatinine clearance. Limited data was available regarding changes of drug plasma protein binding in CKD, with mean f_U values for each CKD stage available only for 7 drugs. The rest of the drugs in the dataset had negligible or low plasma protein binding as reported in healthy subjects. In the original dataset, the estimated R_{nf} in healthy subjects ranged from 28.4 (olmesartan) to 0.11 (lacosamide). A large span in ratio indicates a diverse dataset of solutes with respect to their renal handling, incorporating drugs that, in addition to glomerular filtration, either predominantly undergo proximal tubule secretion, tubular reabsorption, or a mix of both processes.

Of the original dataset, 21 drugs had an estimated $R_{nf} > 0.74$ that indicates minimal or absence of tubular reabsorption; a summary of the relevant parameters for this subset of drugs is presented in Table 5.1. Graphical displays of R_{nf} as a function of GFR for all 21 drugs can be found in Supplementary Materials. Linear regression analysis showed that 13 drugs (62%) displayed statistically significant change in R_{nf} (outcome variable) across GFR (predictor variable), as defined by the slope of linear regression being statistically different from zero. The ratio of renal clearance to filtration clearance thus did not remain constant with disease progression. We further divided drugs in Table 5.1 into the three following groups; **Group A**: significant *increase* in R_{nf} as GFR declines with disease progression; **Group B**: significant

decrease in R_{nf} as GFR declines; **Group C**: no change in R_{nf} across the range of CKD. Typical examples of the R_{nf} versus GFR plots for each of the three classes are shown in Figure 5.1. For all 3 drugs in Group A, an increase in ratio represents a less than proportional decline in drug renal clearance (presumably reflective of secretory clearance) as compared to filtration clearance, indicating preservation of secretory component of renal clearance at later stages of CKD. The GFR significantly under-predicted renal clearance by an average of 20 to 32% in moderately impaired CKD patients (CKD stage 3B). Notably, one of drugs/solutes that showed such behavior is PAH, a marker of renal plasma flow. Among 10 drugs in group B, some have previously been cited as being extensively secreted via the proximal tubule, such as olmesartan, penciclovir, and metformin. A significant decrease in the R_{nf} as GFR decline for drugs in group B indicates a more pronounced decline of drug renal clearance or secretory clearance than GFR. Specifically, the GFR significantly over-predicted renal clearance, on average, by 22 to 48% in moderately impaired CKD patients (CKD stage 3B). For drugs in both Group A and Group B, the most pronounced change in R_{nf} is observed at severe stages of CKD (Supplementary Material). For example, the absolute value of R_{nf} for olmesartan decreased from 22.1 in healthy subjects to 15.6 in CKD stage 3B (Figure 5.1). Eight drugs that did not display statistically significant correlation indicating no change in R_{nf} as CKD progresses, were assigned to group C. R_{nf} in healthy subjects appears to differ among the three groups; Group A had the highest median value of 3.89 (range 5.32 – 2.79), followed by Group B with median value of 1.86 (range 28.4 – 0.79), and lastly Group C with a median value of 1.55 (range 16.30 – 0.81). Many of the drugs from Group A, B and C are reported to be substrates for (multiple) renal transporters.

Table 5.2 shows six drugs which had an estimated ratio in healthy subjects ≤ 0.74, ie, tubular reabsorption is quite evident. All these drugs failed to show statistically significant

deviation of regression slope from zero, implying that passive reabsorption declines in parallel with GFR. Scarce information on interaction with renal transporters exists for drugs in Table 5.2. One of these drugs—fluconazole has been used as a marker of passive distal tubular reabsorption (111).

We compiled the physico-chemical characteristics of the 27 drugs in Table 5.3, specifically their molecular weight, lipophilicity (LogP), ionization (pKa), and charge at physiologic pH. These characteristics should govern the extent of drug passive reabsorption at distal parts of the nephron. All investigated drugs were small molecules with molecular weights up to 650 g/mol (naloxegol having the highest), mainly hydrophilic as indicated by most LogP being below 1 to 2 (with just a few exceptions, eg. olmesartan, mirabegron, 5-HMT), and contain more than one weakly acidic or basic functional groups, generating multiple pKa values. The majority of the drugs that are neutral at physiologic pH were shown to have an estimated R_{nf} in healthy ≤ 0.74 (i.e., drugs in Table 5.2), which suggests passive reabsorption to be an important pathway in renal drug handling.

5.5 Discussion

Prediction of drug renal clearance according to the either measured or estimated creatinine clearance has been the standard approach to drug dosage adjustment in CKD since its introduction by Lucius Dettli and Roger Jellife in the late 1960's (115, 118-121). They invoked the intact nephron hypothesis proposed by Neal Bricker nearly a decade earlier (114, 122) as the basis for the linear relationship between drug renal clearance and creatinine clearance as a measure of GFR. In this particular context, the intact nephron hypothesis has at times been

misrepresented to portray nephrons in the pathological kidneys as being either untouched by disease or totally destroyed.

The intact nephron hypothesis was an attempt to explain the remarkable ability of patients with moderate to severe stage of CKD and substantive reduction in GFR to continue to excrete average dietary loads of water, nitrogenous wastes, and mineral solutes. In fact, the central idea of Bricker's hypothesis was adaptation of the residual nephrons to compensate for the loss of nephrons that succumbed to the disease process. Studies at the time showed that despite a widened range of single nephron GFR in the diseased kidneys, due to compromised functioning in some and hyper-functioning in other remnant nephrons, glomerular and tubule function remain closely integrated as in normal kidneys. The close connection of glomerular and tubular functions is compatible with the general physiological importance of maintaining whole-body fluid and electrolyte homeostasis in the setting of kidney injury. However, in retrospect, the idealized theoretical model of fixed glomerular and tubular loss is incompatible with the marked pathological heterogeneity of the disease processes that encompass the term "CKD." For example, polycystic kidney disease, the most common genetic kidney disease, is characterized by aberrant cyst growth originating within distal and proximal tubule cells. The loss of glomerular function, evidenced by a decline in GFR, occurs late in this course of this disease, after most of the renal interstitium has been replaced by pathological cysts. On the other hand, diabetic nephropathy, the most common acquired kidney disease, is characterized by mesangial expansion and podocyte loss within the glomerulus that manifest clinically as albuminuria long before changes in GFR are detected. Moreover, the physiological process of secreting medications via the proximal tubule, an active process, differs diametrically from that of glomerular filtration, which is passive. Proximal tubule secretion of organic anions and cations

occurs through a series or orchestrated steps that include transporter-mediated uptake at the basolateral membrane, cellular internalization, and efflux transport into the tubular lumen. These active and regulated cellular processes are affected by a wide range of conditions within the kidneys, including oxygenation status, neuroendocrine signaling, and the water and electrolyte composition of the urinary filtrate. In contrast, glomerular filtration is a passive process that is primarily determined by size and charge selectivity of the basement membrane and by the cellular structures that constitute this barrier (i.e. podocytes and endothelial cells). These distinctions provide compelling rationales to investigate the assumption of GFR as a valid proxy of renal drug clearance, which occurs predominantly through proximal tubule secretion.
It is the concept of "homogeneity of glomerulo-tubular balance" that Dettli pointed to as support for assuming parallel decline in drug filtration and secretory clearance during renal impairment. While the preservation of glomerular-tubular balance for essential physiological solutes (eg, sodium, potassium, and phosphate) has been thoroughly investigated by micropuncture studies in various experimental models of renal dysfunction (123), comparable studies with drug solutes (ie, exogenous organic anions or cations) are notably absent. Dettli's creatinine-based approach in prediction of drug renal clearance (ie, the assumption of parallel decline in filtration and secretory clearance) in CKD has long been accepted based upon its empirical success with many older antibiotics (115), the majority of them having drug renal clearance that are close to GFR indicating minimal if not the absence of tubular secretion.

To our knowledge, this is the first systematic literature analysis for drugs with renal clearance in CKD that cannot be accurately described by estimated or measured glomerular filtration function. Among 27 drugs and solutes for which data were available, we demonstrated failure of GFR measure to accurately predict alterations in drug renal clearance in CKD for 13

(48%) drugs. Notably, based on their *initial ratio* R_{nf} index in healthy subjects, these drugs were primarily secreted in the proximal tubule in addition to being filtered through the glomerulus. The observed disconnect between glomerular filtration and overall drug renal clearance (specifically secretory clearance) is most apparent in CKD stages 4 and 5. Furthermore, for 10 out of 13 drugs (Group B), the secretory component of drug renal clearance declines more rapidly than filtration clearance, meaning an over-prediction of renal drug clearance based upon estimated or measured GFR. The latter finding has clinical implications in that for drugs in Group B the measure of residual GFR function alone cannot estimate the full extent of reduction in drug renal clearance during mid to late stages of disease, which could lead to risks of overdosing and adverse drug events. Thus, we hypothesize that dosing of such drugs in the growing population with CKD would be improved if it is based on measures of both glomerular filtration and tubular secretion function. A small number of drugs fall into Group A, which show a lesser reduction in renal drug clearance relative to GFR during progressive deterioration in kidney function. This could be interpreted as sign of some sort of compensatory mechanism(s) within the proximal tubule to preserve secretory function in the face of a falling GFR. Until we fully understand the cellular and molecular mechanisms underlying the contrasting behavior of renal tubular secretion for the drugs in Group A versus Group B, we have no a priori way of predicting how a highly renally secreted drug would behave in CKD.

One difficulty we encountered during the literature search was the inconsistency in reporting of data on pharmacokinetics in renal impairment. Investigations often focused on estimating the effects of renal impairment on overall drug exposure (reported either as changes in *AUC*, or changes in oral clearance, *Cl/F*) rather than effects of renal impairment on the more relevant measure of drug renal clearance. Furthermore, abbreviated pharmacokinetic studies in

renal impairment, often performed as a special population study for a New Drug Application (NDA), only show changes in pharmacokinetics in severe renal impairment (CKD stage 4). While these studies can be informative on the "worst case scenario" for changes in drug exposure and pharmacokinetic parameters, they do not provide detail information about the course of decline in renal clearance processes during progressive stages of CKD. It should also be pointed out that publications tended to group data for each stage of CKD, which deprives other investigators the opportunity for critical, retrospective examination of individual patient data. It was challenging to find publications that contained sufficient information for our analysis. In light of our experience, we strongly recommend a concerted effort for the research community and regulatory agencies to develop a consensus on the essential parameters that should be collected in pharmacokinetic studies on renal impairment, namely renal clearance, plasma unbound fraction, and preferably inulin/iohexol/iothalamate clearance as a measure of actual GFR rather than the usual clinical measurement of creatinine clearance. Creatinine clearance is known to overestimate GFR due to its tubular secretion, which while minimal in the healthy state becomes evident as GFR is lowered during renal dysfunction (124).

What does currently available literature say about the inter-dependence or lack thereof between glomerular and tubular function during the progression of disease? Our group has recently shown substantial inter-individual variation in relationship between filtration and secretion (defined by creatinine and urea clearance estimated from the same timed urine collection) for an organic anion transporter substrate hippuric acid (ρ=0.42); (125). The mechanisms accounting for the discordance between tubular secretion and GFR deserve careful investigation. One important consideration is the marked difference in the amount of medication delivered to the kidneys via glomerular and proximal tubule processes. Glomerular filtration is

limited to ≈20% of renal plasma flow and tightly regulated by afferent and efferent arteriolar tone. The proximal tubules receive the remaining 80% of renal plasma flow, enabling the possibility of near complete clearance of solute and medications in a single pass within the kidneys. A second important consideration is competition among retained substances and drugs for proximal tubule transporters. *In vitro* studies have demonstrated that some prominent uremic solutes, including hippuric acid, indoxyl sulfate, *p*-cresol sulfate inhibit basolateral OAT transporters (39), and may further interact with apical efflux transporters (MATE1/2K, MRP2/4, P-gp). In moderate to severe stages of CKD, these uremic solutes circulate at concentrations high enough to inhibit tubular drug transport (34, 39). Uremic solute interference may thus explain the observed decrease in R_{nf} as GFR declines for Group B drugs. A third consideration is the binding kinetics of specific medications for circulating proteins such as albumin, which could affect the rate of proximal tubule secretion via competition with tubule transporters. In contrast, the impact of protein binding on glomerular filtration is more of an equilibrium phenomenon that is readily predictable by ex vivo plasma unbound or free fraction, and by size and charge characteristics of the basement membrane.

An important limitation to our analysis is the likelihood of measurement error in the estimation of GFR. Different GFR estimation methods are more or less precise, and the accuracy varies over the range of renal function. Measurement error, however, would probably have introduced non-differential misclassification, and the implications for the results of this error would have been to bias the estimates towards the null. We also included publications that displayed the individual patient data across the entire continuum of GFR, with some offering a rich dataset (eg, PAH, Figure 5.1), while others had rather sparse data (n ≈ 4 subjects) for some CKD stages (eg, pravastatin, Supplementary Figure 5.3). It is possible that our test of statistical

significance on the dependence of R_{nf} on GFR and the resulting assignment of the drugs to Group C rather to Group A or B may be biased by the sample size and outliers. Notably, pravastatin was assigned to Group C; it shows almost 8-fold decrease in ratio across the full range of GFR, yet the correlation between ratio and GFR measure failed a test of statistical significance. For sure, further *in vivo* studies are necessary to better define pravastatin's renal handling in CKD (i.e., significant decrease in R_{nf} – Group B *versus* no change in R_{nf} – Group C).

In conclusion, we contend that effective dosing of secreted drugs in CKD patients requires a fundamental redefinition of how the disease modulates renal drug clearance by extending our focus beyond filtration to include measures of renal tubular secretion. This will necessarily lead to re-evaluation of current approaches to drug dosing adjustment in CKD from creatinine-based methods to a more comprehensive approach of encompassing tubular markers that reflect the ongoing interference or pathophysiology of tubular drug transport function (126-128). The successful development of dosing algorithms that incorporate measures of proximal tubular function would refine renal drug dosing strategies, leading to safer and more efficacious use of medications in patients with CKD. Additionally, understanding the relative contributions of filtration and secretion to drug renal clearance in the disease population would facilitate the necessary task of *in vitro-to-in vivo* scaling during the transition of a drug candidate from the preclinical phase to phase 1 and 2 clinical trials in new drug development.

5.6 Study highlights

- What is the current knowledge on the topic?

Intact nephron hypothesis states that all renal excretory processes decline in parallel with CKD progression, which is an underlying assumption for drug dosage adjustments in CKD that

are based on serum creatinine. Since its very introduction, the universal applicability of the hypothesis has been questioned.

- What question did this study address?

Can measures of glomerular filtration accurately predict alterations in drug renal clearance/secretory clearance across the range of CKD for all drugs? If not, what is the pattern and the severity of the observed disconnect between glomerular filtration and tubular secretion, and what are the potential implications?

- What this study adds to our knowledge?

This is the first systematic analysis giving evidence that there is a distinct subset of drugs showing a disconnect between glomerular filtration and tubular secretion in CKD.

- How this might change clinical pharmacology or translational science?

Our data support a re-definition of drug dosing adjustment strategies in CKD. The incorporation of measurements of proximal tubule secretion in renal dosing algorithms could refine renal drug dosing strategies, leading to more personalized use of medications in kidney disease patients.

5.7 Figures and tables

Table 5.1. Drugs with $\frac{Cl\ renal}{fu*GFR} > 0.74$.

Drugs are listed in descending order according to the average ratio in healthy subjects (GFR ≥ 90ml/min).

Drug	Ref.	Method for GFR determination	Fraction unbound (f_U)	Correlation coefficient	Slope of linear regression (95% CI, min/mL)*	p value	Mean ratio when GFR ≥ 90 ml/min	Fold change in ratio**	Substrate for renal transporters? ***
Group A: Increase in ratio across the range of CKD									
PAH	(129)	Measured inulin or ^{51}Cr-EDTA Cl	0.88	-0.4539	-0.045 (-0.065, -0.025)	<0.001	5.32	1.32	OAT1, OAT2, OAT3, MRP2, MRP4
Dexpramipexole	(130)	eGFR by MDRD	0.95	-0.3785	-0.019 (-0.037, -0.001)	0.039	3.89	1.28	OCT2
Prulacopride	(131)	N/A	Mean fu / CKD stage	-0.3769	-0.010 (-0.019, -0.001)	0.028	2.79	1.20	P-gp
Group B: Decrease in ratio across the range of CKD									
Olmesartan	(132)	N/A	Mean fu / CKD stage	0.5239	0.109 (0.045, 0.172)	0.001	28.44	0.71	OAT1, OAT3, OAT4, MRP2, MRP4
Penciclovir	(133)	eGFR by C-G	0.80	0.4020	0.036 (0.001, 0.071)	0.046	6.12	0.72	OAT2
Metformin	(134-136)	Measured CrCl or N/A	1	0.3707	0.012 (0.001, 0.024)	0.04	3.75	0.78	OCT2, MATE1, MATE2K
Lenalidomide	(137)	Measured CrCl	Mean fu / CKD stage	0.5731	0.019 (0.007, 0.031)	0.004	3.30	0.61	P-gp
5-HMT	(138)	Measured CrCl	Mean fu / CKD stage	0.4605	0.012 (0.003, 0.021)	0.009	2.38	0.66	P-gp
Foscarnet	(139)	Measured CrCl	0.83	0.4737	0.005 (0.001, 0.010)	0.022	1.33	0.75	/
Ribavirin	(140)	Measured CrCl	1	0.5768	0.004 (0.0005, 0.008)	0.031	0.94	0.69	CNT2, CNT3, ENT1
(S)-Vigabatrin	(141)	Measured CrCl	1	0.7571	0.373 (0.231, 0.515)****	<0.001	0.81	0.52	/

Dabigatran	(142)	Measured CrCl	Mean fu / CKD stage	0.4459	0.003 (0.001, 0.005)	0.017	0.79	0.78	P-gp
Ceftobiprole	(143)	N/A	0.84	0.9029	0.005 (0.004, 0.006)	<0.001	0.79	0.63	OAT1, OCT2
Group C: No change in ratio across the range of CKD									
Tiotropium	(144)	Measured CrCl	Mean fu / CKD stage	0.4429	0.052 (-0.0001, 0.1045)	0.05	16.30	0.79	OCT2, OCTN1, OCTN2
Pravastatin	(145)	Measured CrCl	Mean fu / CKD stage	0.3828	0.052 (-0.023, 0.126)	0.16	13.63	0.73	OAT3, OAT4, BCRP, MRP2
Mirabegron	(146)	eGFR by MDRD	N/A, measured Cl_u	-0.0469	-0.003 (-0.024, 0.019)	0.80	6.31	1.03	P-gp
Oseltamivir carboxylate	(147)	N/A	0.97	0.4268	0.003 (-0.0004, 0.006)	0.088	2.00	0.91	OAT1, OAT3, MRP4
Lomefloxacin	(148)	N/A	0.90	0.157	0.001 (-0.003, 0.005)	0.47	1.55	0.94	OAT, OATP1A2
Cidofovir	(149)	Measured CrCl	0.94	0.1104	0.001 (-0.003, 0.004)	0.707	0.94	0.96	OAT1, OAT3
Naloxegol	(150)	eGFR by MDRD	0.96	-0.2513	-0.004 (-0.012, 0.003)	0.236	0.92	1.27	P-gp
Cefpirome	(151)	Measured CrCl	0.90	0.0933	0.001 (-0.002, 0.003)	0.643	0.81	0.96	/

N/A: not available, eGFR: estimated GFR, C-G: Cockroft-Gault, MDRD: Modification of Diet in Renal Disease, Cl_u*: unbound clearance. *Linear regression slope is estimated for GFR as independent, and ratio as dependent variable. **Fold change in ratio represents change in ratio when GFR drops from 90 ml/min (healthy subjects) to 30 ml/min (CKD stage 3B). ***Drug has previously been characterized either in vitro and/or in vivo as a substrate for renal transporters. **** (S)-Vigabatrin regression coefficient units are min*kg/mL.*

Figure 5.1. Scatterplots depicting relationship between R_{nf} and GFR for a single drug.

Scatterplots of renal clearance to filtration clearance (R_{nf}) and glomerular filtration rate (GFR) in group A, group B, and group C drugs indicating that the ratio of R_{nf} does not necessarily remain constant with disease progression. Group A shows a significant increase in R_{nf} as GFR declines with disease progression; group B shows a significant decrease in R_{nf} as GFR declines; and group C shows no change in R_{nf} across the range of chronic kidney disease severity. Methods for GFR determination are listed in **Table 4.2**.

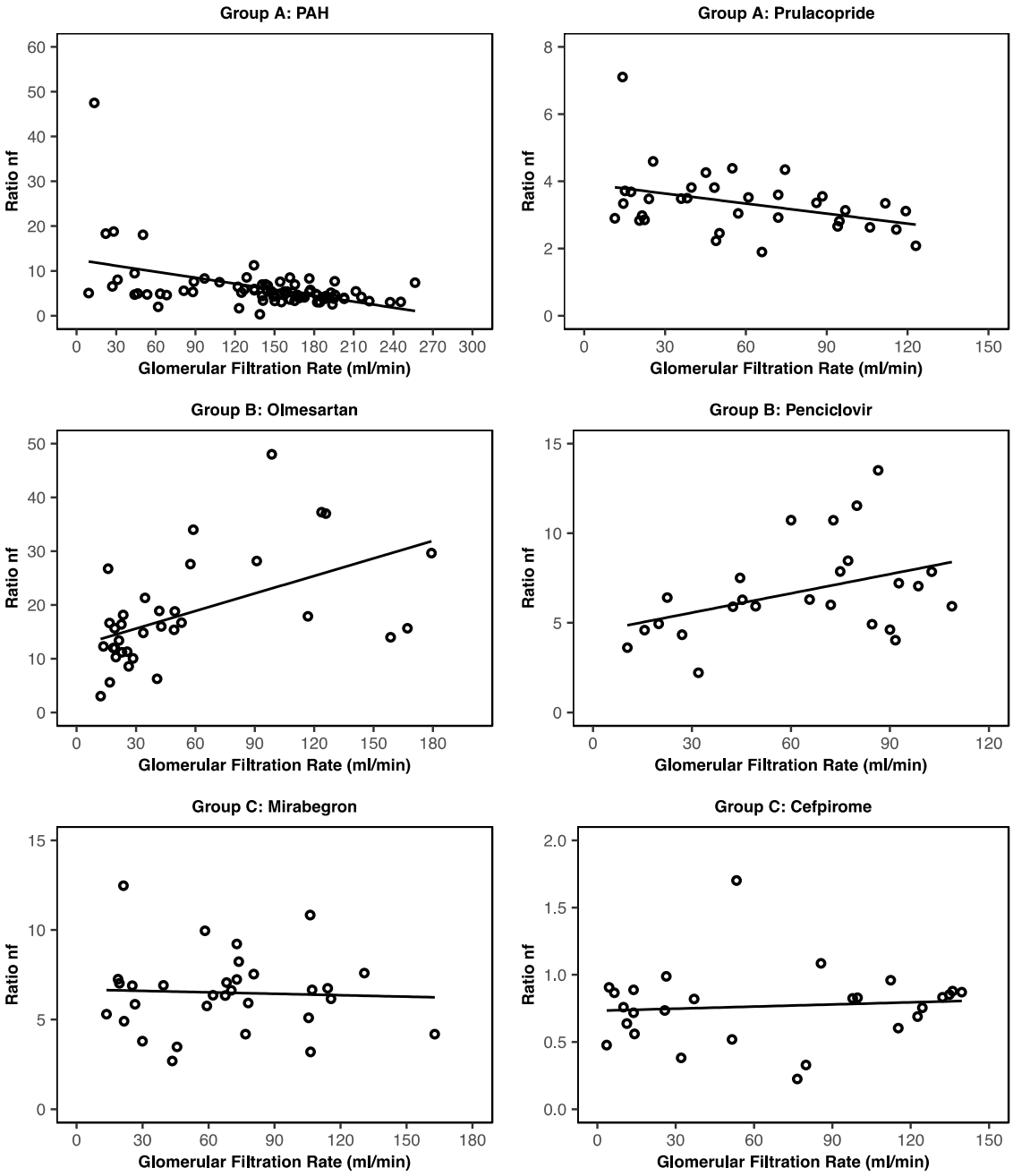
Group A: PAH
Ratio nf
Glomerular Filtration Rate (ml/min)
Group A: Prulacopride
Ratio nf
Glomerular Filtration Rate (ml/min)
Group B: Olmesartan
Ratio nf
Glomerular Filtration Rate (ml/min)
Group B: Penciclovir
Ratio nf
Glomerular Filtration Rate (ml/min)
Group C: Mirabegron
Ratio nf
Glomerular Filtration Rate (ml/min)
Group C: Cefpirome
Ratio nf
Glomerular Filtration Rate (ml/min)

Table 5.2. Drugs with $\frac{Cl\ renal}{fu*GFR} \leq 0.74$.

Drugs are listed in descending order according to the average ratio in healthy subjects (GFR ≥ 90ml/min).

Drug	Ref.	Method for GFR determination	Fraction unbound (f_U)	Correlation coefficient	Slope of linear regression (95% CI, min/mL)*	p value	Ratio when GFR ≥ 90ml/min	Fold change in ratio**	Substrate for renal transporters? ***
Cefsulodin	(152)	Measured CrCl	0.85	-0.31	-0.002 (-0.007, 0.002)	0.275	0.67	1.18	/
Pregabalin	(153)	eGFR by C-G	1	0.24	0.001 (-0.001, 0.003)	0.240	0.57	0.85	OCT2, OCTN1
Nicotine	(154)	Measured ^{51}Cr-EDTA Cl	0.95	-0.31	-0.003 (-0.007, 0.001)	0.189	0.55	1.27	OCT2
Levetiracetam	(155)	N/A	0.90	-0.21	-0.001 (-0.003, 0.001)	0.348	0.30	1.20	/
Fluconazole	(156)	Measured CrCl	0.87	-0.31	-0.001 (-0.002, 0.001)	0.265	0.20	1.18	/
Lacosamide	(157)	eGFR by C-G	0.85	-0.14	-0.0002 (-0.001, 0.0004)	0.443	0.12	1.10	/

*N/A: not available, eGFR: estimated GFR, C-G: Cockroft-Gault. *Linear regression slope is estimated for GFR as independent, and ratio as dependent variable. **Fold change in ratio represents change in ratio when GFR drops from 90 ml/min (healthy subjects) to 30 ml/min (CKD stage 3B). ***Drug has previously been characterized either in vitro and/or in vivo as a substrate for renal transporters.*

Table 5.3. Physico-chemical properties of drugs.

Drug	Molecular weight (g/mol)	LogP	pKa	Charge at physiologic pH
PAH	194.19	-1	2.7,4.24	Anion
Dexpramipexole	211.33	1.9	9.47	Cation
Prulacopride	367.87	0.74	8.98, 14.64	Cation
Olmesartan	446.50	5.9	0.91,4.96,5.57,13.93	Anion
Metformin	129.16	-0.5	12.4	Cation
Penciclovir	253.26	-1.5	2.84, 8.01	Anion
Lenalidomide	259.26	-0.4	2.31, 11.61	Neutral
5-HMT	341.50	4.40	N/A	N/A
Vigabatrin	129.16	-2.1	4.61, 9.91	Zwitterion
Foscarnet	126.00	-2.1	3.13	Anion
Ribavirin	244.20	-2.8	-1.2, 11.88	Neutral
Dabigatran	627.73	3.8	3.87, 17.89	Zwitterion
Ceftobiprole	534.57	-4.8	3.28, 10.33	Zwitterion
Tiotropium	392.51	-1.8	-4.3, 10.35	Neutral
Pravastatin	424.53	1.65	-2.7,4.21	Anion
Mirabegron	396.51	2.9	9.62, 13.84	Cation
Oseltamivir carboxylate	284.40	0.74	4.13, 9.26	Zwitterion
Lomefloxacin	351.35	-0.3	5.64, 8.7	Zwitterion
Cidofovir	279.19	-3.9	1.19, 2.15	Anion
Naloxegol	651.79	-1	10.14, 12.2	Cation
Cefpirome	514.58	0.9	1.7, 2.43	Anion
Cefsulodin	532.55	0.2	0.29	Anion
Nicotine	162.23	1.17	8.5	Neutral
Pregabalin	159.23	-1.3	4.8, 10.23	Zwitterion
Levetiracetam	170.21	-0.6	-1, 16.09	Neutral
Fluconazole	306.27	0.4	2.56, 12.71	Neutral
Lacosamide	250.29	-0.022	-1.5, 12.47	Neutral

N/A: not available.

5.8 Supplementary materials

Supplementary figure 5.1. Drugs and solutes with a ratio greater than 0.74 and showing increase in ratio across the range of CKD (Group A).

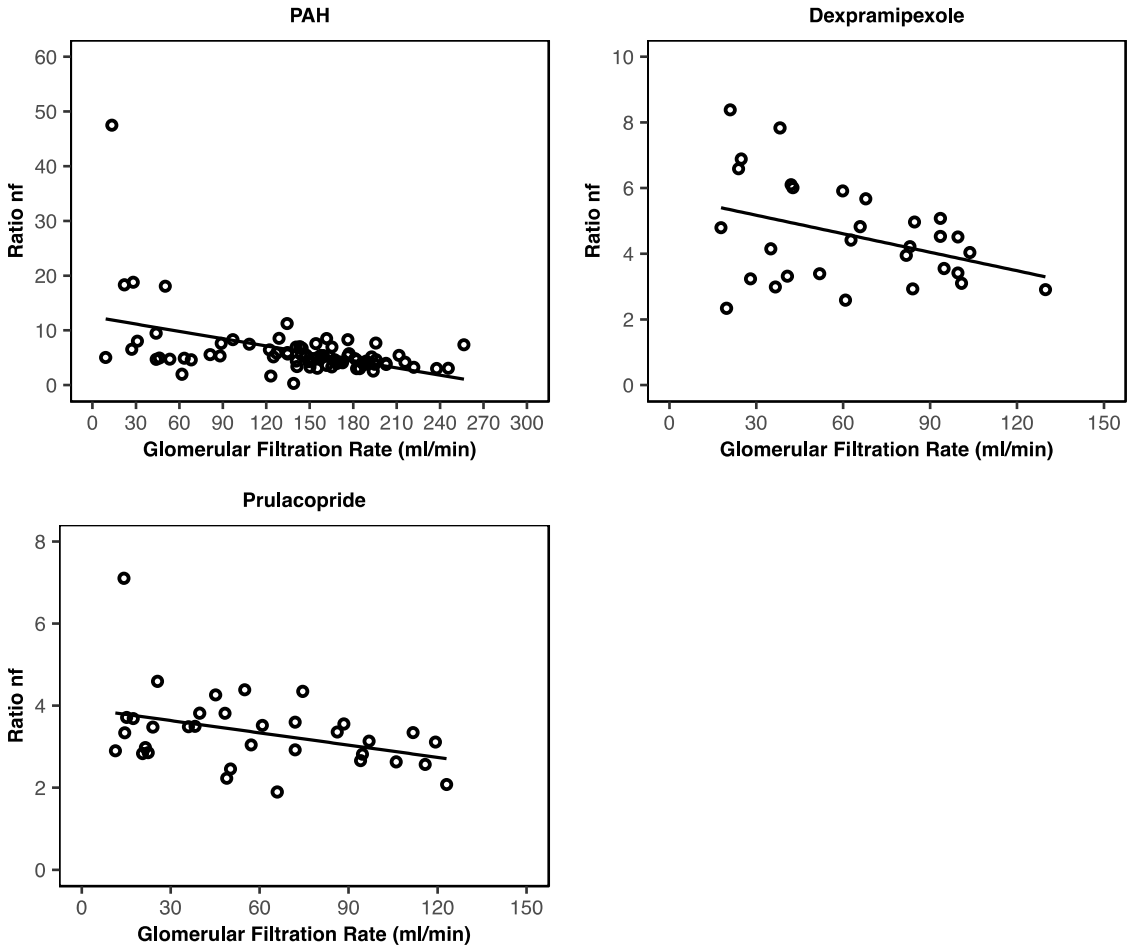

Supplementary figure 5.2. Drugs and solutes with a ratio greater than 0.74 showing decrease in ratio across the range of CKD (Group B).

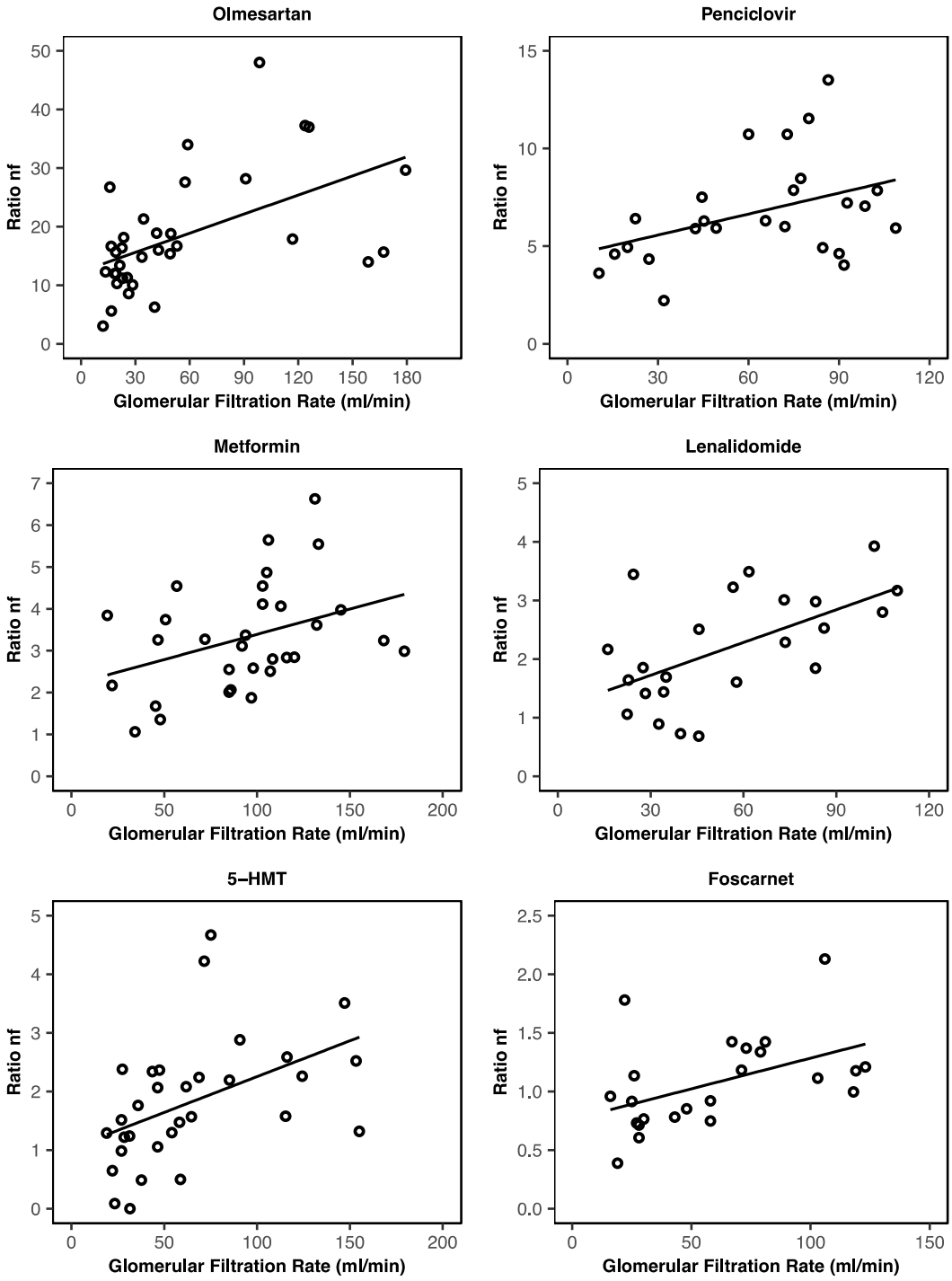

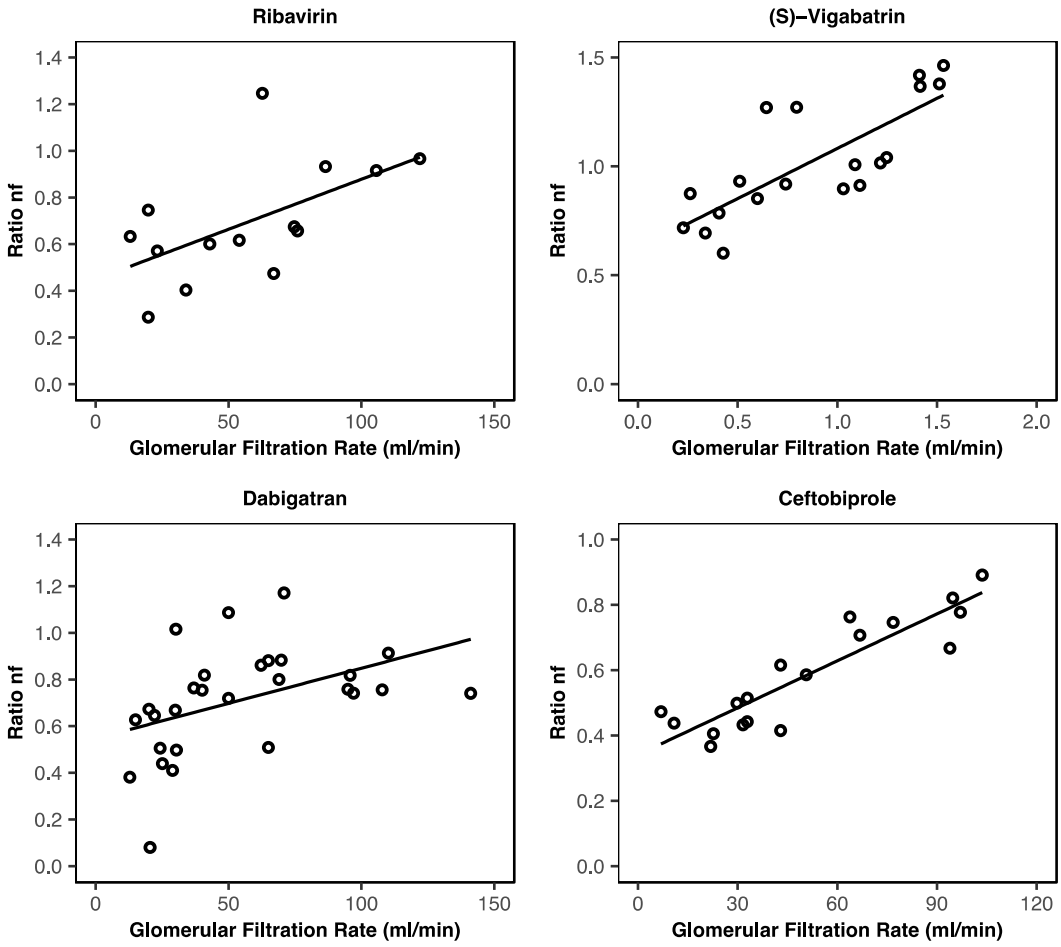
Ribavirin
Ratio nf
Glomerular Filtration Rate (ml/min)
(S)−Vigabatrin
Ratio nf
Glomerular Filtration Rate (ml/min)
Dabigatran
Ratio nf
Glomerular Filtration Rate (ml/min)
Ceftobiprole
Ratio nf
Glomerular Filtration Rate (ml/min)

Supplementary figure 5.3. Drugs and solutes with a ratio greater than 0.74 showing no statistically significant correlation (no change in ratio) across the range of CKD (Group C).

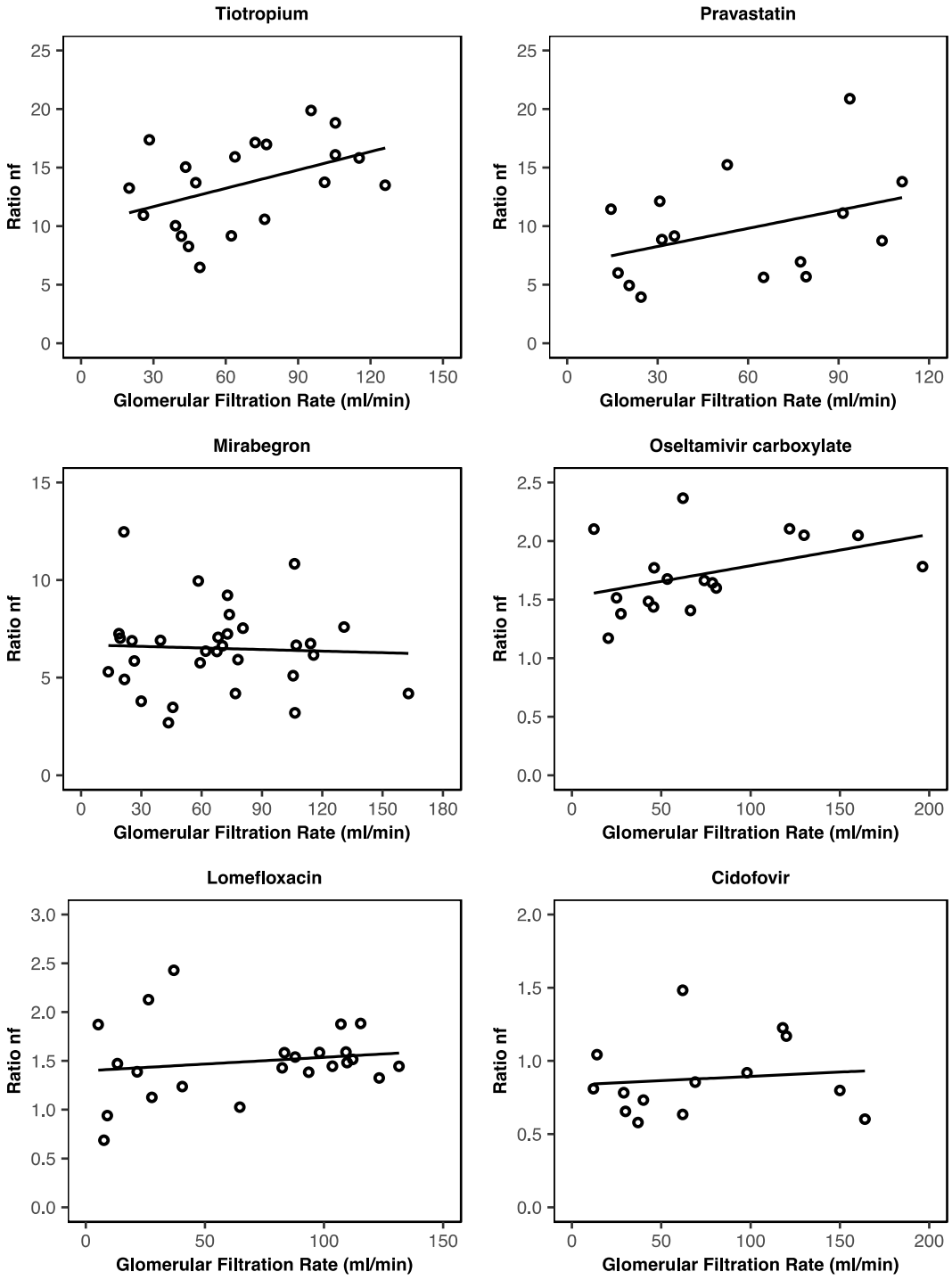

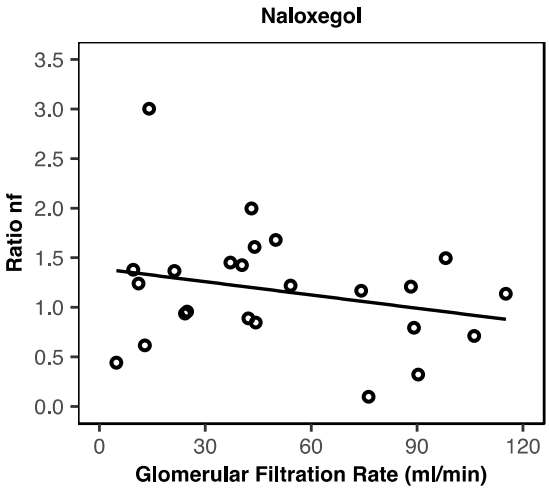
Naloxegol
Ratio nf
3.5
3.0
2.5
2.0
1.5
1.0
0.5
0.0
0
30
60
90
120
Glomerular Filtration Rate (ml/min)

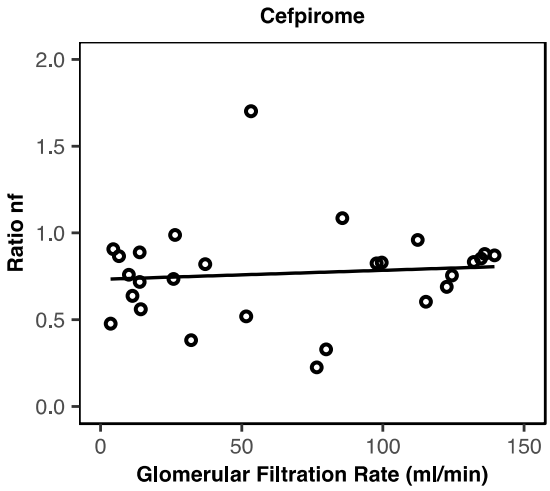
Cefpirome
Ratio nf
2.0
1.5
1.0
0.5
0.0
0
50
100
150
Glomerular Filtration Rate (ml/min)

Supplementary figure 5.4. Drugs and solutes with a ratio less than or equal to 0.74 showing no statistically significant correlation (no change in ratio) across the range of CKD.

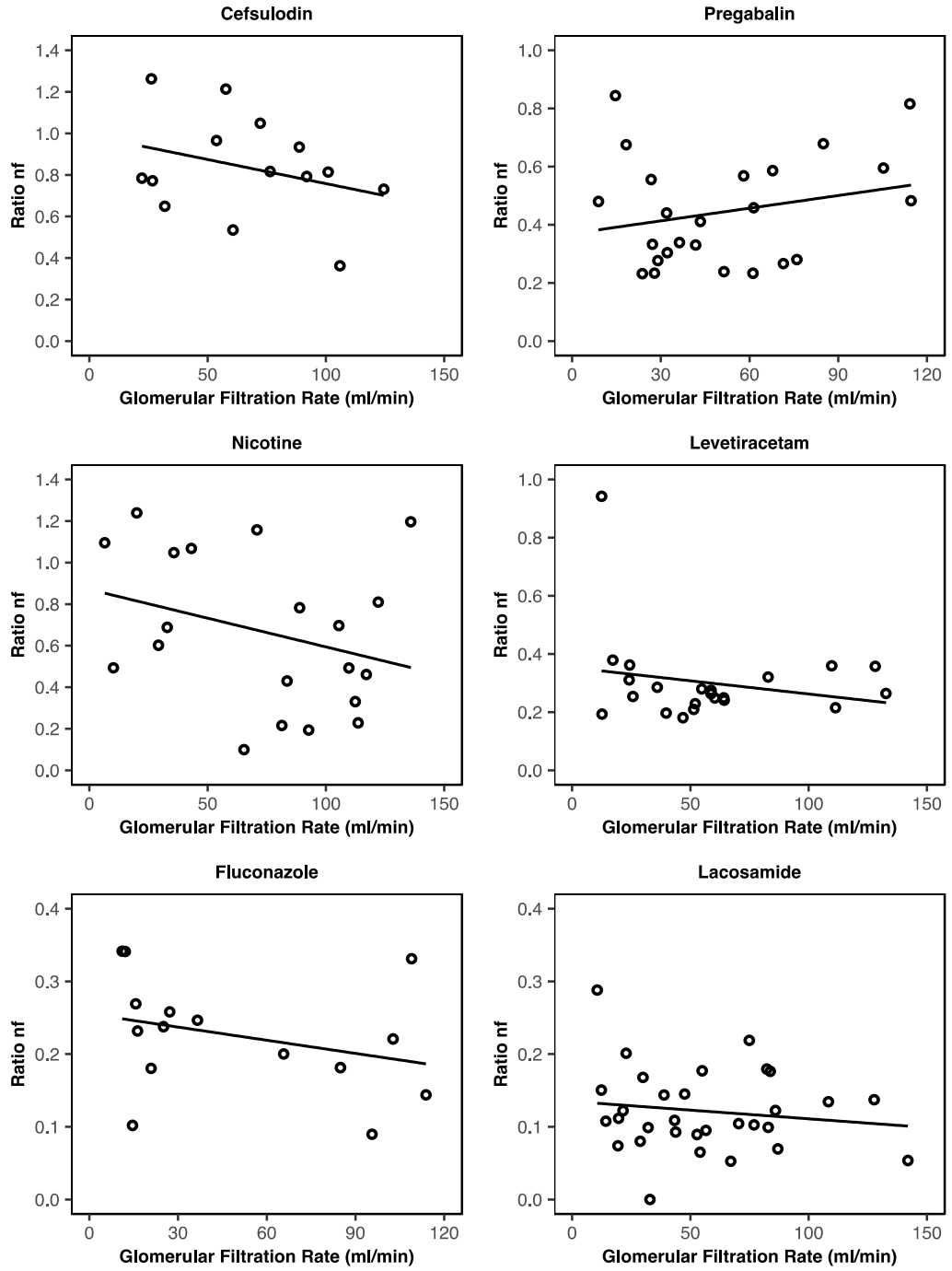

6 Conclusions

My PhD thesis research deals with drug secretion at the human renal proximal tubule. This area of research has gained much attention in recent years, in part due to the increasing number of prescribed medications that are significantly eliminated via the renal route. To advance the understanding of the mechanism and kinetics of drug transport across the human proximal tubular epithelium, I have devoted efforts towards developing an *in vitro* model of cultured human proximal tubule epithelial cells (PTECs) that would allow detailed investigations of the cellular and molecular processes involved.

Chapter 1 provides background information on the existing *in vitro* models for investigating renal tubular drug secretion, with a particular emphasis on the recent advances in 3D cultures and microphysiological systems. The advantages and limitations of the current renal proximal tubule microphysiological systems are discussed, which led to a proposal on the features and capabilities that are desired in the next generation of proximal tubule microphysiological system.

In **Chapter 2**, I characterized the functioning of passaged human PTECs grown on permeable supports. Cells polarized and formed a tight monolayer. The establishment of a PTEC barrier was dependent upon: (i) cell seeding density, (ii) presence and type of extracellular matrix, (iii) cell culturing technique. Furthermore, the expression of transporters relevant in the vectorial transport of drugs was demonstrated either via mRNA or protein expression. This was followed by a series of functional studies on secretory transport of the model anionic drug *p*-aminohippurate (PAH). The measured PAH permeability indicates robust expression and activity of transporters known to mediate the passage of organic anion across the proximal tubule as indicated by sensitivity towards probenecid; PAH permeability was reduced by 61% in the presence of

probenecid. I also found that the choice of buffer used in the transport assays is critical; among the buffers tested, the PAH permeability was the highest in Hank's Balanced Salt Solution (HBSS) buffer. Whereas previous studies have largely relied upon freshly isolated human PTECs for investigation, which severely limits cell supply, my findings demonstrate that, with appropriate culture techniques and a defined time in culture (up to passage #5), it is possible to use passaged human PTECs in studies of vectorial drug transport. This information was crucial for the work presented in subsequent chapters, as until now, these cells were not considered for use due to their presumed loss of polarity, barrier integrity, as well as transporter expression and function.

Recently, accumulating evidence has shown that, when primary cells are cultured in the presence of extracellular matrix and under continuous perfusate flow (both determinants of *in vivo* architecture of native cellular microenvironment), they exhibit prolonged viability and improved functioning. None of these earlier in vitro systems are amenable to drug transport studies that require access and sampling of solute concentrations at both the basolateral and apical aspects of the cell barrier. Thus, a major portion of my thesis work was devoted towards establishing a model of human PTECs cultured in a Nortis microphysiological system (MPS) that recapitulate the in vivo tubule-interstitial environment and allows ready measurement of drug transport permeability. In **Chapter 3**, we reported that our human proximal tubule MPS maintains the following salient morphological and physiological properties relevant to their *in vivo* function: (i) cell viability sustained for over 4 weeks; (ii) cell polarity demonstrated by differential expression of Na+/K+ ATPase and tight junction ZO-1; (iii) expression of typical proximal tubule markers (Aquaporin 1, SGLT2, γ-glutamyl transpeptidase, CD13, E-Cadherin); (iv) glucose reabsorption, glutathione re-uptake, and breakdown of glutamine under acidic pH; and (v) homeostatic regulation of Vitamin D metabolism.

The next step in our model development was to construct an experimental paradigm for drug transport studies using the human proximal tubule MPS validated in Chapter 3. **Chapter 4** described the development of a vascularized proximal tubule MPS (or VPT-MPS), a model that offers rudiments of human tubulointerstitial environment, and is characterized by continuous perfusion of media flow through the vessel (i.e., supply of basolateral flow), and tubule lumen (i.e., apical flow). Critically, this model enabled steady, predictable flow dynamics which allowed for steady measurements of solute tubular secretion over hours of a typical transport experiment. Through a series of studies with FITC-Dextran, I confirmed that the epithelium, not the vessel or interstitium is the limiting barrier for diffusion. Hence, the VPT-MPS appropriately resembled *in vivo* human proximal tubule. There was a multifold-difference between output of mannitol and PAH in the effluent from the tubule lumen. Furthermore, the appearance of PAH in the tubule lumen was inhibited by nearly 50% by probenecid. The utility of the VPT-MPS was also demonstrated with *in vitro – in vivo* scaling and physiological modelling of the secretory transport of PAH, with the predicted value of clearance underestimating the observed value by less than 3-fold. This chapter thus offers for the first-time, proof-of-concept approach to modelling drug tubular secretion with the aid of microphysiological systems; the work may represent a paradigm shift in studying tubular secretion of drugs.

The focus of the last portion of my dissertation was assessments of changes in drug renal clearance in chronic kidney disease (CKD). In **Chapter 5**, I collected published pharmacokinetic data to assess if measures of decline in glomerular filtration rate (GFR) predict lowering of renal drug clearance across varying stages of CKD. For each of the drugs identified in this literature analysis, I calculated $R_{nf,}$ a ratio of renal drug clearance to estimated GFR. Tweny-one drugs had R_{nf} >0.74 in subjects with normal GFR (>90ml/min), implying simultaneous filtration and

secretion. Thirteen drugs with R_{nf} >0.74 displayed statistically significant change in R_{nf} (outcome variable) across GFR (predictor variable), as defined by a slope of regression coefficient being statistically different from zero. This indicates, for those drugs, a complex, nonlinear relationship exists between renal drug clearance and GFR that is dependent upon severity of disease; in other words, GFR is not a simple or straighforward predictor of changes in drug renal clearance/secretory clearance. The dependence of R_{nf} on GFR was either positive (n=3, Group A) or negative (n=10, Group B). The former case suggest that, as renal function deterioates, decline in tubular secretion is worse than GFR; whereas, the latter case sugests the opposite trend. Behavior of drugs in Group A could be interpreted as some sort of compensatory mechanism(s) within the proximal tubule to preserve secretory function in the face of a falling GFR. Behavior of drugs in Group B could be explained by the circulating uremic solute inhibition of proximal tubule transporters involved in the vectorial translocation of drugs in the tubule lumen. For 8 drugs, the regression slope did not significantly deviate from zero (Group C). This analysis strongly suggested that, for drugs that have a significant secretory component relative to the overall drug renal clearance, dosing adjustment in CKD requires a re-definition which includes both measures of GFR and tubular secretion function. Further work is required to identify an endogenous biomarker of tubular secretion function.

7 References

1. Brenner BM, Rector FC. Brenner and Rector's the kidney. 8th Edition ed. United States: Philadelphia : Saunders Elsevier, 2008.
2. Morrissey KM, Stocker SL, Wittwer MB, Xu L, Giacomini KM. Renal transporters in drug development. Annual review of pharmacology and toxicology. 2013;53:503-29.
3. Kelly EJ, Wang Z, Voellinger JL, Yeung CK, Shen DD, Thummel KE, et al. Innovations in preclinical biology: ex vivo engineering of a human kidney tissue microperfusion system. Stem cell research & therapy. 2013;4 Suppl 1:S17.
4. Paine SW, Menochet K, Denton R, McGinnity DF, Riley RJ. Prediction of human renal clearance from preclinical species for a diverse set of drugs that exhibit both active secretion and net reabsorption. Drug metabolism and disposition: the biological fate of chemicals. 2011;39(6):1008-13.
5. Tahara H, Shono M, Kusuhara H, Kinoshita H, Fuse E, Takadate A, et al. Molecular cloning and functional analyses of OAT1 and OAT3 from cynomolgus monkey kidney. Pharmaceutical research. 2005;22(4):647-60.
6. Eraly SA, Vallon V, Vaughn DA, Gangoiti JA, Richter K, Nagle M, et al. Decreased renal organic anion secretion and plasma accumulation of endogenous organic anions in OAT1 knock-out mice. The Journal of biological chemistry. 2006;281(8):5072-83.
7. Johnson BM, Zhang P, Schuetz JD, Brouwer KL. Characterization of transport protein expression in multidrug resistance-associated protein (Mrp) 2-deficient rats. Drug metabolism and disposition: the biological fate of chemicals. 2006;34(4):556-62.
8. Deguchi T, Kusuhara H, Takadate A, Endou H, Otagiri M, Sugiyama Y. Characterization of uremic toxin transport by organic anion transporters in the kidney. Kidney international. 2004;65(1):162-74.
9. Geng W, Pang KS. Differences in excretion of hippurate, as a metabolite of benzoate and as an administered species, in the single-pass isolated perfused rat kidney explained. The Journal of pharmacology and experimental therapeutics. 1999;288(2):597-606.
10. Yin J, Duan H, Shirasaka Y, Prasad B, Wang J. Atenolol Renal Secretion Is Mediated by Human Organic Cation Transporter 2 and Multidrug and Toxin Extrusion Proteins. Drug metabolism and disposition: the biological fate of chemicals. 2015;43(12):1872-81.
11. Sato T, Masuda S, Yonezawa A, Tanihara Y, Katsura T, Inui K. Transcellular transport of organic cations in double-transfected MDCK cells expressing human organic cation transporters hOCT1/hMATE1 and hOCT2/hMATE1. Biochemical pharmacology. 2008;76(7):894-903.
12. Shu Y, Bello CL, Mangravite LM, Feng B, Giacomini KM. Functional characteristics and steroid hormone-mediated regulation of an organic cation transporter in Madin-Darby canine kidney cells. The Journal of pharmacology and experimental therapeutics. 2001;299(1):392-8.
13. Kuteykin-Teplyakov K, Luna-Tortos C, Ambroziak K, Loscher W. Differences in the expression of endogenous efflux transporters in MDR1-transfected versus wildtype cell lines affect P-glycoprotein mediated drug transport. British journal of pharmacology. 2010;160(6):1453-63.
14. Lash LH, Putt DA, Cai H. Membrane transport function in primary cultures of human proximal tubular cells. Toxicology. 2006;228(2-3):200-18.

15. Brown CD, Sayer R, Windass AS, Haslam IS, De Broe ME, D'Haese PC, et al. Characterisation of human tubular cell monolayers as a model of proximal tubular xenobiotic handling. Toxicology and applied pharmacology. 2008;233(3):428-38.
16. Gozalpour E, Fenner KS. Current State Of In Vitro Cell-Based Renal Models. Current drug metabolism. 2018.
17. Orosz DE, Woost PG, Kolb RJ, Finesilver MB, Jin W, Frisa PS, et al. Growth, immortalization, and differentiation potential of normal adult human proximal tubule cells. In vitro cellular & developmental biology Animal. 2004;40(1-2):22-34.
18. Van der Hauwaert C, Savary G, Gnemmi V, Glowacki F, Pottier N, Bouillez A, et al. Isolation and characterization of a primary proximal tubular epithelial cell model from human kidney by CD10/CD13 double labeling. PloS one. 2013;8(6):e66750.
19. Ichimura T, Asseldonk EJ, Humphreys BD, Gunaratnam L, Duffield JS, Bonventre JV. Kidney injury molecule-1 is a phosphatidylserine receptor that confers a phagocytic phenotype on epithelial cells. The Journal of clinical investigation. 2008;118(5):1657-68.
20. Baer PC, Nockher WA, Haase W, Scherberich JE. Isolation of proximal and distal tubule cells from human kidney by immunomagnetic separation. Technical note. Kidney international. 1997;52(5):1321-31.
21. Qi W, Johnson DW, Vesey DA, Pollock CA, Chen X. Isolation, propagation and characterization of primary tubule cell culture from human kidney. Nephrology (Carlton, Vic). 2007;12(2):155-9.
22. DesRochers TM, Suter L, Roth A, Kaplan DL. Bioengineered 3D human kidney tissue, a platform for the determination of nephrotoxicity. PloS one. 2013;8(3):e59219.
23. Jansen J, Schophuizen CM, Wilmer MJ, Lahham SH, Mutsaers HA, Wetzels JF, et al. A morphological and functional comparison of proximal tubule cell lines established from human urine and kidney tissue. Experimental cell research. 2014;323(1):87-99.
24. Brown CD. Development of predictive in vitro models of the proximal tubule for drug development and safety assessment studies http://www.solvobiotech.com/documents/Colin_Brown-prez.pdf [Available from: http://www.solvobiotech.com/documents/Colin_Brown-prez.pdf.
25. Jansen J, De Napoli IE, Fedecostante M, Schophuizen CM, Chevtchik NV, Wilmer MJ, et al. Human proximal tubule epithelial cells cultured on hollow fibers: living membranes that actively transport organic cations. Scientific reports. 2015;5:16702.
26. Blackburn JG, Hazen-Martin DJ, Detrisac CJ, Sens DA. Electrophysiology and ultrastructure of cultured human proximal tubule cells. Kidney international. 1988;33(2):508-16.
27. Raghavan V, Rbaibi Y, Pastor-Soler NM, Carattino MD, Weisz OA. Shear stress-dependent regulation of apical endocytosis in renal proximal tubule cells mediated by primary cilia. Proceedings of the National Academy of Sciences of the United States of America. 2014;111(23):8506-11.
28. Fukuda Y, Kaishima M, Ohnishi T, Tohyama K, Chisaki I, Nakayama Y, et al. Fluid shear stress stimulates MATE2-K expression via Nrf2 pathway activation. Biochemical and biophysical research communications. 2017;484(2):358-64.
29. Jang KJ, Mehr AP, Hamilton GA, McPartlin LA, Chung S, Suh KY, et al. Human kidney proximal tubule-on-a-chip for drug transport and nephrotoxicity assessment. Integrative biology : quantitative biosciences from nano to macro. 2013;5(9):1119-29.

30. Tourovskaia A, Fauver M, Kramer G, Simonson S, Neumann T. Tissue-engineered microenvironment systems for modeling human vasculature. Experimental biology and medicine (Maywood, NJ). 2014;239(9):1264-71.
31. Coresh J, Selvin E, Stevens LA, Manzi J, Kusek JW, Eggers P, et al. Prevalence of chronic kidney disease in the United States. Jama. 2007;298(17):2038-47.
32. Go AS, Chertow GM, Fan D, McCulloch CE, Hsu CY. Chronic kidney disease and the risks of death, cardiovascular events, and hospitalization. The New England journal of medicine. 2004;351(13):1296-305.
33. Meyer TW, Hostetter TH. Approaches to uremia. Journal of the American Society of Nephrology : JASN. 2014;25(10):2151-8.
34. Duranton F, Cohen G, De Smet R, Rodriguez M, Jankowski J, Vanholder R, et al. Normal and pathologic concentrations of uremic toxins. Journal of the American Society of Nephrology : JASN. 2012;23(7):1258-70.
35. Cantu TG, Ellerbeck EF, Yun SW, Castine SD, Kornhauser DM. Drug prescribing for patients with changing renal function. American journal of hospital pharmacy. 1992;49(12):2944-8.
36. Hu KT, Matayoshi A, Stevenson FT. Calculation of the estimated creatinine clearance in avoiding drug dosing errors in the older patient. The American journal of the medical sciences. 2001;322(3):133-6.
37. Leendertse AJ, van Dijk EA, De Smet PA, Egberts TC, van den Bemt PM. Contribution of renal impairment to potentially preventable medication-related hospital admissions. The Annals of pharmacotherapy. 2012;46(5):625-33.
38. Kearney BP, Yale K, Shah J, Zhong L, Flaherty JF. Pharmacokinetics and dosing recommendations of tenofovir disoproxil fumarate in hepatic or renal impairment. Clinical pharmacokinetics. 2006;45(11):1115-24.
39. Masereeuw R, Mutsaers HA, Toyohara T, Abe T, Jhawar S, Sweet DH, et al. The kidney and uremic toxin removal: glomerulus or tubule? Seminars in nephrology. 2014;34(2):191-208.
40. Detrisac CJ, Sens MA, Garvin AJ, Spicer SS, Sens DA. Tissue culture of human kidney epithelial cells of proximal tubule origin. Kidney international. 1984;25(2):383-90.
41. Gibson-D'Ambrosio RE, Samuel M, Chang CC, Trosko JE, D'Ambrosio SM. Characteristics of long-term human epithelial cell cultures derived from normal human fetal kidney. In vitro cellular & developmental biology : journal of the Tissue Culture Association. 1987;23(4):279-87.
42. Taub M. Primary kidney proximal tubule cells. Methods in molecular biology (Clifton, NJ). 2005;290:231-47.
43. Grantham JJ, Irish JM, 3rd, Hall DA. Studies of isolated renal tubules in vitro. Annual review of physiology. 1978;40:249-77.
44. Delie F, Rubas W. A human colonic cell line sharing similarities with enterocytes as a model to examine oral absorption: advantages and limitations of the Caco-2 model. Critical reviews in therapeutic drug carrier systems. 1997;14(3):221-86.
45. Humes HD, Cieslinski DA. Interaction between growth factors and retinoic acid in the induction of kidney tubulogenesis in tissue culture. Experimental cell research. 1992;201(1):8-15.
46. Liu Y. Epithelial to mesenchymal transition in renal fibrogenesis: pathologic significance, molecular mechanism, and therapeutic intervention. Journal of the American Society of Nephrology : JASN. 2004;15(1):1-12.

47. Giacomini KM, Huang SM, Tweedie DJ, Benet LZ, Brouwer KL, Chu X, et al. Membrane transporters in drug development. Nature reviews Drug discovery. 2010;9(3):215-36.
48. Prasad B, Johnson K, Billington S, Lee C, Chung GW, Brown CD, et al. Abundance of Drug Transporters in the Human Kidney Cortex as Quantified by Quantitative Targeted Proteomics. Drug metabolism and disposition: the biological fate of chemicals. 2016;44(12):1920-4.
49. Breljak D, Ljubojevic M, Hagos Y, Micek V, Balen Eror D, Vrhovac Madunic I, et al. Distribution of organic anion transporters NaDC3 and OAT1-3 along the human nephron. American journal of physiology Renal physiology. 2016;311(1):F227-38.
50. Nigam SK, Bush KT, Martovetsky G, Ahn SY, Liu HC, Richard E, et al. The organic anion transporter (OAT) family: a systems biology perspective. Physiological reviews. 2015;95(1):83-123.
51. Hwang JS, Park EY, Kim WY, Yang CW, Kim J. Expression of OAT1 and OAT3 in differentiating proximal tubules of the mouse kidney. Histology and histopathology. 2010;25(1):33-44.
52. Van der Hauwaert C, Savary G, Buob D, Leroy X, Aubert S, Flamand V, et al. Expression profiles of genes involved in xenobiotic metabolism and disposition in human renal tissues and renal cell models. Toxicology and applied pharmacology. 2014;279(3):409-18.
53. Jenkinson SE, Chung GW, van Loon E, Bakar NS, Dalzell AM, Brown CD. The limitations of renal epithelial cell line HK-2 as a model of drug transporter expression and function in the proximal tubule. Pflugers Archiv : European journal of physiology. 2012;464(6):601-11.
54. Nieskens TT, Peters JG, Schreurs MJ, Smits N, Woestenenk R, Jansen K, et al. A Human Renal Proximal Tubule Cell Line with Stable Organic Anion Transporter 1 and 3 Expression Predictive for Antiviral-Induced Toxicity. The AAPS journal. 2016;18(2):465-75.
55. Weber EJ, Chapron A, Chapron BD, Voellinger JL, Lidberg KA, Yeung CK, et al. Development of a microphysiological model of human kidney proximal tubule function. Kidney international. 2016;90(3):627-37.
56. Liu L, Cui Y, Chung AY, Shitara Y, Sugiyama Y, Keppler D, et al. Vectorial transport of enalapril by Oatp1a1/Mrp2 and OATP1B1 and OATP1B3/MRP2 in rat and human livers. The Journal of pharmacology and experimental therapeutics. 2006;318(1):395-402.
57. Maeda K, Tian Y, Fujita T, Ikeda Y, Kumagai Y, Kondo T, et al. Inhibitory effects of p-aminohippurate and probenecid on the renal clearance of adefovir and benzylpenicillin as probe drugs for organic anion transporter (OAT) 1 and OAT3 in humans. European journal of pharmaceutical sciences : official journal of the European Federation for Pharmaceutical Sciences. 2014;59:94-103.
58. Cunningham RF, Israili ZH, Dayton PG. Clinical pharmacokinetics of probenecid. Clinical pharmacokinetics. 1981;6(2):135-51.
59. Wang Z, Schuetz EG, Xu Y, Thummel KE. Interplay between vitamin D and the drug metabolizing enzyme CYP3A4. The Journal of steroid biochemistry and molecular biology. 2013;136:54-8.
60. Fan J, Liu S, Du Y, Morrison J, Shipman R, Pang KS. Up-regulation of transporters and enzymes by the vitamin D receptor ligands, 1alpha,25-dihydroxyvitamin D3 and vitamin D analogs, in the Caco-2 cell monolayer. The Journal of pharmacology and experimental therapeutics. 2009;330(2):389-402.

61. Bahn A, Hauss A, Appenroth D, Ebbinghaus D, Hagos Y, Steinmetzer P, et al. RT-PCR-based evidence for the in vivo stimulation of renal tubularp-aminohippurate (PAH) transport by triiodothyronine (T3) or dexamethasone (DEXA) in kidney tissue of immature and adult rats. Experimental and toxicologic pathology : official journal of the Gesellschaft fur Toxikologische Pathologie. 2003;54(5-6):367-73.
62. Kikuchi R, Kusuhara H, Hattori N, Shiota K, Kim I, Gonzalez FJ, et al. Regulation of the expression of human organic anion transporter 3 by hepatocyte nuclear factor 1alpha/beta and DNA methylation. Molecular pharmacology. 2006;70(3):887-96.
63. Sauvant C, Hesse D, Holzinger H, Evans KK, Dantzler WH, Gekle M. Action of EGF and PGE2 on basolateral organic anion uptake in rabbit proximal renal tubules and hOAT1 expressed in human kidney epithelial cells. American journal of physiology Renal physiology. 2004;286(4):F774-83.
64. Yuan X, Ta TC, Lin M, Evans JR, Dong Y, Bolotin E, et al. Identification of an endogenous ligand bound to a native orphan nuclear receptor. PloS one. 2009;4(5):e5609.
65. Wang ZQ, Lu FE, Leng SH, Fang XS, Chen G, Wang ZS, et al. Facilitating effects of berberine on rat pancreatic islets through modulating hepatic nuclear factor 4 alpha expression and glucokinase activity. World journal of gastroenterology. 2008;14(39):6004-11.
66. Alpers CE, Hudkins KL, Pritzl P, Johnson RJ. Mechanisms of clearance of immune complexes from peritubular capillaries in the rat. The American journal of pathology. 1991;139(4):855-67.
67. Wang Z, Senn T, Kalhorn T, Zheng XE, Zheng S, Davis CL, et al. Simultaneous measurement of plasma vitamin D(3) metabolites, including 4beta,25-dihydroxyvitamin D(3), using liquid chromatography-tandem mass spectrometry. Analytical biochemistry. 2011;418(1):126-33.
68. Itoh Y, Ezawa A, Kikuchi K, Tsuruta Y, Niwa T. Protein-bound uremic toxins in hemodialysis patients measured by liquid chromatography/tandem mass spectrometry and their effects on endothelial ROS production. Analytical and bioanalytical chemistry. 2012;403(7):1841-50.
69. Brenner B, Rector FC. Brenner and Rector's the kidney (8th Ed.). Philadelphia: Saunders Elsevier; 2008.
70. Humes HD, MacKay SM, Funke AJ, Buffington DA. Tissue engineering of a bioartificial renal tubule assist device: in vitro transport and metabolic characteristics. Kidney international. 1999;55(6):2502-14.
71. Wickham S, West MB, Cook PF, Hanigan MH. Gamma-glutamyl compounds: substrate specificity of gamma-glutamyl transpeptidase enzymes. Analytical biochemistry. 2011;414(2):208-14.
72. Vallon V, Platt KA, Cunard R, Schroth J, Whaley J, Thomson SC, et al. SGLT2 mediates glucose reabsorption in the early proximal tubule. Journal of the American Society of Nephrology : JASN. 2011;22(1):104-12.
73. Liu JJ, Lee T, DeFronzo RA. Why Do SGLT2 inhibitors inhibit only 30-50% of renal glucose reabsorption in humans? Diabetes. 2012;61(9):2199-204.
74. Vander Heiden MG, Cantley LC, Thompson CB. Understanding the Warburg effect: the metabolic requirements of cell proliferation. Science (New York, NY). 2009;324(5930):1029-33.
75. Omdahl JL, Morris HA, May BK. Hydroxylase enzymes of the vitamin D pathway: expression, function, and regulation. Annual review of nutrition. 2002;22:139-66.

76. Inui KI, Masuda S, Saito H. Cellular and molecular aspects of drug transport in the kidney. Kidney international. 2000;58(3):944-58.
77. Smith PL, Buffington DA, Humes HD. Kidney epithelial cells. Methods in enzymology. 2006;419:194-207.
78. Schophuizen CM, De Napoli IE, Jansen J, Teixeira S, Wilmer MJ, Hoenderop JG, et al. Development of a living membrane comprising a functional human renal proximal tubule cell monolayer on polyethersulfone polymeric membrane. Acta biomaterialia. 2015;14:22-32.
79. Kim S, Takayama S. Organ-on-a-chip and the kidney. Kidney research and clinical practice. 2015;34(3):165-9.
80. Sekiya S, Shimizu T, Yamato M, Okano T. Hormone supplying renal cell sheet in vivo produced by tissue engineering technology. BioResearch open access. 2013;2(1):12-9.
81. Maeshima A, Sakurai H, Nigam SK. Adult kidney tubular cell population showing phenotypic plasticity, tubulogenic capacity, and integration capability into developing kidney. Journal of the American Society of Nephrology : JASN. 2006;17(1):188-98.
82. Thery M. Micropatterning as a tool to decipher cell morphogenesis and functions. Journal of cell science. 2010;123(Pt 24):4201-13.
83. Martinez E, Engel E, Planell JA, Samitier J. Effects of artificial micro- and nano-structured surfaces on cell behaviour. Annals of anatomy = Anatomischer Anzeiger : official organ of the Anatomische Gesellschaft. 2009;191(1):126-35.
84. Engler AJ, Sen S, Sweeney HL, Discher DE. Matrix elasticity directs stem cell lineage specification. Cell. 2006;126(4):677-89.
85. Discher DE, Janmey P, Wang YL. Tissue cells feel and respond to the stiffness of their substrate. Science (New York, NY). 2005;310(5751):1139-43.
86. Maschmeyer I, Lorenz AK, Schimek K, Hasenberg T, Ramme AP, Hubner J, et al. A four-organ-chip for interconnected long-term co-culture of human intestine, liver, skin and kidney equivalents. Lab on a chip. 2015;15(12):2688-99.
87. Humes HD, Weitzel WF, Bartlett RH, Swaniker FC, Paganini EP, Luderer JR, et al. Initial clinical results of the bioartificial kidney containing human cells in ICU patients with acute renal failure. Kidney international. 2004;66(4):1578-88.
88. O'Callaghan C. The renal system at a glance (3rd ed.). Hoboken, NJ: Wiley-Blackwell; 2009.
89. Ligresti G, Nagao RJ, Xue J, Choi YJ, Xu J, Ren S, et al. A Novel Three-Dimensional Human Peritubular Microvascular System. Journal of the American Society of Nephrology : JASN. 2016;27(8):2370-81.
90. Jansen J, Fedecostante M, Wilmer MJ, Peters JG, Kreuser UM, van den Broek PH, et al. Bioengineered kidney tubules efficiently excrete uremic toxins. Scientific reports. 2016;6:26715.
91. Homan KA, Kolesky DB, Skylar-Scott MA, Herrmann J, Obuobi H, Moisan A, et al. Bioprinting of 3D Convoluted Renal Proximal Tubules on Perfusable Chips. Scientific reports. 2016;6:34845.
92. Denic A, Mathew J, Lerman LO, Lieske JC, Larson JJ, Alexander MP, et al. Single-Nephron Glomerular Filtration Rate in Healthy Adults. The New England journal of medicine. 2017;376(24):2349-57.
93. Gross AS, McLachlan AJ, Minns I, Beal JB, Tett SE. Simultaneous administration of a cocktail of markers to measure renal drug elimination pathways: absence of a pharmacokinetic interaction between fluconazole and sinistrin, p-aminohippuric acid and pindolol. British journal of clinical pharmacology. 2001;51(6):547-55.

94. Vanderbilt Institute for Integrative Biosystems Research and Education (VIIBRE). OoC Scaling Spreadsheet 2013 [Available from: https://www.vanderbilt.edu/viibre/organs-on-a-chip.php.
95. Maass C, Stokes CL, Griffith LG, Cirit M. Multi-functional scaling methodology for translational pharmacokinetic and pharmacodynamic applications using integrated microphysiological systems (MPS). Integrative biology : quantitative biosciences from nano to macro. 2017;9(4):290-302.
96. Bertram JF, Douglas-Denton RN, Diouf B, Hughson MD, Hoy WE. Human nephron number: implications for health and disease. Pediatric nephrology (Berlin, Germany). 2011;26(9):1529-33.
97. Janku I. Physiological modelling of renal drug clearance. European journal of clinical pharmacology. 1993;44(6):513-9.
98. Beese M, Wyss K, Haubitz M, Kirsch T. Effect of cAMP derivates on assembly and maintenance of tight junctions in human umbilical vein endothelial cells. BMC cell biology. 2010;11:68.
99. Hubatsch I, Ragnarsson EG, Artursson P. Determination of drug permeability and prediction of drug absorption in Caco-2 monolayers. Nature protocols. 2007;2(9):2111-9.
100. Mitchell LA, Overgaard CE, Ward C, Margulies SS, Koval M. Differential effects of claudin-3 and claudin-4 on alveolar epithelial barrier function. American journal of physiology Lung cellular and molecular physiology. 2011;301(1):L40-9.
101. Abaci HE, Shuler ML. Human-on-a-chip design strategies and principles for physiologically based pharmacokinetics/pharmacodynamics modeling. Integrative biology : quantitative biosciences from nano to macro. 2015;7(4):383-91.
102. Low LA, Tagle DA. Organs-on-chips: Progress, challenges, and future directions. Experimental biology and medicine (Maywood, NJ). 2017:1535370217700523.
103. Lee-Montiel FT, George SM, Gough AH, Sharma AD, Wu J, DeBiasio R, et al. Control of oxygen tension recapitulates zone-specific functions in human liver microphysiology systems. Experimental biology and medicine (Maywood, NJ). 2017:1535370217703978.
104. Maoz BM, Herland A. Organs-on-Chips with combined multi-electrode array and transepithelial electrical resistance measurement capabilities. 2017;17(13):2294-302.
105. Phan DTT, Wang X, Craver BM, Sobrino A, Zhao D, Chen JC, et al. A vascularized and perfused organ-on-a-chip platform for large-scale drug screening applications. Lab on a chip. 2017;17(3):511-20.
106. Hailey DW, Esterberg R, Linbo TH, Rubel EW, Raible DW. Fluorescent aminoglycosides reveal intracellular trafficking routes in mechanosensory hair cells. The Journal of clinical investigation. 2017;127(2):472-86.
107. Miller DS, Letcher S, Barnes DM. Fluorescence imaging study of organic anion transport from renal proximal tubule cell to lumen. The American journal of physiology. 1996;271(3 Pt 2):F508-20.
108. Hall AM. Update on tenofovir toxicity in the kidney. Pediatric nephrology (Berlin, Germany). 2013;28(7):1011-23.
109. Enomoto A, Niwa T. Roles of organic anion transporters in the progression of chronic renal failure. Therapeutic apheresis and dialysis : official peer-reviewed journal of the International Society for Apheresis, the Japanese Society for Apheresis, the Japanese Society for Dialysis Therapy. 2007;11 Suppl 1:S27-31.

110. Motojima M, Hosokawa A, Yamato H, Muraki T, Yoshioka T. Uraemic toxins induce proximal tubular injury via organic anion transporter 1-mediated uptake. British journal of pharmacology. 2002;135(2):555-63.
111. Putt TL, Duffull SB, Schollum JB, Walker RJ. GFR may not accurately predict aspects of proximal tubule drug handling. European journal of clinical pharmacology. 2014;70(10):1221-6.
112. Tett SE, Kirkpatrick CM, Gross AS, McLachlan AJ. Principles and clinical application of assessing alterations in renal elimination pathways. Clinical pharmacokinetics. 2003;42(14):1193-211.
113. Petitpierre B, Perrin L, Rudhardt M, Herrera A, Fabre J. Behaviour of chlorpropamide in renal insufficiency and under the effect of associated drug therapy. International journal of clinical pharmacology, therapy and toxicology. 1972;6(2):120-4.
114. Bricker NS. On the meaning of the intact nephron hypothesis. The American journal of medicine. 1969;46(1):1-11.
115. Dettli L. Drug dosage in renal disease. Clinical pharmacokinetics. 1976;1(2):126-34.
116. Tozer TN, Rowland M, Rowland M. Clinical pharmacokinetics and pharmacodynamics : concepts and applications. 4th ed. ed. Tozer TN, Rowland M, editors. Philadelphia: Philadelphia : Wolters Kluwer Health/Lippincott William & Wilkins; 2011.
117. Maher FT, Strong CG, Elveback LR. Renal extraction ratios and plasma-binding studies of radioiodinated o-iodohippurate p-aminohippurate in man. Mayo Clinic proceedings. 1971;46(3):189-92.
118. Dettli L. Elimination kinetics and drug dosage in renal insufficiency patients. Triangle; the Sandoz journal of medical science. 1975;14(3-4):117-23.
119. Dettli L, Spring P, Habersang R. Drug dosage in patients with impaired renal function. Postgraduate medical journal. 1970:Suppl:32-5.
120. Dettli LC. Drug dosage in patients with renal disease. Clinical pharmacology and therapeutics. 1974;16(1):274-80.
121. Jelliffe RW. A mathematical analysis of digitalis kinetics in patients with normal and reduced renal function. Mathematical Biosciences. 1967;1(2):305-25.
122. Bricker NS, Morrin PA, Kime SW, Jr. The pathologic physiology of chronic Bright's disease. An exposition of the "intact nephron hypothesis". The American journal of medicine. 1960;28:77-98.
123. Brenner BM, Rector FC. The Kidney. Brenner BM, Rector FC, editors. Philadelphia: Philadelphia : Saunders; 1976.
124. The Cleveland Clinic Foundation. Kidney Function Assessment by Creatinine-Based Estimation Equations 2010 [Available from: http://www.clevelandclinicmeded.com/medicalpubs/diseasemanagement/nephrology/kidney-function/.
125. Suchy-Dicey AM, Laha T, Hoofnagle A, Newitt R, Sirich TL, Meyer TW, et al. Tubular Secretion in CKD. Journal of the American Society of Nephrology : JASN. 2015.
126. Nauta FL, Boertien WE, Bakker SJ, van Goor H, van Oeveren W, de Jong PE, et al. Glomerular and tubular damage markers are elevated in patients with diabetes. Diabetes care. 2011;34(4):975-81.
127. Vaidya VS, Bonventre JV. Mechanistic biomarkers for cytotoxic acute kidney injury. Expert opinion on drug metabolism & toxicology. 2006;2(5):697-713.

128. Vaidya VS, Waikar SS, Ferguson MA, Collings FB, Sunderland K, Gioules C, et al. Urinary biomarkers for sensitive and specific detection of acute kidney injury in humans. Clinical and translational science. 2008;1(3):200-8.
129. Clericetti N, Beretta-Piccoli C. Lithium clearance in patients with chronic renal diseases. Clinical nephrology. 1991;36(6):281-9.
130. He P, Kerr D, Marbury T, Ries D, Farwell W, Stecher S, et al. Pharmacokinetics of renally excreted drug dexpramipexole in subjects with impaired renal function. Journal of clinical pharmacology. 2014;54(12):1383-90.
131. Smith WB, Mannaert E, Verhaeghe T, Kerstens R, Vandeplassche L, Van de Velde V. Effect of renal impairment on the pharmacokinetics of prucalopride: a single- dose open-label Phase I study. Drug design, development and therapy. 2012;6:407-15.
132. von Bergmann K, Laeis P, Puchler K, Sudhop T, Schwocho LR, Gonzalez L. Olmesartan medoxomil: influence of age, renal and hepatic function on the pharmacokinetics of olmesartan medoxomil. Journal of hypertension Supplement : official journal of the International Society of Hypertension. 2001;19(1):S33-40.
133. Boike SC, Pue MA, Freed MI, Audet PR, Fairless A, Ilson BE, et al. Pharmacokinetics of famciclovir in subjects with varying degrees of renal impairment. Clinical pharmacology and therapeutics. 1994;55(4):418-26.
134. Noel M. Kinetic study of normal and sustained release dosage forms of metformin in normal subjects. Res Clin For. 1979;1:35-45.
135. Tucker GT, Casey C, Phillips PJ, Connor H, Ward JD, Woods HF. Metformin kinetics in healthy subjects and in patients with diabetes mellitus. British journal of clinical pharmacology. 1981;12(2):235-46.
136. Sirtori CR, Franceschini G, Galli-Kienle M, Cighetti G, Galli G, Bondioli A, et al. Disposition of metformin (N,N-dimethylbiguanide) in man. Clinical pharmacology and therapeutics. 1978;24(6):683-93.
137. Chen N, Lau H, Kong L, Kumar G, Zeldis JB, Knight R, et al. Pharmacokinetics of lenalidomide in subjects with various degrees of renal impairment and in subjects on hemodialysis. Journal of clinical pharmacology. 2007;47(12):1466-75.
138. Malhotra B, Gandelman K, Sachse R, Wood N. Assessment of the effects of renal impairment on the pharmacokinetic profile of fesoterodine. Journal of clinical pharmacology. 2009;49(4):477-82.
139. Aweeka FT, Jacobson MA, Martin-Munley S, Hedman A, Schoenfeld P, Omachi R, et al. Effect of renal disease and hemodialysis on foscarnet pharmacokinetics and dosing recommendations. Journal of acquired immune deficiency syndromes and human retrovirology : official publication of the International Retrovirology Association. 1999;20(4):350-7.
140. Watanabe H, Sakaguchi Y, Sugimoto R, Kaneko K, Iwata H, Kotani S, et al. Human organic anion transporters function as a high-capacity transporter for p-cresyl sulfate, a uremic toxin. Clinical and experimental nephrology. 2014;18(5):814-20.
141. Haegele KD, Huebert ND, Ebel M, Tell GP, Schechter PJ. Pharmacokinetics of vigabatrin: implications of creatinine clearance. Clinical pharmacology and therapeutics. 1988;44(5):558-65.
142. Stangier J, Rathgen K, Stahle H, Mazur D. Influence of renal impairment on the pharmacokinetics and pharmacodynamics of oral dabigatran etexilate: an open-label, parallel-group, single-centre study. Clinical pharmacokinetics. 2010;49(4):259-68.

143. Murthy B, Schmitt-Hoffmann A. Pharmacokinetics and pharmacodynamics of ceftobiprole, an anti-MRSA cephalosporin with broad-spectrum activity. Clinical pharmacokinetics. 2008;47(1):21-33.
144. Turck D, Weber W, Sigmund R, Budde K, Neumayer HH, Fritsche L, et al. Pharmacokinetics of intravenous, single-dose tiotropium in subjects with different degrees of renal impairment. Journal of clinical pharmacology. 2004;44(2):163-72.
145. Halstenson CE, Triscari J, DeVault A, Shapiro B, Keane W, Pan H. Single-dose pharmacokinetics of pravastatin and metabolites in patients with renal impairment. Journal of clinical pharmacology. 1992;32(2):124-32.
146. Dickinson J, Lewand M, Sawamoto T, Krauwinkel W, Schaddelee M, Keirns J, et al. Effect of renal or hepatic impairment on the pharmacokinetics of mirabegron. Clinical drug investigation. 2013;33(1):11-23.
147. He G, Massarella J, Ward P. Clinical pharmacokinetics of the prodrug oseltamivir and its active metabolite Ro 64-0802. Clinical pharmacokinetics. 1999;37(6):471-84.
148. Nilsen OG, Saltvedt E, Walstad RA, Marstein S. Single-dose pharmacokinetics of lomefloxacin in patients with normal and impaired renal function. The American journal of medicine. 1992;92(4a):38s-40s.
149. Brody SR, Humphreys MH, Gambertoglio JG, Schoenfeld P, Cundy KC, Aweeka FT. Pharmacokinetics of cidofovir in renal insufficiency and in continuous ambulatory peritoneal dialysis or high-flux hemodialysis. Clinical pharmacology and therapeutics. 1999;65(1):21-8.
150. Bui K, She F, Sostek M. The effects of renal impairment on the pharmacokinetics, safety, and tolerability of naloxegol. Journal of clinical pharmacology. 2014;54(12):1375-82.
151. Lameire N, Malerczyk V, Drees B, Lehr K, Rosenkranz B. Single-dose pharmacokinetics of cefpirome in patients with renal impairment. Clinical pharmacology and therapeutics. 1992;52(1):24-30.
152. Gibson TP, Granneman GR, Kallal JE, Sennello LT. Cefsulodin kinetics in renal impairment. Clinical pharmacology and therapeutics. 1982;31(5):602-8.
153. Molander L, Hansson A, Lunell E, Alainentalo L, Hoffmann M, Larsson R. Pharmacokinetics of nicotine in kidney failure. Clinical pharmacology and therapeutics. 2000;68(3):250-60.
154. Randinitis EJ, Posvar EL, Alvey CW, Sedman AJ, Cook JA, Bockbrader HN. Pharmacokinetics of pregabalin in subjects with various degrees of renal function. Journal of clinical pharmacology. 2003;43(3):277-83.
155. Yamamoto J, Toublanc N, Kumagai Y, Stockis A. Levetiracetam pharmacokinetics in Japanese subjects with renal impairment. Clinical drug investigation. 2014;34(11):819-28.
156. Toon S, Ross CE, Gokal R, Rowland M. An assessment of the effects of impaired renal function and haemodialysis on the pharmacokinetics of fluconazole. British journal of clinical pharmacology. 1990;29(2):221-6.
157. Cawello W, Fuhr U, Hering U, Maatouk H, Halabi A. Impact of impaired renal function on the pharmacokinetics of the antiepileptic drug lacosamide. Clinical pharmacokinetics. 2013;52(10):897-906.